VNIVERSITAT DE VALÈNCIA

PhD Program in Neurosciences

RD 99/2011

INDUCTION OF NEURONAL PLASTICITY DURING ADULTHOOD. ROLE OF CORTICAL INTERNEURONS AND PLASTICITY-RELATED MOLECULES

Héctor Carceller Cerdá

November 2019

Dr. Juan Nácher Roselló
Dr. Ramón Guirado Guillén

Facultat de Ciències Biològiques

Departament de Biologia Cel·lular, Biologia Funcional i Antropologia Física

The supervisors of the present doctoral thesis, Drs. Ramón Guirado Guillén and Juan Salvador Nácher Roselló,

CERTIFY:

That, Ms. Héctor Carceller Cerdà, graduated in Biology and MSc in Neuroscience at the University of Valencia, has carried out the present Doctoral Thesis entitled:

"INDUCTION OF NEURONAL PLASTICITY DURING ADULTHOOD. ROLE OF CORTICAL INTERNEURONS AND PLASTICITY-RELATED MOLECULES",

and that being concluded, authorize its presentation to be judged by the corresponding court and qualified for obtaining the PhD in Neuroscience.

What we sign as required in Burjassot, on November the 7th , 2019

Juan Nacher

Firmado digitalmente por Juan Nacher
Fecha: 2019.11.07 16:36:42 +01'00'

GUIRADO GUILLEN RAMON - 18444847C

Digitally signed by GUIRADO GUILLEN RAMON - 18444847C
Date: 2019.11.10 19:45:53 +01'00'

Dr. Juan Salvador Nácher Roselló

Dr. Ramón Guirado Guillén

Para la realización de esta tesis, el autor ha sido beneficiario de un contrato predoctoral asociado a la convocatoria Prometeo para grupos de excelencia de la Generalitat Valenciana (PROMETEO 2013/069) y de una beca predoctoral de Formación de Profesorado Universitario concedida por el Ministerio de Educación, Cultura y Deporte (FPU 15/01233) según la resolución del 5 de agosto de 2016, de la Secretaría General de Universidades.

“Sometimes science is more art than science, Morty.
Lot of people don’t get that”

Rick Sanchez, Rick and Morty

Table of contents

Agraïments

Arriba el moment d'escriure la part més llegida de la tesi, quina pressió! La llista d'autors d'aquesta secció és llarga, així que anem per feina. Per suposat la primera menció amb tots els honors és per a Joan. Quan vaig arribar al seu antic despatx (quin despatx!) fa quasi 10 anys no m'imaginava ni per un moment que després de molts experiments, mal de caps, lab meetings i somriures, acabaria escrivint la meva pròpia tesi doctoral. He tingut molta sort de tenir-te com a pare científic i espere poder tornar almenys una part de tot el que he après al teu costat. El meu deute és també immens amb Ramón. Si Joan és el meu pare científic, Ramón és el germà gran. Sempre disposat a ensenyar i compartir el seu coneixement sobre el sistema nerviós, o sobre teoría política, o sobre quasi qualsevol cosa.

Tota la gent amb la que en algún moment he compartit la meva segona casa durant aquests anys. La vella guàrdia que sempre aporta la veu de l'experiència (José Miguel, Carlos, Emilio); els que em van ensenyar tot un món quan vaig arribar (Javi, Esther); les que m'han precedit (Clara, Marta, María, Yasmina); les que venen després (Clara, Júlia, Simona) i els amb els en algun punt he coincidit i compartit bancada (Pablo, Estroflo, Ana Paula, Edna...). Ha estat un plaer passar aquests anys amb vosaltres.

Thanks a lot to Dr. Alexander Dityatev for hosting me during my short stay in his amazing lab. All the people in the lab: Hussam, Eduardo, Rahul, Pedro, Maura, Carla, Gabriela, Shaobo and Antonia. You made me feel one more there and showed me the secret gems of Magdeburg, including the amazing BlocSchmeide! I wish you the best for the future.

I com que no tot en la vida es treball, a tota la gent que m'envolta en el meu dia a dia i amb els que he compartit moments meravellosos (i els que ens queden!): Javi, Tomás, Jordi, Alex, Cassandra, Sebas, Poxo, Silvia i tants altres que fan la meva existència molt millor del que seria sense ells.

Menció especial per als meus pares i la meva germana, amb els que el temps s'atura i els problemes que hi ha a València, es queden a València. Però no les alegries.

Per finalitzar, aquesta tesi també és un poc de Rosa i per la paciència infinita que ha d'utilitzar a canvi d'un mecànic per a la bicicleta i una estufa a l'hivern. Perquè tot el temps que compartim és un sospir.

Abbreviations

5-HT serotonin
5-HTT serotonin transporter
AIS axonal initial segment
AnkG ankyrin G
BA basal amygdala
BLA basolateral amygdala
BMA basomedial amygdala
CA1 *Cornu Ammonis* 1 from the hippocampus
CAMKII calcium/calmodulin-dependent protein kinase II
CB calbindin
CB1r cannabinoid receptor 1
CCK cholecystokinin
CeA central amygdala
CG cingulate cortex
ChABC chondroitinase ABC
CNS Central nervous system
CP critical period
CR calretinin
CSPGs chondroitin sulfate proteoglycans
dLGN dorsal lateral geniculate nucleus
dSC deep superior colliculus
EndoN endo neuraminidase-N
GABA ɣ-aminobutyric acid
GAD glutamic acid decarboxylase
GHT geniculohypothalamic tract
GIN mice FVB-Tg(GadGFP)45704Swn/J mice
IGL intergeniculate leaflet
IL infralimbic cortex
LA lateral amygdala
LFP local field potential
LGN lateral geniculate nucleus
mPFC medial prefrontal cortex
NCAM neural cell adhesion molecule
NMDA N-methyl-D-aspartate
NPY neuropeptide Y
OFC orbitofrontal cortex
PB phosphate buffer
PBS phosphate saline buffer
PNNs perineuronal nets
PNS Peripheral nervous system
PrL prelimbic cortex

PSA polysialic acid
PSA-NCAM polysialylated form of the neural cell adhesion molecule
PSD postsynaptic density
PV parvalbumin
PV-Tdt mice C57BL/6-Tg(Pvalb-tdTomato)15Gfng/J mice
RGC retinal ganglion cells
SC superior colliculus
SChN suprachiasmatic nucleus
SEM standard error of the mean
SGL superficial gray layer
sSC superficial superior colliculus
SSRI selective serotonin reuptake inhibitors
SST somatostatin
SYN synaptophysin
V1 primary visual cortex
V2 secondary visual cortex
VGAT vesicular GABA transporter
VGLUT vesicular glutamate transporter
VIP vasoactive intestinal peptide
vLGN ventral lateral geniculate nucleus
WFA *Wisteria Floribunda* agglutinin

List of figures

List of tables

Resumen en castellano

Introducción

La complejidad del sistema nervioso de los vertebrados representa un reto a la hora de conocer su funcionamiento. Hace ya más de cien años que se postuló la neurona como unidad básica de procesamiento, generación y transmisión de la información a través de este sistema, y, con el paso de los años, ha evolucionado el conocimiento sobre esta unidad funcional (Jermakowicz and Casagrande, 2007). La idea clásica del sistema nervioso central (SNC) adulto es la de un tejido asombrosamente interconectado y complejo, pero prácticamente inmutable y muy poco adaptable a los cambios. No obstante, esta visión se ha ido desplazando, formándose una nueva idea del SNC adulto que, aunque de manera más limitada que durante el desarrollo, también tiene la propiedad de adaptarse a cambios tanto extrínsecos como intrínsecos, la denominada plasticidad neuronal. Esta plasticidad neuronal comprende múltiples procesos, desde los cambios en la eficiencia de las sinapsis (plasticidad sináptica) al remodelado de la estructura de las neuronas (plasticidad estructural) y la generación de nuevas células en el SNC adulto (neurogénesis). A su vez, estos fenómenos plásticos se encuentran mediados por neurotransmisores y otras moléculas que facilitan o limitan el remodelado de la estructura y conectividad de las neuronas. En la presente tesis voy a estudiar cómo afectan diversos tratamientos potenciadores de la plasticidad neuronal en el SNC a la estructura y conectividad de las neuronas en la corteza prefrontal medial, la corteza visual, el núcleo geniculado lateral, el colículo superior y la amígdala.

Neuronas

De entre los tipos celulares que se pueden encontrar en el SNC, se ha abordado el efecto de diferentes tratamientos sobre la estructura de neuronas excitadoras e inhibidoras o interneuronas. Las neuronas piramidales constituyen la población celular más abundante de neuronas excitadoras en la corteza cerebral, donde se encuentran mayoritariamente agrupadas en dos estratos, uno superficial (capas II/III) y otro profundo (capa V) (Elston, 2003). Se trata de neuronas glutamatérgicas, es decir, producen y liberan al espacio sináptico mayoritariamente glutamato, el principal neurotransmisor excitador del SNC, mediante proyecciones tanto locales

como dirigidas a otras regiones del SNC. A nivel morfológico presentan una estructura canónica: un soma triangular, que recibe sinapsis tanto inhibidoras como excitadoras, de cuya base emerge un axón (generalmente mielinizado) que se ramifica y produce numerosos contactos sinápticos excitadores. El segmento inicial del axón (AIS) no presenta cubierta de mielina y recibe numerosos contactos sinápticos procedentes de neuronas inhibidoras (Kubota, 2014). En cuanto a la estructura dendrítica, ésta se divide en dos dominios principales: 1) la dendrita apical que emerge del ápice del soma y sigue un patrón de bifurcación en dendritas de menor calibre que se desarrollan en perpendicular a la dendrita apical y 2) las dendritas basales, que emergen de la base del soma y suelen estar menos desarrolladas. Las dendritas presentan protuberancias membranosas de morfología variada denominadas espinas dendríticas, que reciben contactos sinápticos, principalmente excitadores, mientras que los contactos que se producen directamente sobre las dendritas son mayoritariamente inhibitorios, procedentes de interneuronas.

En cuanto a las interneuronas, aunque menores en número, presentan una gran diversidad en cuanto a morfología, expresión de marcadores y actividad sináptica (Tremblay et al., 2016). En términos generales, se trata de neuronas que producen y secretan ácido γ-aminobutírico (GABA), principalmente mediante proyecciones locales. En esta tesis, se han estudiado tres poblaciones de interneuronas en base a la expresión de distintos marcadores moleculares: las interneuronas que expresan parvalbúmina (PV), somatostatina (SST) y colecistoquinina (CCK). Las interneuronas que expresan PV forman el principal grupo de interneuronas en la corteza cerebral (Rudy et al., 2011). Presentan un patrón de actividad característico, rápido y no adaptativo (Tremblay et al., 2016), por lo que forman parte fundamental en la generación de las oscilaciones neuronales, tanto rápidas como lentas.

Morfológicamente, estas neuronas que expresan PV constituyen dos poblaciones características: las neuronas “candelabro” que forman contactos sinápticos sobre el AIS de otras neuronas, y las neuronas en “cesto”, que forman contactos sinápticos alrededor la soma y la parte proximal de las dendritas. El otro grupo de interneuronas que forman cestos son aquellas que expresan CCK, aunque su patrón actividad difiere respecto a las que expresan PV. La actividad de éstas células puede ser inhibida por el elemento postsináptico mediante la activación del receptor de cannabinoides 1 (CB1r) en un proceso conocido como inhibición sináptica inducida por despolarización. Así pues, estas interneuronas tienen un patrón de actividad más sutil y modulable, complementando la actividad robusta y no adaptativa de las interneuronas que expresan PV (Freund and Katona, 2007). El último grupo de interneuronas

estudiado corresponde a las interneuronas que expresan SST. Estas interneuronas realizan contactos sinápticos sobre las dendritas de neuronas piramidales y otras interneuronas (Wang et al., 2004; Pfeffer et al., 2013). Morfológicamente se pueden distinguir dos grupos; las células no Martinotti y las Martinotti, éstas últimas estudiadas en la presente tesis. Las células Martinotti se encuentran dispersas en todas las capas de la corteza cerebral excepto la capa I. A nivel estructural, presentan un axón ascendente que contacta con la porción distal de dendritas apicales en la capa I. Otra característica significativa de esta población de interneuronas es la presencia de espinas dendríticas, una cualidad poco frecuente en las neuronas inhibidoras (Wang et al., 2004).

De la actividad combinada y sincrónica de todas las poblaciones neuronales surgen las oscilaciones neuronales, que pueden ser detectadas mediante el registro del potencial de campo local (LFP) y revelan patrones rítmicos de la actividad neuronal (Buzsáki et al., 2012). Las oscilaciones con una frecuencia de entre 30 y 90 Hz, conocidas como oscilaciones gamma, contribuyen a la formación de la memoria y el procesamiento sensitivo, y se encuentran alteradas en diversos desórdenes neuropsiquiátricos (Bartos et al., 2007). Estas oscilaciones emergen de la interacción coordinada entre neuronas piramidales e interneuronas, especialmente las que expresan PV, que juegan un papel fundamental en su generación y mantenimiento, gracias a su patrón de actividad de alta frecuencia y poco modulable (Buzsáki and Wang, 2012).

Áreas de estudio

Durante los últimos años, diferentes tratamientos han demostrado la capacidad de potenciar la plasticidad neuronal en diversas regiones del sistema nervioso adulto. En la presente tesis se han estudiado la corteza prefrontal medial (mPFC), la amígdala y el sistema visual, compuesto por el núcleo geniculado lateral (LGN), el colículo superior (SC) y la corteza visual, concretamente la corteza visual primaria (V1).

La citoarquitectura de la mPFC y la V1 corresponde al esquema general de la corteza cerebral, organizada en 6 capas. Las neuronas piramidales se agrupan en las capas II/III y la capa V y el resto de neuronas y células gliales se reparten en proporciones variables por todas las capas, formando patrones de contactos sinápticos propios en cada capa (Fuster, 2001). La única excepción es la ausencia de la capa IV en la mPFC. En cuanto al LGN, se compone de tres áreas: el LGN dorsal, principal centro de relevo en la transmisión de estímulos visuales a la

corteza visual; el foliolo intergeniculado (IGL) y el LGN ventral, estos últimos implicados en la regulación del sistema circadiano mediante el tracto geniculohipotalámico que proyecta el IGL al núcleo supraquiasmático (Moore and Card, 1994). Por su parte, el SC es una estructura integrativa que recibe estímulos visuales directamente de la retina, pero también de otras cortezas sensoriales primarias y de la corteza motora. El SC está implicado en el control de los movimientos coordinados ojo/cabeza (May, 2006; Krauzlis et al., 2013).

Por último, la amígdala es un área clave en la generación de memorias relacionadas con el miedo, la ansiedad y la recompensa (Campeau and Davis, 1995; Pape and Pare, 2010). Está compuesta por múltiples núcleos interconectados, entre los que destaca la amígdala basolateral (BLA), el principal centro de procesamiento de la información que llega a la amígdala (Campeau and Davis, 1995).

Neurotransmisión

La transmisión de información a través de los diferentes elementos de la circuitería neuronal es susceptible de ser afectada por cambios tanto extrínsecos como intrínsecos. A su vez, esta alteración puede producir otros cambios que abarcan diferentes niveles, desde la alteración en la expresión de moléculas relacionadas con la plasticidad hasta la remodelación estructural de las neuronas. En la presente tesis, se han estudiado los efectos de diferentes tratamientos sobre la plasticidad de tres sistemas de neurotransmisión: el sistema glutamatérgico, el GABAérgico y el serotoninérgico.

El sistema glutamatérgico está compuesto principalmente por neuronas excitadoras o principales que liberan el glutamato al espacio sináptico. La unión de este neurotransmisor a receptores específicos produce la despolarización de la membrana plasmática en el elemento postsináptico. Esta liberación se produce mediante la fusión de vesículas sinápticas que contienen el glutamato con la membrana plasmática en la zona del terminal axónico. La entrada del glutamato en las vesículas sinápticas se produce a través de la acción del transportador vesicular de glutamato (VGLUT), cuya función es imprescindible para el correcto desarrollo de las sinapsis excitadoras (Divito and Underhill, 2014). Otra proteína presente en la membrana de las vesículas sinápticas, tanto excitadoras como inhibidoras, es la sinaptofisina (SYN). Aunque la función específica de la SYN no está completamente clara, esta proteína resulta un buen marcador general de la zona presináptica (Masliah et al., 1990; Eshkind and Leube, 1995).

El sistema GABAérgico corresponde al conjunto de contactos sinápticos producidos por las interneuronas, tanto sobre neuronas excitadoras como sobre otras interneuronas, que liberan GABA al espacio sináptico y cuya unión a receptores específicos provoca la hiperpolarización de la membrana plasmática de la neurona postsináptica. En el proceso de síntesis y liberación del GABA intervienen dos moléculas cuya expresión ha sido analizada en la presente tesis. Por un lado, la ácido glutámico descarboxilasa (GAD) cataliza la síntesis de GABA mediante sus dos isoformas: GAD65 y GAD67 (Martin and Rimvall, 1993). Por otro lado, la incorporación del GABA a las vesículas sinápticas se realiza mediante el transportador vesicular de GABA (VGAT). Ambas moléculas constituyen buenos marcadores de la zona presináptica de las sinapsis inhibitorias.

En cuanto al sistema serotoninérgico, utiliza la serotonina (5-hidroxitriptamina: 5-HT) como neurotransmisor y está implicado en múltiples comportamientos, especialmente aquellos relacionados con el estado de ánimo (Castrén, 2005). La 5-HT es sintetizada por las células ubicadas en los núcleos del raphe que proyectan de forma masiva a todo el neocórtex y otras estructuras como la amígdala (Beliveau et al., 2017). El estudio de los efectos de la neurotransmisión serotoninérgica es complejo, ya que existen siete familias diferentes de receptores ($5\text{-}HT_1$-$5\text{-}HT_7$), mayoritariamente metabotrópicos y un transportador situado en la membrana presináptica (5-HTT) que se encarga de la recaptación de 5HT hacia el espacio presináptico. El 5-HTT constituye la principal diana de un numeroso grupo de antidepresivos, los inhibidores específicos de la recaptación de serotonina, entre los que se encuentra la fluoxetina (Prozac, Lilly).

Plasticidad estructural

La estructura, tanto de neuronas principales como de interneuronas, es dinámica y puede cambiar tanto en condiciones estándar, como en respuesta a alteraciones en la neurotransmisión producidas por cambios en el ambiente, tratamientos farmacológicos o enfermedades neuropsiquiátricas, entre otros (Spruston, 2008). Estos cambios se pueden producir tanto en las dendritas como en el axón e incluyen alteraciones en la longitud y complejidad del árbol dendrítico, la densidad y tipología de las espinas dendríticas, así como en la densidad y tamaño de los botones axónicos (Keck et al., 2008, 2011; Sammons et al., 2018). En la presente tesis, se estudiará el efecto de diferentes tratamientos inductores de plasticidad neuronal en el SNC adulto sobre la estructura de las interneuronas, especialmente de aquellas que expresan SST, mediante la utilización de una cepa transgénica de ratón que expresa la

proteína verde fluorescente (GFP) específicamente en esta población de interneuronas (Oliva et al., 2000).

PSA-NCAM y PNNs

Otra línea de investigación trata de comprender qué tipo de moléculas pueden estar relacionadas con la plasticidad neuronal y mediar los cambios a nivel sináptico y estructural observados. En esta tesis se han estudiado en detalle los efectos de diferentes tratamientos inductores de plasticidad en la forma polisializada de la molécula de adhesión celular neural (PSA-NCAM) y las moléculas que constituyen las redes perineuronales (PNNs).

Debido a sus propiedades antiadhesivas, la PSA-NCAM se expresa en amplias zonas del SNC durante el desarrollo y está implicada en múltiples procesos como la migración neuronal, el remodelado sináptico y la expansión de las neuritas (Rutishauser, 2008). Aunque mucho más restringida, la expresión de PSA-NCAM se mantiene en algunas zonas durante la etapa adulta. Su expresión es especialmente intensa en los nichos neurogénicos (giro dentado del hipocampo y zona subventricular/ruta migratoria rostral/bulbo olfatorio), pero también se puede encontrar PSA-NCAM en otras zonas como el neocórtex y la amígdala, en las que esta molécula se encuentra exclusivamente expresada por diferentes grupos de interneuronas (Nacher et al., 2002; Prosser et al., 2003; Varea et al., 2005). Las interneuronas que expresan PSA-NCAM muestran características estructurales particulares en comparación con otras interneuronas que no presentan esta molécula en su membrana: reciben menos contactos sinápticos en la zona del soma y tienen un menor número de dendritas y espinas dendríticas (Gómez-Climent et al., 2011). Asimismo, la eliminación enzimática del ácido polisiálico (PSA) tiene múltiples efectos estructurales en la corteza cerebral: aumenta los contactos sinápticos de la interneuronas que expresan PV sobre neuronas piramidales (Castillo-Gómez et al., 2011) y altera la densidad de espinas dendríticas en las interneuronas que expresan SST (Castillo-Gómez et al., 2016). Se ha hipotetizado que todos estos efectos se deben a las propiedades antiadhesivas de la PSA-NCAM, que facilitan el remodelado sináptico y estructural de las neuronas de la corteza (Nacher et al., 2013).

Por otro lado, las PNNs son estructuras formadas a partir de moléculas de la matriz extracelular que se depositan alrededor del cuerpo celular, dendritas proximales y en ocasiones la parte inicial del AIS, mayoritariamente de interneuronas que expresan PV (Celio et al., 1998). Se forman a partir de la unión de proteoglicanos de condroitin sulfato (GSPGs) a un esqueleto

de hialuronato. La composición y densidad de las PNNs presenta variaciones regionales a lo largo de las corteza cerebral (Ueno et al., 2018). Las PNNs se forman al final el desarrollo, coincidiendo con el cierre del periodo crítico (Brückner et al., 2000) y su aparición marca una abrupta reducción de la plasticidad de las interneuronas que expresan PV (Fawcett et al., 2019). La digestión de las PNNs mediante la inyección de la enzima de origen bacteriano CondroitinasaABC (ChABC) promueve un aumento significativo de la plasticidad neuronal en diferentes áreas del cerebro, alcanzando niveles similares a los presentes durante el desarrollo, antes de su aparición (Xue et al., 2014; Lensjø et al., 2017b; Fawcett et al., 2019). De la misma manera, ratones transgénicos con mutaciones en diferentes componentes de las PNNs presentan unos mayores niveles de plasticidad en la etapa adulta (Bukalo et al., 2001; Favuzzi et al., 2017).

Oscilaciones neuronales

Las fluctuaciones rítmicas de la actividad de conjuntos de neuronas pueden ser registradas mediante la inserción de electrodos de la región de interés, que permite la detección de los potenciales de campo local (LFP). Los LFP se clasifican en función de su frecuencia, predominando determinadas frecuencias en diferentes estados, comportamientos o enfermedades (Buzsáki and Draguhn, 2004). Dos de las bandas de LFP más estudiadas son la theta (5-10 Hz) y la gamma (30-90 Hz), así como su acoplamiento, que tiene un papel clave en el procesamiento y el flujo de la información a través de las redes neuronales (Buzsáki and Wang, 2012).

Plasticidad neuronal en el sistema nervioso adulto

Aunque los estudios pioneros de Hubel y Wiesel apuntaban a un sistema nervioso central poco plástico una vez concluido el periodo crítico durante el desarrollo (Hubel and Wiesel, 1970), durante los últimos años numerosos tratamientos han demostrado poder inducir niveles de plasticidad similares a los alcanzados durante el periodo crítico en la corteza cerebral de animales adultos. En esta tesis, se ha estudiado el efecto de tres tratamientos potenciadores de la plasticidad neuronal sobre la circuiteria inhibitoria y la expresión de moléculas relacionadas con la plasticidad.

Primero se ha realizado un tratamiento ambiental mediante deprivación visual, en el que se aislaron las cajas de estabulación de la luz ambiental, conocido como exposición a la oscuridad. Este tipo de deprivación visual promueve la plasticidad en la corteza visual,

permitiendo la recuperación de la agudeza visual en ratones adultos con ambliopía (He et al., 2007). Se ha observado que el aumento de plasticidad en la corteza visual mediante deprivación visual tiene efectos sobre la composición de los receptores de glutamato y las espinas dendríticas de neuronas piramidales (He et al., 2006; Tropea et al., 2010). No obstante, no se conoce el efecto de este tratamiento sobre las estructura de las interneuronas, más allá de la reducción en la expresión de PV (Stodieck et al., 2014).

En el siguiente tratamiento se ha observado el efecto de una administración crónica de fluoxetina sobre las interneuronas de la amígdala. Además de su uso como antidepresivo, se ha demostrado la capacidad de la fluoxetina para aumentar la plasticidad en el neocortex (Maya Vetencourt et al., 2008) y en la amígdala (Karpova et al., 2011). En relación a su efecto sobre la estructura de las interneuronas, se ha visto que afecta a la densidad de espinas dendríticas de las células Martinotti en la mPFC (Guirado et al., 2014b) y a la dinámica del árbol dendrítico de las interneuronas de las capas II/III de la corteza visual (Chen et al., 2011). Sin embargo, el efecto de la fluoxetina sobre la estructura de las interneuronas de la amígdala no ha sido explorado todavía.

Por último, se ha analizado el efecto de la eliminación enzimática de las PNNs sobre las interneuronas que expresan PV en la mPFC, mediante la inyección intracerebral de la enzima de origen bacteriano ChABC. La ChABC actúa sobre los CSPGs de las PNNs, produciendo su eliminación temporal y potenciando la plasticidad neuronal. La primera evidencia del efecto de la ChABC sobre la plasticidad neuronal proviene de un estudio en la corteza visual primaria (Pizzorusso et al., 2002), aunque posteriormente se han descrito efectos similares en otras áreas como la amígdala (Thompson et al., 2018). No obstante, sus efectos sobre la corteza prefrontal se encuentran menos explorado, especialmente su efecto sobre la inervación alrededor del soma de las interneuronas que expresan PV.

Objetivos

El objetivo principal de la tesis doctoral es estudiar los efectos de diferentes manipulaciones farmacológicas y ambientales sobre la estructura de las neuronas excitadoras e inhibidoras en el cerebro adulto de los ratones, su conectividad y la expresión de moléculas relacionadas con la plasticidad, en un intento de comprender mejor los mecanismos de

plasticidad estructural del sistema nervioso adulto. Para lograr este objetivo principal, derivamos los siguientes objetivos específicos:

1. Estudiar el impacto de la deprivación visual por exposición a la oscuridad en la estructura y conectividad de las interneuronas corticales y la expresión de moléculas sinápticas y relacionadas con la plasticidad en todo el sistema visual.

2. Estudiar el impacto de un tratamiento crónico con fluoxetina sobre la estructura de las interneuronas y la expresión de moléculas relacionadas con la plasticidad en la amígdala basolateral.

3. Analizar los efectos de la presencia de redes perineuronales y su eliminación enzimática sobre la inervación perisomática de neuronas piramidales e interneuronas y sobre la fisiología de la corteza prefrontal.

Metodología y resultados

Efecto de la deprivación visual sobre la expresión de moléculas sinápticas, moléculas relacionadas con la plasticidad y sobre la estructura de interneuronas del sistema visual

Con el objetivo de comprender cómo la eliminación de la estimulación visual afecta a las interneuronas del sistema visual, se cubrieron por completo las jaulas de estabulación de unos ratones transgénicos que expresan EGFP en una subpoblación de interneuronas. Tras diez días de total aislamiento visual, hemos sacrificado los animales y procesado sus cerebros para el análisis de expresión de diferentes moléculas, así como de la estructura de las interneuronas.

Primero, se analizó el efecto de la deprivación sobre la expresión de moléculas sinápticas, tanto excitadoras como inhibidoras, de diferentes áreas pertenecientes al sistema visual: el núcleo geniculado lateral, el colículo superior y la corteza visual primaria. Los resultados mostraron una reducción en la densidad de puncta que expresaban los marcadores sinápticos analizados, así como un descenso en la expresión de estas moléculas, excepto en el caso de la SYN que aumentaba su expresión en la corteza visual primaria. Además, se caracterizó el fenotipo de las interneuronas que expresaban EGFP en la corteza visual primaria, encontrando que pertenecen a una subpoblación de interneuronas que expresan SST, y que se pueden clasificar como células Martinotti.

A continuación se analizó el impacto de la deprivación visual sobre la estructura de dichas interneuronas, hallando una reducción en la complejidad del árbol dendrítico y una disminución de las espinas dendríticas asociadas a sinapsis estables (espinas de tipo "hongo/mushroom") y un aumento de aquellas relacionadas con sinapsis débiles y poco estables (espinas "rechonchas/stubby"). Respecto al efecto sobre el axón de las células Martinotti, se observó un descenso en el tamaño y la intensidad de fluorescencia de sus botones axónicos. Por otro lado, se analizó el efecto sobre la expresión de moléculas relacionadas con la plasticidad: PSA-NCAM y componentes de las PNNs. Se halló una reducción tanto en la densidad de células que expresan PSA-NCAM en la corteza visual primaria como en la expresión de PSA-NCAM en el neuropilo de la corteza visual primaria. También se encontró una reducción en la densidad de interneuronas que expresan PV y un aumento en la intensidad de fluorescencia de las PNNs que envuelven este tipo de interneuronas. Se analizó el efecto del tratamiento sobre la inervación inhibitoria del soma de las neuronas piramidales, que no resultó alterada por la deprivación visual.

También se estudió el efecto de la deprivación visual sobre la expresión de moléculas sinápticas y moléculas relacionadas con plasticidad en los núcleos extracorticales del sistema visual: el LGN y SC. En el LGN se encontró un aumento en la densidad de puncta que expresaban SYN así como de VGAT, mientras que en el SC el aumento se ha limitado a los que expresaban SYN. En cuanto a la expresión de PSA-NCAM, ésta no se vió afectada por la deprivación visual.

Efecto del antidepresivo fluoxetina sobre las interneuronas que expresan somatostatina en la amígdala basolateral

Para ahondar en el conocimiento de los efectos de un tratamiento crónico con antidepresivos sobre la plasticidad estructural y el funcionamiento de las interneuronas de la BLA, se llevó a cabo un tratamiento mediante una inyección intraperitoneal diaria de fluoxetina durante dos semanas. El tratamiento, al igual que el experimento de deprivación visual, se realizó en ratones transgénicos que expresan EGFP en una subpoblación de interneuronas, característica que permite analizar su estructura. Finalizado el tratamiento, los ratones fueron sacrificados y sus cerebros procesados para diferentes análisis inmunohistoquímicos y su observación en el microscopio confocal.

Primero se estudió el efecto de la fluoxetina sobre la expresión de la PSA-NCAM y las enzimas encargadas de la síntesis de GABA: GAD65 y GAD67. Se encontró un aumento en la expresión de PSA-NCAM como consecuencia del tratamiento, no así de GAD65 y GAD67. A continuación se analizó la distribución y fenotipo de las interneuronas que expresaban EGFP. Se confirmó que, tal y como ocurre en el resto de regiones cerebrales, estas interneuronas expresaban el neuropéptido SST. Además, se observó que estas neuronas eran muy escasas dentro de la BLA, esencialmente concentradas en la región basal. Posteriormente, se llevó a cabo un análisis del efecto de la fluoxetina sobre la estructura de estas interneuronas, encontrándose un aumento de las espinas “stubby” y una disminución de las espinas “hongo” en las dendritas de las interneuronas que expresaban EGFP. Respecto a la porción axónica, se halló una disminución tanto de la densidad de botones axónicos, como de su tamaño, como consecuencia de la administración de fluoxetina.

Finalmente, se estudió el efecto de la fluoxetina sobre la actividad basal de las interneuronas de la BLA. Para ello, se cuantificó la intensidad de expresión del marcador de actividad basal FosB, tanto en neuronas excitadoras como en diferentes grupos de interneuronas. Se observó un aumento en la intensidad de fluorescencia de este marcador, tanto en neuronas excitadoras como en interneuronas que expresaban PV. Por otro lado, la expresión de FosB en interneuronas que expresaban SST se vio fuertemente reducida.

Las redes perineuronales regulan la densidad de puncta que expresan marcadores inhibitorios en la región perisomática de neuronas parvalbúmina positivas, así como la generación de ritmos gamma, en el área prelímbica de la corteza prefrontal medial

Con el objetivo de profundizar en el conocimiento sobre el impacto que la presencia de PNNs tiene sobre la estructura y conectividad de las interneuronas que expresan PV en la región prelímbica (PrL) de la mPFC de ratones adultos, se comparó la intensidad de fluorescencia, la densidad de puncta perisomáticos, tanto excitadores como inhibidores, y la longitud del AIS de aquellas interneuronas que expresaban PV y estaban rodeadas de PNNs respecto a aquellas que no presentaban estas estructuras. Se halló que las interneuronas que expresaban PNNs tenían una mayor intensidad de fluorescencia de PV y una mayor densidad de puncta inhibitorios sobre su cuerpo celular. Concretamente, este aumento se debía a una mayor densidad de puncta procedentes de otras interneuronas que expresaban PV. Además, se encontró que el ratio entre los puncta excitadores e inhibidores está desplazado en estas células y es significativamente menor que en las interneuronas que no presentan PNNs. Por último, se

estudió si la estructura del AIS del axón puede verse también afectada. Efectivamente, se encontró que las interneuronas que expresan redes perineuronales tienen un AIS significativamente mayor que aquellas interneuronas que no expresan redes perineuronales.

A continuación, se planteó estudiar el efecto de la digestión enzimática de las PNNs sobre la conectividad de las interneuronas que expresan PV, así como la actividad de la corteza prefrontal. Primero se realizó un estudio sobre la dinámica temporal de la digestión de las PNNs tras la inyección de ChABC en la mPFC de ratón. Se halló que, aunque eficiente, la digestión de las redes perineuronales es muy limitada en el tiempo. Seis días después de la inyección de la enzima, se apreció la reaparición de redes perineuronales alrededor de los cuerpos celulares de algunas células de la PrL. Así pues, se estableció el sacrificio de los animales y el procesado de los cerebros cuatro días después de la inyección como protocolo para analizar los cambios producidos por la ChABC.

Posteriormente, se realizó la inyección de ChABC y, tras cuatro días, se sacrificó a los animales y se procesaron sus cerebros para el análisis de diversas moléculas bajo el microscopio confocal. Primero se analizó la intensidad de fluorescencia de la PV en las interneuronas que expresaban esta proteína de unión al calcio y no se encontraron cambios asociados al tratamiento realizado. Después, se pasó a analizar en detalle el efecto del tratamiento enzimático sobre la densidad de puncta perisomáticos sobre las interneuronas que expresaban PV. Se halló una disminución de la densidad de los puncta SYN+ alrededor del cuerpo celular de estas interneuronas. Concretamente, esta reducción en la densidad de puncta que expresaban un marcador general de sinapsis se correspondió con un descenso de los puncta inhibitorios procedentes de otras interneuronas que expresaban PV. Por otro lado, el ratio de puncta excitadores respecto a inhibitorios se desplazó hacia la excitación como consecuencia del tratamiento. Una vez analizada la inervación sobre los somas de interneuronas que expresaban PV, se pasó a analizar la inervación sobre los somas de neuronas piramidales. Se analizó la densidad de puncta PV+ en la región perisomática, no encontrando cambios significativos como consecuencia de la inyección de ChABC. Una vez analizados los cambios en la zona circundante al cuerpo celular, se analizaron posibles cambios en zonas del neuropilo. En ambos casos no se encontraron cambios significativos en la densidad de puncta que expresaban las diferentes moléculas sinápticas analizadas. Finalmente, se estudió la proteína FosB, cuya expresión está relacionada con el nivel de activación de las neuronas. Se analizó la intensidad de fluorescencia de FosB en las neuronas piramidales y las interneuronas que

expresan PV, tras la inyección con ChABC. Se halló una disminución muy robusta en la expresión de esta molécula en ambas poblaciones neuronales de la PrL.

Por último, con el objetivo de comprobar si la digestión de las PNNs altera la actividad de la circuitería cortical de la mPFC, se realizaron registros extracelulares (LFP) tanto en la mPFC como en el hipocampo, utilizado como estructura control. Se observó un aumento de la actividad theta y una disminución de la actividad gamma como consequencia de la inyección de de ChABC.

Conclusiones

1. La deprivación visual reduce la densidad de puncta que expresan sinaptofisina y el transportador vesicular de glutamato 1, mientras que aumenta la intensidad de fluorescencia de sinaptofisina y reduce la del transportador vesicular de glutamato 1 y el transportador vesicular de GABA en la corteza visual primaria de ratones adultos.

2. Las células que expresan EGFP en la corteza visual primaria de ratones GIN son, mayoritariamente, células Martinotti.

3. La deprivación visual reduce de complejidad del árbol dendrítico, altera la densidad de varios tipos de espinas dendríticas y reduce el tamaño y la intensidad de fluorescencia de los botones axónicos de las interneuronas que expresan EGFP en la corteza visual primaria.

4. La deprivación visual provoca una reducción tanto del número de células que expresan PSA-NCAM como de la densidad de puncta que expresa PSA-NCAM, una reducción en la densidad de interneuronas que expresan parvalbúmina y un aumento en la intensidad de fluorescencia de las redes perineuronales en la corteza visual primaria.

5. En el núcleo geniculado lateral, hay una gran expresión de PSA-NCAM en el foliolo intergeniculado y la parte ventral del núcleo geniculado lateral, mientras que apenas se expresa en la parte dorsal del núcleo geniculado lateral de ratones adultos.

6. Los somas de las interneuronas que expresan parvalbúmina se encuentran rodeados tanto de PSA-NCAM como de redes perineuronales en la parte ventral del núcleo geniculado lateral.

7. Las interneuronas que expresan parvalbúmina en el colículo superior se encuentran segregadas espacialmente en base a la expresión de redes perineuronales.

8. El tratamiento con fluoxetina aumenta la densidad de puncta que expresan PSA-NCAM y la densidad de puncta que coexpresan PSA-NCAM y GAD65/67, pero no los que expresan GAD65/67 en la amígdala basolateral de ratones adultos.

9. Las interneuronas que expresan EGFP en la amígdala basolateral se encuentran dispersas y expresan somatostatina.

10. El tratamiento con fluoxetina reduce la densidad de espinas dendríticas maduras y la densidad y el tamaño de los botones axónicos, a la vez que aumenta la densidad de espinas dendríticas inmaduras en las interneuronas que expresan somatostatina en la amígdala basolateral de ratones adultos.

11. La expresión del marcador de actividad neuronal FosB aumenta en neuronas piramidales e interneuronas que expresan parvalbúmina, mientras que se reduce en las interneuronas que expresan somatostatina en la amígdala basolateral de ratones adultos tratados con fluoxetina.

12. Las interneuronas que expresan parvalbúmina y redes perineuronales expresan más parvalbúmina y reciben una mayor densidad de contactos sinápticos inhibitorios procedente de otras interneuronas que expresan parvalbúmina que aquellas que no están rodeadas por redes perineuronales.

13. La condroitinasa ABC elimina completamente las redes perineuronales durante 4 días en la corteza prefrontal medial de ratones adultos, aunque éstas empiezan a reaparecer 6 días después.

14. La digestión de las redes perineuronales mediante la condroitinasa ABC produce una disminución en la densidad de puncta inhibitorios, concretamente aquellos que expresan parvalbúmina, sobre la zona del soma de interneuronas que expresan parvalbúmina.

15. La eliminación de las redes perineuronales no afecta a la densidad de puncta que expresan el transportador vesicular de glutamato 1, el transportador vesicular de GABA y la sinaptofisina en el neuropilo de la corteza prefrontal medial.

16. La eliminación de las redes perineuronales reduce la expresión del marcador de actividad neuronal FosB en la región prelímbica, tanto en neuronas piramidales como en interneuronas que expresan parvalbúmina.

17. La eliminación de las redes perineuronales produce una disminución de las oscilaciones gamma y un aumento de las oscilaciones theta en la región prelímbica tras la estimulación producida por el pinzamiento de la cola de ratones adultos

I. INTRODUCTION

1. Neuronal diversity in the central nervous system

The nervous system is constituted by a complex neuronal network that enables an organism to interact with its environment. The sensory components detect environmental and internal stimuli that are stored and processed in order to modulate behaviour. Anatomically, the nervous system is formed by the central nervous system (CNS), which comprises the brain and spinal cord, and the peripheral nervous system (PNS) composed by the rest of nervous elements distributed throughout the organism (Watson et al., 2012).

Regarding the organization of the mammalian nervous system, an extraordinary cell diversity is finely interconnected during development to give rise to this complex system. Cells present within the CNS can be broadly classified into neurons, cells able to generate and communicate an electric signal, and glial cells, which have multiple roles supporting neuronal activity. In the present thesis, I will focus on neurons or neuronal cells. The great diversity of neuronal types present in the CNS has been classified following multiple criteria attending to their morphology, electrophysiological and neurochemical properties, and, more recently, single-cell transcriptomics (Kandel et al., 2012). Morphologically, neurons are classified using criteria like the morphology and location of their soma, the terminal field of their axonal output or the shape and orientation of their dendritic tree. This classification has given rise to neuronal categories such as bipolar cells, chandelier cells or pyramidal cells. Regarding their electrophysiological properties, neurons are classified on the basis of the response that they evoke on their postsynaptic targets. If they reduce their membrane potential, facilitating the generation of an action potential, they are considered excitatory, or principal neurons, which represent approximately 80% of the total neuronal population in the adult brain. The neurotransmitter (i.e. the chemical messenger released from the presynaptic side of a synapse,

which is able to activate receptors in the postsynaptic side), mainly used by these excitatory neurons is the L-glutamate (henceforth glutamate). On the other hand, neurons that raise the membrane potential of their postsynaptic targets, inducing a hyperpolarization of their membrane, are referred to as inhibitory neurons, interneurons or GABAergic neurons. This type of neuron uses ɣ-aminobutyric acid (GABA) as neurotransmitter. These interneurons can be classified in different groups or subpopulations based on the expression of different molecular markers, such as calcium binding proteins, neuropeptides or neurotransmitter receptors. Interneurons show a higher diversity than excitatory neurons (Tremblay et al., 2016). Recently, the development of high-throughput single-cell RNA sequencing allowed the possibility to profile gene expression in individual cells and classify neurons based on similar molecular properties (Poulin et al., 2016). In the present thesis, I will focus on excitatory neurons and different interneuronal subpopulations.

1.1. Pyramidal neurons

Pyramidal neurons constitute the most abundant neuronal population throughout the cerebral cortex (Elston, 2003). Morphologically, they display a well stereotyped structure: a pyramidal-shaped soma from which base emanates one axon that branches and produces numerous excitatory glutamatergic contacts or axonal boutons. The axonal initial segment (AIS) sits between the cell body and the axon and receives numerous synaptic contacts (Kubota, 2014). Regarding its dendritic structure, pyramidal neurons have two different domains: (1) the apical dendrite, which emerges from the apex of the soma and bifurcates several times to produce a tuft of dendrites, and (2) the basal dendrites, which descend from the base of the soma and are typically less developed than the apical tree (Spruston, 2008).

Although these features are characteristic of pyramidal neurons, they can vary considerably between different layers, cortical regions and species (Kasper et al., 1994). The dendrites of pyramidal cells display membranous specializations, called dendritic spines, which cluster together synaptic receptors and compartmentalize the electric signal (Koch and Zador, 1993). These dendritic structures mainly receive excitatory synapses and they are, therefore, defined usually as excitatory postsynaptic specializations, whereas the dendritic shaft receives inhibitory input, especially from somatostatin (SST) expressing interneurons. On the other hand, inhibitory synaptic contacts on pyramidal neurons are commonly found on the perisomatic region, the AIS and the shaft of dendrites (Kubota, 2014). In this thesis, I have analyzed the effects of different plasticity-inducing treatments on the inhibitory input on pyramidal cells,

especially on their perisomatic region. This inhibitory input is produced either by cholecystokinin (CCK) expressing interneurons and parvalbumin (PV) positive basket cells. Regarding the inhibitory input on the AIS, it is produced by another subpopulation of parvalbumin expressing interneurons known as chandelier cells (Kubota, 2014).

1.2. Interneurons

Interneurons are derived from the ganglionic eminences, structures located in the ventral part of the developing telencephalon. They are classified regarding the expression of selective markers, morphological and electrophysiological properties (Markram et al., 2004; Tremblay et al., 2016). However, new methods to examine gene expression in single cells have been able to find new subtle differences among interneurons, upgrading the refinement of the classification of interneuronal types (Poulin et al., 2016). Based on the Petilla terminology, I studied the PV cells and the SST cells, both originated in the medial part of the ganglionic eminence, and the CCK cells, derived from the caudal ganglionic eminence (**Figure 1**).

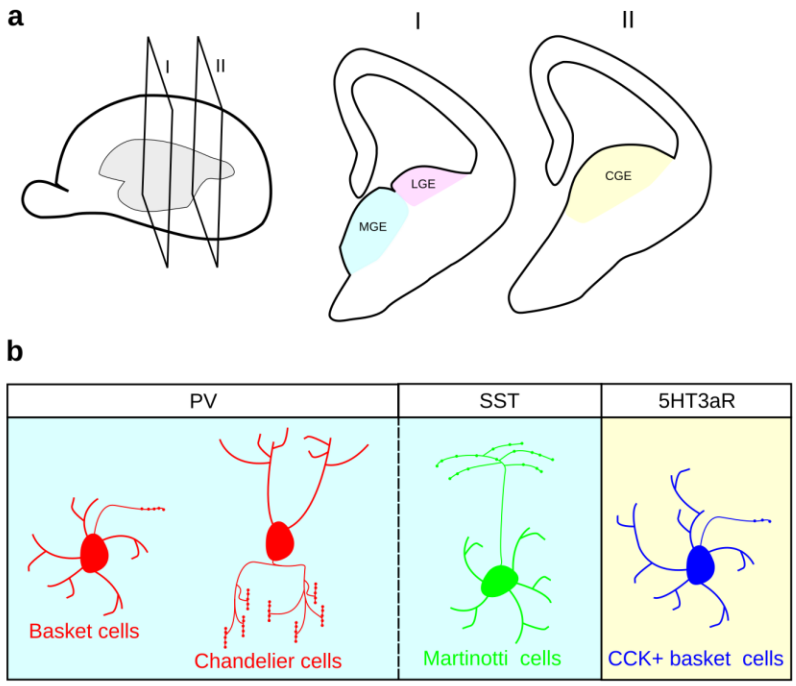

Figure 1. Origin, morphology and neurochemical phenotype of cortical interneurons. **(a)** Scheme of the spatial distribution of ganglionic eminences in the developing telencephalon. Neocortical interneurons are derived from medial and caudal ganglionic eminences. **(b)** Schematic representation of structural and phenotypic characteristics of the interneuronal subpopulations of interest. Adapted from (Sultan et al., 2013).

1.2.1. Parvalbumin expressing interneurons

PV expressing interneurons are the largest group of interneurons in the cerebral cortex (Rudy et al., 2011). They display a characteristic fast-spiking firing activity pattern (Tremblay et

al., 2016). Attending to the morphology of their axons, two major subpopulations are found: chandelier cells and basket cells. Chandelier or axo-axonic cells display a characteristic shape of their axonal arbour, with arrays of boutons or cartridges. They form synapses on the AIS of pyramidal neurons, controlling their output (**Figure 2**). Although their dominant effect is inhibitory, they appear to play a dual role in the circuitry, promoting the activity of quiescent pyramidal neurons (Woodruff et al., 2011). However, the function of chandelier cells is not yet fully understood. On the other hand, the most abundant PV+ interneurons are basket cells, which innervate the cell bodies and proximal dendrites of pyramidal cells and other interneurons (**Figure 2**), mainly other PV+ cells (Pfeffer et al., 2013). Due to their fast and non-adaptive firing pattern, PV+ cells play a key role in the generation of neuronal oscillations i.e. the rhythmic patterns of neural activity generated as a consequence of the dynamic interplay among neuronal populations in the CNS (Buzsáki and Draguhn, 2004). Especifically, PV+ cells are critically involved in the generation of slow *theta* (4 to 10 Hz)(Buzsáki, 2002) and fast *gamma* (30 to 100 Hz) (Sohal et al., 2009) oscillations. Moreover, they constitute the main cortical target of thalamocortical inputs (Ji et al., 2016).

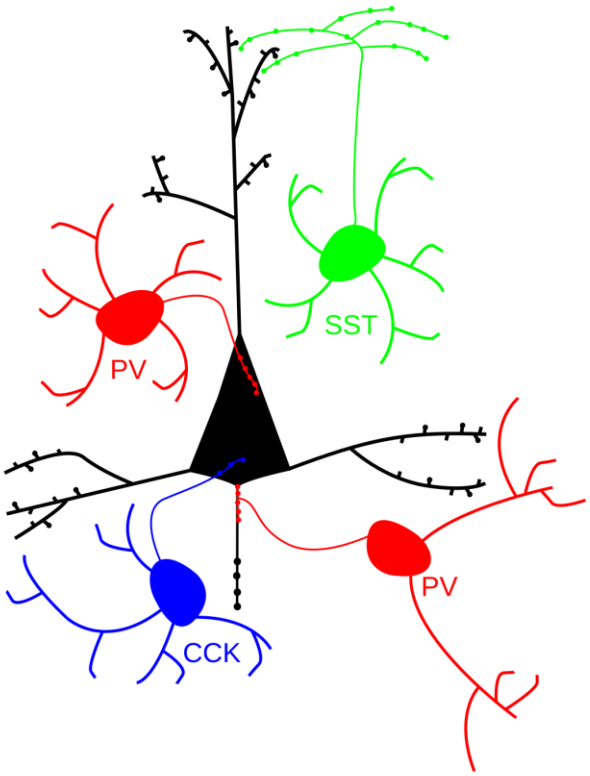

Figure 2. Cortical microcircuitry. Representative scheme of the interneuronal connectivity on different compartments of a pyramidal cell within the cortical microcircuitry.

1.2.2. Cholecystokinin expressing interneurons

CCK+ interneurons belong to the heterogeneous group of interneurons that express the serotonin receptor 5HT3aR and are derived from the caudal ganglionic eminence (Tremblay et al., 2016). These interneurons innervate the somata of pyramidal neurons and other interneurons (**Figure 2**). They can be classified on the basis of the coexpression of vasoactive intestinal peptide (VIP) in small basket cells (VIP positive) and large basket cells (VIP negative). In the present thesis, I have studied the large CCK+ basket cells. They express the cannabinoid receptor 1 (CB1r) in their axonal terminals and provide, together with PV+ basket cells, the perisomatic inhibition to pyramidal neurons. Nevertheless, their activity patterns present some remarkable differences: The activity of CCK+ large basket cells can be inhibited through the activation of CB1r by endocannabinoids generated as a consequence of depolarization of the postsynaptic cell, the so-called depolarization-induced synaptic inhibition. Moreover, the activity of CCK+ basket cells is modulated by serotonin, in contrast to that of PV+ cells. Moreover, CCK+ large basket cells form smaller baskets and display an adapting firing pattern, allowing a finer tuning of the network that complements the robust, non-adapting activity of PV+ basket cells (Freund and Katona, 2007). Interestingly, the CCK+ basket cells are relatively more abundant in relation to PV+ cells in secondary and association areas, such as the medial prefrontal cortex (mPFC) (Whissell et al., 2015).

1.2.3. Somatostatin expressing interneurons

Somatostatin (SST) expressing interneurons constitute the second largest group of cortical interneurons (Rudy et al., 2011) and target the dendrites of pyramidal neurons and other interneurons (Wang et al., 2004; Pfeffer et al., 2013). SST interneurons can be subdivided into two groups based on their morphology: Martinotti and non-Martinotti cells. In the present thesis, I have investigated Martinotti cells. Martinotti cells are widely distributed throughout the isocortex, from layer II to layer V, where they are particularly abundant. The structure of Martinotti cells displays two distinctive characteristics. First, the presence of an ascending axon that profusely arborizes in layer I and targets the distal portion of the apical dendrite of pyramidal neurons (Figure 2), but also PV+ and VIP+ interneurons (Pfeffer et al., 2013); moreover, Martinotti cells also display a significant proportion of their axonal arbor contacting the basal dendrites of pyramidal neurons in the layer where the soma is located. Second, these cells present dendritic spines, a rare feature in interneurons (Tremblay et al., 2016). The

targeting of large dendritic areas, either from pyramidal neurons or from other interneurons, along with their adapting firing pattern, allows Martinotti interneurons to tune the horizontal and feedback connectivity.

2. Areas of study

In recent years, several studies have reported an increased neuronal plasticity under different treatments in different areas of the adult nervous system. In the present thesis, I have studied the impact of plasticity-inducing treatments on the prefrontal cortex, the primary visual cortex, the amygdala, the superior colliculus and the lateral geniculate complex.

2.1. Medial prefrontal cortex

The mouse prefrontal cortex can be divided into the medial prefrontal cortex (mPFC) and the orbitofrontal cortex (OFC) (Watson et al., 2012). The mPFC is a cognitive area located in the frontal lobe in humans and the rostral part of the neocortex in rodents. This area is massively interconnected to other cortical and extracortical areas and it is associated with multiple functions, such as decision making, recent and remote memories and sensory perception (Brown and Bowman, 2002; Dalley et al., 2004). Based on anatomical and functional features, in rodents it can be divided into three areas: cingulate cortex (CG), infralimbic cortex (IL) and prelimbic cortex (PrL) (**Figure 3**). In general terms, there is a dorsoventral shift in the input to mPFC. CG receives a wide range of sensory cortical and extracortical input and presumably integrates this information. In contrast, the ventral mPFC (PrL and IL) is involved in the processing of input from limbic regions such as the amygdala, the claustrum and the medial basal forebrain, as well as the hippocampus and monoaminergic nuclei of the brainstem, among others (Hoover and Vertes, 2007). Regarding its cytoarchitectural configuration, i.e. the density and size of cells and neuropil, it follows the same scheme of the neocortex, consisting of 6 horizontal layers, but lacking the internal granule cell layer (layer IV) present in the rest of the neocortex (**Figure 3**). Therefore, the rodent mPFC is organized in five layers from the outer surface as follows: (**Figure 3**) (Fuster, 2015; Paxinos and Franklin, 2007):

- Layer I (molecular or plexiform layer): contains very few neuronal bodies, most of them of interneurons. It is mainly composed by apical dendrites and axons that emerge from pyramidal neurons in deeper layers of the neocortex. These dendrites receive their input from thalamic and intracortical afferents.

- Layer II (external granule cell layer) is mainly composed of granular neurons (small excitatory neurons) and it connects with other cortical areas from the same hemisphere.

- Layer III (external pyramidal cell layer) is composed of medium-sized pyramidal neurons, which project mainly within their region or to other cortical areas.

- Layer V (internal pyramidal layer) contains large and densely packed pyramidal neurons. These neurons project mainly outside their local region to other cortical areas or subcortical structures.

- Layer VI (polymorphic layer) is the most heterogeneous layer throughout the mPFC. It contains few pyramidal neurons, which are interconnected with thalamic neurons. This layer constitutes the deep limit of the cortex, which is in contact with the white matter.

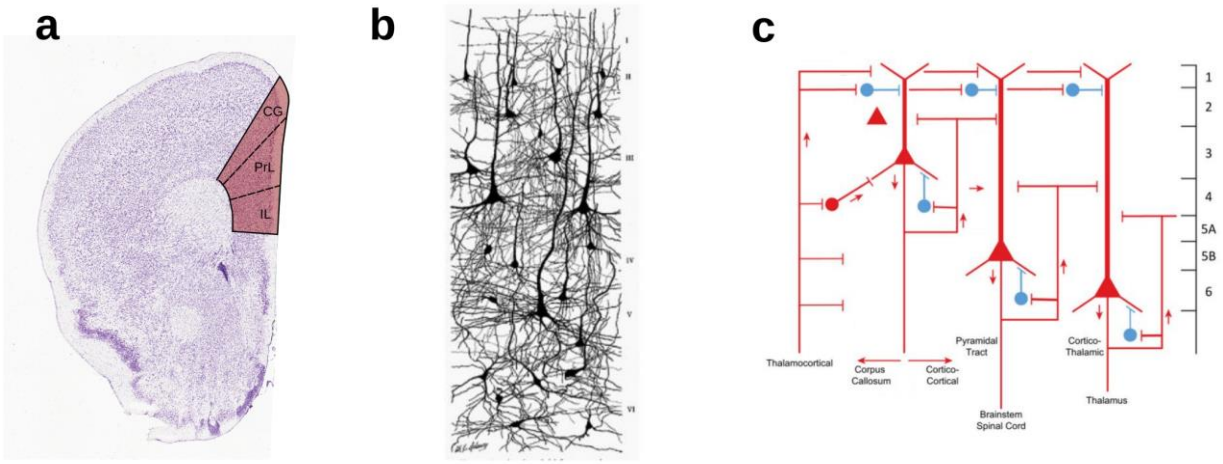

Figure 3. The medial prefrontal cortex in rodents **a)** Mouse brain coronal section (-2.00 mm from Bregma) showing the areas of mPFC. **b)** Drawing of Golgi stained prefrontal cortex section (from Conel, 1939). **c)** Representative scheme of neuronal connectivity in the mPFC, adapted from (Shepherd and Rowe, 2017).

2.2. Visual system

In the mouse central nervous system, visual information is projected from retinal ganglion cells (RGC) to the suprachiasmatic nucleus (SChN) (Hattar et al., 2006), the lateral geniculate nucleus (LGN) and, mainly, to the superior colliculus (SC) of the midbrain (Ellis et al., 2016). From these primary afferences, visual stimuli arrive to the primary (V1) and secondary

(V2) visual cortices, and other association areas (**Figure 4**). Like in other sensory systems, the visual information maintains the spatial organization from RGC to the visual cortex, the so-called retinotopy.

2.2.1. Lateral geniculate nucleus

The LGN is composed by different subregions: the dorsal part (dLGN), which represents the principal relay center of retinal information to the visual cortex; the intergeniculate leaflet (IGL), which projects the visual information to the main circadian rhythm master: the SChN, and the ventral part (vLGN), which is highly connected to the IGL (Moore and Card, 1994). The dLGN receives visual information from both eyes through the RGC, forming retinotopic maps on thalamocortical neurons (Kerschensteiner and Guido, 2017). The 90% of dLGN neurons are thalamocortical excitatory neurons that project mainly to layer IV, but also the layer I, of the V1, whereas the rest are interneurons (Arcelli et al., 1997). The dLGN also receives feedback cortical projections from the V1. Regarding the vLGN, it is organized in the magnocellular external part, which receives innervation from the retina, and the parvocellular internal part, which lacks retinal input (Kolmac and Mitrofanis, 2000). In contrast to the dLGN, the main majority of neuronal cells in both the vLGN and the IGL are GABAergic (Harrington, 1997). Importantly, the axons from the IGL and the vLGN target wide and diverse regions, but not the visual cortex (Moore et al., 2000). They form the largest thalamic input to the ipsilateral SC, i.e. to the same brain hemisphere. Moreover, the main interneuronal subpopulation in the IGL expresses NPY and projects to the suprachiasmatic nucleus, forming the geniculohypothalamic tract (GHT) (Moore and Card, 1994). The GHT mediates responses to non-photic stimuli, which can be blocked by lesions in this tract and mimic electrical stimulation or the application of GABA agonists (Morin and Allen, 2006).

2.2.2. Superior colliculus

The SC is an integrative sensorimotor structure, i.e. a region that receives information from different regions and provides an output, located in the tectum of the midbrain (Ellis et al., 2016). In rodents, the SC is involved in the control of eye/head movements and innate defensive behaviors (May, 2006). It is broadly split into two parts: the superficial SC (sSC) and the deep SC (dSC). The sSC receives 90% of all projections from the RGC and the V1, forming a retinotopic map and projects to the dLGN (Dräger and Olsen, 1980). On the other hand, the dSC is composed mainly by the stratum griseum intermedium and it receives input from the

sSC, the primary motor, somatosensory and auditory cortices and the brainstem nuclei (Zingg et al., 2017).

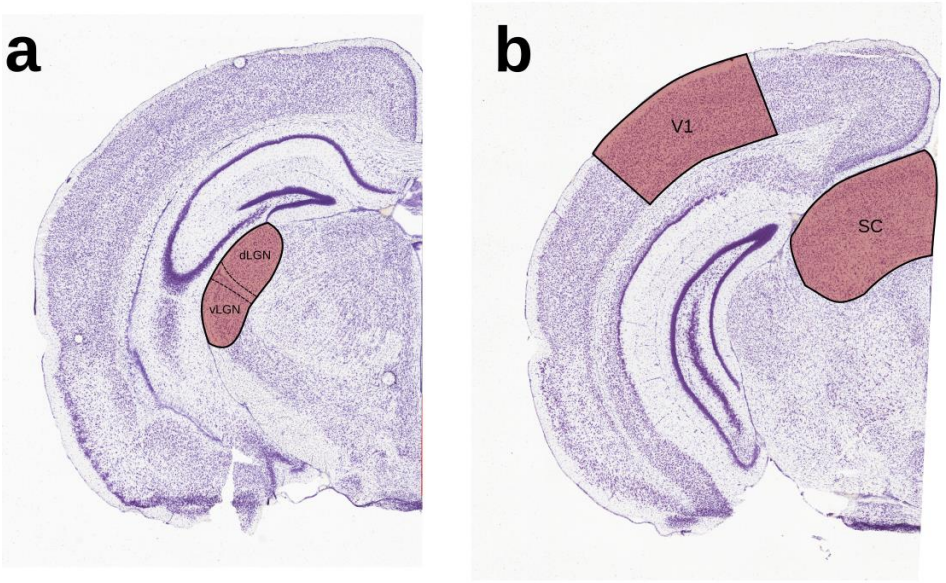

Figure 4. Visual areas of study. **a)** Coronal section (1.90mm from Bregma) with different regions of LGN highlighted. **b)** Coronal section (3.30 mm from Bregma) with the location of V1 and SC highlighted.

2.2.3. Primary visual cortex

The organization of the V1 follows the canonical neocortical division into six layers. In addition to the five layers described in the mPFC, the V1 presents a proper layer IV, which receives the visual information from cells in the dLGN, or from layer V through SC (Genç et al., 2016). An important feature of the V1 is the presence of bands of ocular dominance. These bands represent alternatively the information arriving from the left and right eye through neuronal projections as described above (Shatz and Stryker, 1978).

2.3. Amygdala

The amygdala is a key structure for the generation of emotional behavior and the formation and retrieval of memories related to fear, anxiety (Pape and Pare, 2010) and reward processing (Campeau and Davis, 1995). Anatomically, it is composed of multiple interconnected

nuclei (**Figure 5)**, generally encompassed in the lateral (LA), basolateral (BLA), the basomedial (BMA), the central (CeA), the medial and the cortical amygdala (Sah et al., 2003). In this thesis I will focus on the BLA, the main stage in the information processing through the amygdala, which has a prominent role in the acquisition of fear conditioning and the response to stress (Ehrlich et al., 2009; Padival et al., 2013). The LA receives sensory input from high order association areas (McDonald, 1998) and sends a glutamatergic input to the BLA and CeA. The BLA also projects to CeA (Duvarci and Pare, 2014). In both nuclei, glutamatergic principal neurons constitute 80% of the neuronal subpopulation and the remaining 20% is constituted by different interneuronal subpopulations (McDonald, 1982). Two interneuronal subpopulations comprise 60% of total interneurons in BLA: PV expressing interneurons (~40%) and SST+ interneurons (~20%), both coexpressing calbindin (McDonald and Mascagni, 2001, 2002). As in the cerebral cortex, PV+ interneurons target the perisomatic region while SST+ interneurons innervate the distal dendrites of principal neurons, but they have been less explored compared to cortical interneurons (Capogna, 2014). The BLA projects to different neocortical areas, the hippocampal formation and various subcortical areas (Pitkänen et al., 2000).

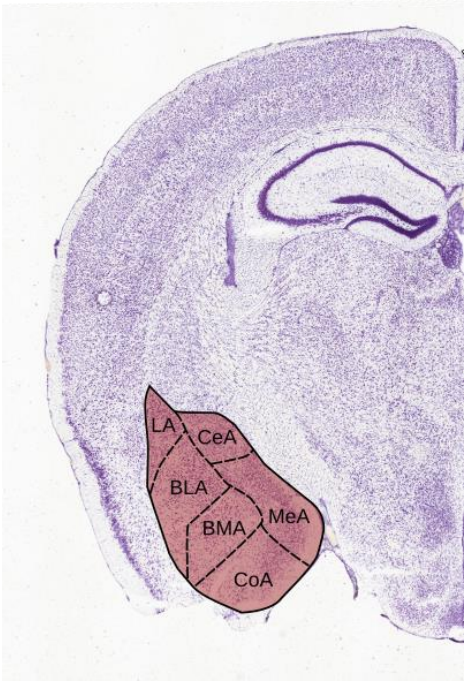

Figure 5. Amygdaloid regions of study. Coronal section (1.50 mm from Bregma) depicting the different nuclei that compose the rodent amygdala

3. Neuronal plasticity

The ability of the neuronal circuitry to adapt their connectivity in an experience-dependent manner is a process known as plasticity. This capacity raises from the ability of the neuronal circuits to form new connections or to change the strength of preexisting connections based on the encoded information collected (Xerri, 2008). This ability can adopt a broad range of forms, from changes in the expression of molecules involved in the efficiency of neurotransmission (synaptic plasticity) to structural changes, such as those involving the shape of dendritic spines, the morphology of dendritic trees or the density and size of axonal boutons (structural plasticity). Studies conducted by Hubel and Wiesel on the V1 of cats constituted a milestone for the study of neuronal plasticity of cortical circuits (Wiesel and Hubel, 1963; Hubel and Wiesel, 1970) and lead to the definition of critical periods. Critical periods (CPs) are defined as a time window in the early postnatal period during which the neuronal circuitry is highly plastic and sensitive to stimulation (Hensch, 2005). Hubel and Wiesel worked on how, during this period, the V1 integrates the visual input from both eyes. Therefore, during the CP, they manipulated the input from the eyes and altered the neuronal configuration, causing a shift in the ocular dominance. Once the CP is closed, this shift in the cortical circuitry of the visual cortex can not be reversed during adulthood (Hubel and Wiesel, 1970). Different factors have been identified as key players in the correct development of the CP, but the maturation of inhibitory circuitry has a central role in the development and modification of the CP (Levelt and Hübener, 2012). The onset and closure of the CPs can be modified by treatments that affect the GABAergic circuitry, like the administration of benzodiazepines, the alteration of the $GABA_A$ receptors or the promotion of the maturation of interneurons (Hensch, 2005).

3.1. Structural plasticity

Structural plasticity can be defined as the changes that neurons experience in their morphology under different conditions. These structural adaptations are the result of molecular changes, some of which affect synaptic efficacy, such as neurotransmitter receptor dynamics, adhesion molecules or extracellular matrix components. Morphological changes can occur both in the input and output neuronal domains. Regarding those in the input domain, the dendritic tree is considered the main target of synaptic contacts from other neurons. Structurally, we can distinguish the dendritic tree and the dendritic spines, which are present in pyramidal neurons and some interneuronal subpopulations. Changes in the complexity of the dendritic arbour are usually analyzed by Sholl's analysis (Sholl, 1953). A classical study of this structural remodeling

is the retraction of dendritic tree of pyramidal neurons after chronic stress (McEwen, 1999). The dendritic complexity of interneurons can also be affected by different factors, including visual deprivation (Chen et al., 2012) and chronic stress (Gilabert-Juan et al., 2013). Regarding the dendritic spines, their density and morphology can be used has an indicator of the strength of the synaptic input (Yuste et al., 2000). The density of dendritic spines of pyramidal neurons is affected by benzodiazepines (Curto et al., 2016) and fluoxetine administration (Guirado et al., 2009). In a similar way, the dendritic spine density of interneurons can be also affected by multiple treatments, such as the depletion of PSA-NCAM (Guirado et al., 2014a; Castillo-Gómez et al., 2016), visual deprivation (Keck et al., 2011; Chen et al., 2012) or chronic stress (Gilabert-Juan et al., 2013). Considering the output domain, axonal length and the density and size of axonal buttons are also structural correlates of experience-dependent alterations (Marik et al., 2010; Keck et al., 2011; Sammons et al., 2018).

The classic methodology to study neuronal morphology is based on the staining of random subsets of neurons using Golgi's method (Golgi, 1873). However, the emergence of transgenic mice has allowed researchers to study the morphology of particular neuronal populations through the constitutive expression of fluorescent proteins. In particular, I have used in the present thesis GIN mice, which express the green fluorescent protein in a subpopulation of somatostatin expressing interneurons (Oliva et al., 2000; Gilabert-Juan et al., 2013) and PV-Tdt mice, which express the red fluorophore tdTomato in PV expressing interneurons (Kaiser et al., 2016).

3.1.1. Excitatory neurotransmission

The amino acid glutamate is the main mediator of excitatory neurotransmission in the mammalian brain (Orrego and Villanueva, 1993). Glutamate is released by principal neurons and it can be found throughout the brain. Glutamate can be synthesized *de novo* from glucose through the Krebs cycle, recycled through the glutamate/glutamine cycle (Erecińska and Silver, 1990) and it can also be transported through the blood brain barrier (Smith, 2000). In excitatory neurons, glutamate is stored in synaptic vesicles before being released by exocytosis to the synaptic cleft in a Ca^{2+}-dependent manner. One of the proteins that can be found in synaptic vesicles is synaptophysin (SYN) (Masliah et al., 1990). Although SYN is present, at least virtually, in all synaptic vesicles of the SNC, the role of this protein in synaptic transmission is not yet clearly understood. The lack of synaptophysin induces only soft behavioural alterations (Schmitt et al., 2009) and it is not necessary to form synaptic vesicles or to induce

neurotransmitter release (Eshkind and Leube, 1995; McMahon et al., 1996), suggesting a highly subtle function. On the other hand, different treatments, such as environmental enrichment (Greifzu et al., 2014), induce an increase in synaptophysin expression (Saito et al., 1994), suggesting a role of SYN in the efficiency of neurotransmission. The transport of glutamate into synaptic vesicles and their stabilization at presynaptic terminals is undertaken by vesicular glutamate transporters (VGLUTs). The type of this transporter expressed in the presynaptic terminal indicates the location of the excitatory input. Pyramidal cells with their soma located in the cortex express VGLUT-1 in their presynaptic terminals, whereas excitatory cells with extracortical somata express VGLUT-2 (Varoqui et al., 2002). By contrast, VGLUT-3 expression is found in a broad but scattered pattern throughout the brain, even in some GABAergic synapses (Herzog et al., 2004). In the postsynaptic terminal, glutamate activates different ionotropic and metabotropic receptors, which can be found throughout the brain. Eight types of metabotropic G protein-coupled receptors and three ionotropic glutamate receptors have been identified to date (Willard and Koochekpour, 2013). These receptors are expressed in both pyramidal neurons and interneurons (Traynelis et al., 2010). Glutamate receptors are usually anchored to the postsynaptic density (PSD), a large supramolecular ensemble, constituted by anchoring cytoskeletal and signaling proteins (Peng et al., 2004). The activation of certain subtypes of glutamate receptors also induces the flow of Ca^{2+} from the extracellular space to the cytosol. The glutamate is cleared from the synaptic cleft by excitatory amino acid transporters of astrocytes and brought back to pyramidal cells through the glutamate/glutamine cycle (Divito and Underhill, 2014). The alteration of this balanced glutamatergic neurotransmission system leads to a broad range of nervous system disorders (Choi, 1988).

3.1.2. Inhibitory neurotransmission

GABA is the main inhibitory neurotransmitter in the mature brain. It is produced and released by interneurons and it is synthesized from glutamate by two isoforms of the enzyme glutamic acid decarboxylase: GAD67 and GAD65 (Pinal and Tobin, 1998). These two isoforms show multiple differences: GAD67 has a cytosolic localization and it provides a basal level of GABA synthesis, whereas GAD65 is located in the presynaptic terminal and it constitutes an additional GABA supply on metabolic demand (Buddhala et al., 2009). GABA is packed in synaptic vesicles by the vesicular GABA transporter (VGAT), which can be used as a reliable marker of GABAergic synapses. Once released, GABA acts on ionotropic $GABA_A$ and $GABA_c$ receptors, permeable to chloride and bicarbonate, as well as on metabotropic $GABA_B$ receptors

(Jembrek and Vlainic, 2015). GABA is reuptaken by GABA transporters located in the cell membrane of presynaptic terminals and astrocytes (Lee et al., 2006). Inhibitory neurotransmission efficiency can be modulated in an activity-dependent manner, allowing different forms of plasticity (Méndez and Bacci, 2011). During development, sensory deprivation leads to a decrease in the local intracortical activity of somatosensory (Jiao et al., 2006) and visual cortex (Fagiolini et al., 1994). Moreover, the stimulation of inhibitory neurotransmission through the administration of the $GABA_A$ agonists benzodiazepines increases cortical plasticity (Fagiolini and Hensch, 2000). During adulthood, visual deprivation leads to a reduction of the dendritic complexity (Chen et al., 2012), as well as to a loss of presynaptic axonal boutons of cortical interneurons (Keck et al., 2011; van Versendaal et al., 2012). This interneuronal plasticity can even be detected in control conditions, when a basal turnover of ~10% of axonal boutons has been described (Marik et al., 2010).

3.1.3. Serotonergic neurotransmission

In contrast to the fast, binary and precise effects of glutamatergic and GABAergic neurotransmission, monoamine neurotransmission underlies a slower and more diffuse form of neuronal communication, which allows the tuning of neuronal circuitry and its adaptation to the stimuli (Bucher and Marder, 2013). Monoamine neurotransmission is exerted through a wide range of molecules, whose receptors are found in all neuronal compartments, influencing each aspect of neuronal signaling. In the CNS, the main monoamines are dopamine, histamine, norepinephrine and serotonin. In this thesis, I have examined the serotonergic system in adult mice.

Serotonin (5-Hydroxytryptamine, 5-HT) is a biogenic amine produced by neurons in the raphe nuclei, which have long axonal projections throughout the brain (Pollak Dorocic et al., 2014). The serotonergic system is highly diverse, with seven families of receptors ($5\text{-}HT_1$ to $5\text{-}HT_7$). 5-HT is reuptaken to the presynaptic terminals by a transporter (5-HTT) (Beliveau et al., 2017), which constitutes the prime target of Selective Serotonin Reuptake Inhibitors (SSRIs) like fluoxetine (Prozac, Lilly). 5-HT is involved in multiple physiological functions, especially related to mood (Castrén, 2005). Likewise, disturbances in the serotonergic system are linked to different neuropsychiatric disorders (Adell, 2015).

3.2. Plasticity-related molecules: PSA-NCAM and extracellular matrix

The polysialylated form of the neural cell adhesion molecule (PSA-NCAM) is the result of the posttranslational addition of polysialic acid (PSA) to the neural cell adhesion molecule (NCAM) by the polysialyltransferases enzymes (**Figure 6**). PSA-NCAM is widely expressed during development, when it is involved in multiple processes, such as neuronal migration, neurite extension and synaptic remodeling (Rutishauser, 2008). Although its expression is more restricted in the adult CNS, PSA-NCAM is also involved in multiple plasticity-related responses during adulthood (Rutishauser, 2008). Remarkably, PSA-NCAM is almost exclusively expressed by some interneuronal populations in the adult neocortex (Varea et al., 2005) and amygdala (Nacher et al., 2002). Cortical PSA-NCAM expressing interneurons display characteristic structural features: they receive less perisomatic input, display a reduced dendritic arborization and have a less dendritic spines when compared to PSA-NCAM non expressing interneurons (Gómez-Climent et al., 2011). Recent studies from our laboratory have shown the role of PSA-NCAM in the modulation of structural plasticity of these interneurons (Nacher et al., 2013). Interestingly, PSA can be depleted from NCAM using the enzyme Endo Neuraminidase-N (EndoN). The depletion of PSA from NCAM has multiple structural effects: it increases the perisomatic innervation from PV expressing interneurons on pyramidal neurons (Castillo-Gómez et al., 2011) and alters the spine density of SST expressing interneurons in organotypic cultures (Castillo-Gómez et al., 2016). These effects of PSA-NCAM on neuronal structure may be due to its antiadhesive properties, which facilitate structural remodeling of neuronal elements. Therefore, PSA-NCAM is a promising candidate to mediate structural alterations of cortical interneurons during adulthood. Moreover, PSA-NCAM expression is altered in different neuropsychiatric disorders (Nacher et al., 2013).

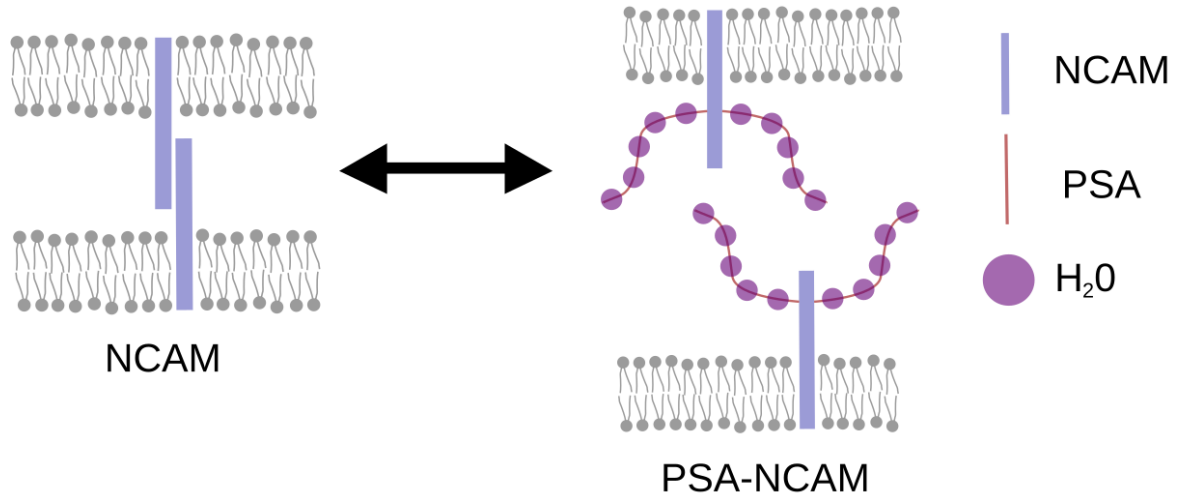

Figure 6. Plasticity-related molecules: PSA-NCAM. Scheme of an homotypic union between two NCAM molecules. The incorporation of negatively charged PSA molecules inverts abruptly the adhesive properties of NCAM molecules.

Perineuronal nets (PNNs) are structures of aggregated and condensed pericellular extracellular matrix (**Figure 7**), which cover the soma, proximal dendrites and often the AIS of neurons (Celio et al., 1998). PNNs surround the synaptic contacts present in these regions. PNNs are composed by a backbone of hyaluronan produced by PNN-bearing neurons, to which a family of four chondroitin sulfate proteoglycans (CSPGs) are bound: aggrecan, neurocan, brevican and versican. Moreover, the glycoprotein tenascin-R links the lecticans to each other and link proteins, such as hyaluronan and proteoglycan link protein 1 and 4, stabilize the CSPG-hyaluronan binding (Carulli et al., 2010). Nevertheless, the composition of PNNs varies between cortical regions (Dauth et al., 2016).

In the neocortex, PNNs are mainly associated to PV expressing cells, although some pyramidal cells in deep cortical layers are also surrounded by them (Matthews et al., 2002). However, surprisingly, there are more pyramidal neurons than PV expressing cells surrounded by PNNs in the amygdala (Morikawa et al., 2017). In general terms, PNNs can bind the lectin *Wisteria Floribunda* agglutinin (WFA), which is used frequently as a marker of these structures, although it is important to note that a small fraction of PNNs are WFA-negative (Matthews et al., 2002). PNNs are formed at the end of neural development, coinciding with the closure of CPs (Brückner et al., 2000) in an activity-dependent manner (Dityatev et al., 2007). The appearance of PNNs surrounding PV+ interneurons signals an abrupt reduction of neuronal plasticity at the

end of the CPs (Pizzorusso et al., 2002; Barritt et al., 2006) and are considered a maturation marker of these cells. The mechanisms through which PNNs fix the connectivity of PV+ cells are diverse: CSPGs interact with glutamate receptors and potassium channels and restrict their mobility (Frischknecht et al., 2009), affecting also the binding of NCAM at perisomatic synapses (Sullivan et al., 2018). The presence of PNNs alters the structure and physiology of interneurons, modulating processes such as drug-seeking behaviors and cognitive deficits associated with a chronic depressive-like states (Van den Oever et al., 2010; Riga et al., 2017).

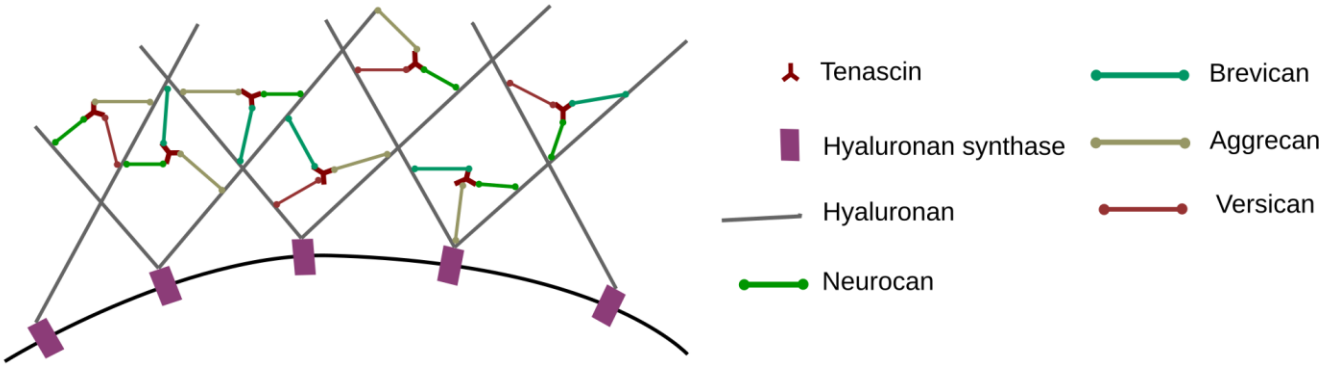

Figure 7. Scheme depicting the molecular components and organization of PNNs.

4. Neuronal oscillations

The neuronal activity gives rise to transmembrane currents in the extracellular medium. The synchronous activity of neuronal ensembles can be explored inserting metal or glass electrodes into the brain to record the local field potential (LFP). The LFP can reveal oscillatory patterns in neuronal activity during brain states and behaviours (Buzsáki and Draguhn, 2004). Gamma oscillations are high frequency neuronal oscillations (30-90 Hz), which provide a temporal structure for information processing in neuronal circuitry. They contribute to memory formation and sensory processing, and are disturbed in some psychiatric disorders (Bartos et al., 2007). These oscillations emerge from the coordinated interactions of excitatory and inhibitory neurons, especially from the activity of PV+ basket cells (Buzsáki and Wang, 2012). PV expressing basket cells display distinctive features supporting their key role in gamma oscillations: low spike threshold, high frequency firing, narrow spikes and resonance at gamma frequency when they are stimulated (Buzsáki and Wang, 2012).

5. Inducing plasticity during adulthood

Although more restricted in its responses than during early life, the adult CNS is also sensitive to experience, treatments and environmental alterations. These changes induce persistent alterations in cortical circuits. In the present thesis, I have used three different treatments to induce structural plasticity, both environmental and pharmacological.

5.1. Fluoxetine

Since its discovery in the early 1970s, fluoxetine hydrochloride (Prozac) has become one of the most widely used drugs to treat depression (Wong et al., 2005). Fluoxetine action is based on the inhibition of the reuptake of monoamines from the synaptic cleft, through the blockade of the 5-HTT. Despite its massive use to treat anxiety and depression, the effects of chronic exposure to fluoxetine on neuronal circuitry are not clearly known. A landmark study performed 10 years ago, demonstrated that chronic treatment with fluoxetine is able to reactivate neuronal plasticity in the adult visual cortex, reaching levels similar to those found during the CP and allowing the recovery of visual acuity in amblyopic rats (Maya Vetencourt et al., 2008). Moreover, fluoxetine treatment also activates neuronal plasticity related to cognitive processes, such as the facilitation of the extinction of fear memories (Karpova et al., 2011) and social learning (Mikics et al., 2018). Regarding its effects on neuronal circuitry, fluoxetine reduces the extracellular levels of GABA in the visual cortex (Maya Vetencourt et al., 2008). This reduction in GABAergic transmission is also reflected at the structural level in interneurons of layer II/III of visual cortex, in which fluoxetine promotes dendritic tip dynamics (Chen et al., 2011). Regarding the mPFC, a chronic treatment with fluoxetine increases the dendritic spine density of SST expressing interneurons (Guirado et al., 2014b). Nevertheless, the effects of fluoxetine on the structure of interneurons and the expression of molecules related to interneuronal plasticity, such as PSA-NCAM, have not been explored yet in the BLA.

5.2. Dark exposure

Different approaches have shown enhancements of neuronal plasticity in the adult visual cortex similar to those found in the critical period (Stryker and Löewel, 2018), including PNNs digestion (Pizzorusso et al., 2002), fluoxetine administration (Maya Vetencourt et al., 2008) or environmental manipulations. The environmental boosting of plasticity can be achieved when mice are raised in complex cages with multisensory and motor enrichment (Greifzu et al., 2014). This environmental manipulation is translated into a reduction of PV and GAD65 expression

within interneurons of the visual cortex. Intriguingly, an environmental manipulation with opposite effects on sensory inputs, this is the visual deprivation through dark exposure, also reactivates robust plasticity in the adult visual cortex (He et al., 2006; Stodieck et al., 2014; Erchova et al., 2017). It has been shown that dark exposure during adulthood alters the composition of glutamate N-methyl-D-aspartate (NMDA) receptors to that of a predominant form during the critical period, which contains the NR2B subunit and exhibits enhanced temporal summation (He et al., 2006). Moreover, this deprivation induces the shift of the dendritic spines of pyramidal neurons towards an immature configuration (Tropea et al., 2010) and immature excitatory synapses are strengthened (Goel and Lee, 2007). On the other hand, dark exposure reduces PV expression in the V1 (Stodieck et al., 2014), as well as the excitability of basket cells (Gu et al., 2016). The reactivation of plasticity also strengthens the thalamic input from the LGN to the visual cortex (Montey and Quinlan, 2011). Therefore, different studies have shown that dark exposure promotes the recovery of visual function in adult animals with amblyopia (He et al., 2007; Stodieck et al., 2014; Mitchell et al., 2016; Erchova et al., 2017). This suggests that a combination of dark exposure and a focused visual experience to stimulate properly the cortical circuitry, may allow the visual cortex to recover from amblyopia. Nevertheless, the effects of dark exposure during adulthood on the structure and connectivity of interneurons, as well as its impact on molecules related to the plasticity of these inhibitory neurons has not been not explored yet.

5.3. Chondroitinase ABC

The formation of PNNs at the end of the critical period and the subsequent decrease of neuronal plasticity have highlighted these structures as tools for the manipulation of plasticity during adulthood. Different knock-out mice deficient for PNNs components show persistent plasticity after the closure of CPs: aggrecan (Rowlands et al., 2018), tenascin-R (Bukalo et al., 2001; Morellini et al., 2010) and brevican (Favuzzi et al., 2017). Nevertheless, the most used manipulation of PNNs is the digestion of CSPGs, using the bacterial enzyme Chondroitinase ABC (ChABC). The first evidence of PNNs digestion as a trigger of cortical plasticity was observed through the reactivation of ocular dominance plasticity in the V1 of adult mice (Pizzorusso et al., 2002). Recently, it has been shown the efficacy of this treatment in the modulation of remote fear memory (Thompson et al., 2018), drug memories (Xue et al., 2014) and the restoration of cognitive deficits associated with a chronic depressive-like state (Riga et al., 2017). Thus, PNNs are good candidates to regulate both memory and experience-

dependent plasticity in adulthood, although the mechanisms underlying the reactivation of plasticity by ChABC administration are not yet completely understood.

II. OBJECTIVES

The main objective of this doctoral thesis is to study the effects of different pharmacological and environmental manipulations on the structure of excitatory and inhibitory neurons in the adult mouse brain, their connectivity and the expression of plasticity-related molecules, in an attempt to gain a better understanding of the mechanisms of structural plasticity in the adult nervous system. In order to achieve this main goal, we derive the following specific objectives:

1. To study the impact of visual deprivation by dark exposure on the structure and connectivity of cortical interneurons and the expression of synaptic and plasticity-related molecules throughout the visual system.

2. To study the impact of a chronic treatment with fluoxetine on the structure of interneurons and the expression plasticity-related molecules in the basolateral amygdala.

3. To analyze the effects of the presence of perineuronal nets and their enzymatic depletion on the perisomatic synaptic puncta on pyramidal and inhibitory neurons and on the physiology of the medial prefrontal cortex.

III. MATERIAL AND METHODS

Experiment 1. Dark exposure affects plasticity-related molecules and interneurons throughout the visual system during adulthood

Animals and visual deprivation

For the visual deprivation experiment, sixteen male GIN (EGFP-expressing inhibitory interneurons, FVB-Tg (Gad-GFP) 45704Swn) three-months-old mice were used. The animals were housed in a standard environment (12 h light/dark cycle) and with *ad libitum* access to food and water in groups of four animals per cage. All animal experimentation was conducted in accordance with the Directive 2010/63/EU of the European Parliament and of the Council of 22 September 2010 on the protection of animals used for scientific purposes. Mice used for the visual deprivation experiment were randomly separated into two groups (control and deprived, n = 8 each) at postnatal day 90. For dark exposure, half of the cages were previously covered with an opaque-black adhesive plastic and the absence of light entrance inside the cage was checked with a photometer. All cages were placed in a ventilated rack and bedding changes were performed during the dark phase of the cycle, using a far-red light. We confirmed that dark cages were ventilated in the same manner as control cages. After 10 days of darkness, at postnatal day 100, mice were deeply anesthetized with sodium pentobarbital (0.01 mg/g dw, i.p.) and perfused transcardially. Each animal was perfused briefly with saline solution (0.9%) and then with 4% paraformaldehyde in 0.1 M phosphate saline buffer (PBS) for 20 minutes. After perfusion, the brains were extracted and stored in phosphate buffer (PB) 0.1 M with sodium azide (0.05%) at 4 ºC. Extracted brains were examined in order to detect poor fixation.

Two animals of each group were discarded, letting n = 6 animals per group used for the rest of the stainings and analysis. Then, the hemispheres were separated and the right hemisphere was cut into 50 µm thick sections, while the left one was cut into 100 µm thick sections, both coronal, with a vibratome (Leica VT1000S). The slices were collected in six and three subseries respectively and stored at 4 ºC in a solution of PB 0.1 M and sodium azide (0.05%).

Immunohistochemistry

Free-floating sections were processed for fluorescence immunohistochemistry as follows. After washing with PBS, non-specific binding was blocked for 1 hour by incubating the sections in PBS containing 5% normal donkey serum (Jackson ImmunoResearch Laboratories) and PBS-0.2% Triton X-100 (Sigma-Aldrich). Subsequently, slices were incubated for 48 hours at 4 ºC with different primary antibody cocktails diluted in PBS-0.2% Triton X-100 (see Table 1) except for the PNNs, which were labeled using a 1:200 diluted biotinylated WFA against the N-acetyl-D-galactosamine component of the PNNs (Sigma-Aldrich Cat# L-1516). After this, slices were washed with PBS and incubated for 2 hours at room temperature with different secondary antibody cocktails diluted in PBS-0.2% Triton X-100 (see **Table 1**). Afterwards, sections were washed with PB. The sections were then mounted on gelatinized slides using Dako Fluorescent Mounting Medium *(Dako North America)* and coverslipped. Sections were processed together for immunohistochemistry to reduce the variability of staining and allow comparisons between groups. To avoid any bias in the analysis, all slides were coded prior to image acquisition and remained coded until the experiment was completed. The extension of V1 was determined for all analyses described with the aid of a stereotaxic atlas and a subseries of sections stained with toluidine blue. Image acquisition parameters were kept unchanged in the confocal imaging of each of the experiments.

Primary antibodies				
Anti	**Host**	**Isotype**	**Dilution**	**Company**
CAMKII	Mouse	Monoclonal IgG1	1:500	Abcam
CB	Mouse	Monoclonal IgG1	1:5000	Swant
CB1r	Rabbit	Polyclonal	1:2000	Synaptic Systems
CCK	Rabbit	Polyclonal	1:10000	Millipore

CR	Mouse	Monoclonal IgG	1:1000	Swant
GFP	Chicken	Polyclonal IgY	1:1000	Abcam
NPY	Rabbit	Whole antiserum	1:5000	Sigma-Aldrich
PSA-NCAM	Mouse	Monoclonal IgM	1:700	DSHB
PV	Guinea Pig	Polyclonal	1:2000	Synaptic Systems
SST	Rabbit	Polyclonal	1:500	Millipore
SYN	Rabbit	Polyclonal	1:1000	Millipore
VGAT	Mouse	Monoclonal IgG	1:1000	Synaptic Systems
VGLUT1	Guinea Pig	Polyclonal	1:2000	Millipore
Secondary antibodies				
Anti	**Host**	**Label**	**Dilution**	**Company**
Biotin	Donkey	Avidin	1:400	Jackson
Biotin	Donkey	Avidin-Cy3	1:400	Invitrogen
Chicken	Donkey	CF488	1:1000	Biotium
Guinea Pig	Donkey	A647	1:400	Jackson
Guinea Pig	Donkey	A405	1:400	Abcam
Mouse IgG1	Donkey	DL549	1:400	Jackson
Mouse IgG1	Donkey	A488	1:400	Invitrogen
Mouse IgG	Donkey	DL649	1:400	Jackson
Mouse IgG	Donkey	A555	1:400	Molecular probes
Mouse IgM	Donkey	DL649	1:400	Jackson
Mouse IgM	Donkey	DL549	1:400	Jackson
Rabbit	Donkey	A405	1:400	Invitrogen
Rabbit	Donkey	A649	1:400	Invitrogen
Rabbit IgG	Donkey	A555	1:400	Invitrogen

Table 1. List of primary and secondary antibodies used in the experiment 1.

Analysis of immunoreactive puncta in the neuropil

We analyzed the density of puncta expressing different synaptic markers in single confocal planes of the mouse V1 neuropil, obtained with a confocal microscope (Leica TCS-SPE). Images were obtained using a 63x oil-immersion objective and an additional 2x digital zoom. We took images from four different coronal sections containing the V1 of each brain (Bregma -2.70, -3.00, -3.30 and -3.60 mm). For each section, three single confocal planes were selected from layer I, layer IV and layer VI. On these planes, four small areas of the neuropil (300 μm^2 each) were selected for analysis, in order to avoid blood vessels and cell somata. Images were processed using different customized macros. In short, noise was reduced using a gaussian blur filter, images were binarized, creating a mask containing the 2% brightest pixels, and the outline of that mask was used in the original image to measure the number and fluorescence intensity of puncta.

Analysis of the neurochemical phenotype of GAD67-EGFP expressing neurons

Sections double labeled for GFP and interneuronal markers (PV, CB, CR, SST, CCK) or PSA-NCAM were observed under a confocal microscope (Leica TCS-SPE) using a 40x objective. Stacks of confocal images (Z-step size of 0.8 µm) were obtained from V1 region. Fifty GAD67-EGFP-expressing neurons were randomly selected from visual cortex layers II-VI of each animal in the control group and from each immunostaining to determine the co-expression. Percentages of co-localization were determined for each animal and mean ± SEM were calculated.

Structural analysis of EGFP-expressing interneurons

The structural features of the EGFP-expressing interneurons were studied with a confocal laser microscope (Leica TCS-SPE), using sections immunostained with anti-GFP antibody, in order to enhance fluorescence. For the analysis of dendritic arborization, six different interneurons from the whole V1 were studied per animal. Interneurons were chosen randomly from layers II-V but they had to meet different criteria to be included in the study: 1) the cell must not show any truncated dendrites, 2) the soma must be located at least 30 µm deep from the surface of the tissue and 3) the cell and their dendrites must not show any sign of neurodegeneration. The scarcity of cells meeting all these criteria did not allow a more detailed

analysis by layers. Stacks of confocal images (Z-step size of 0.8 µm) were obtained a 40x objective covering the whole dendritic tree of selected interneurons. Then, stacks were analyzed using the FIJI software (Schindelin et al., 2012). Simple Neurite Tracer plugin (Longair et al., 2011) of FIJI was used to obtain 3D projections. The dendritic projections from each cell were manually traced, using the presence of dendritic spines, the absence of *en passant* boutons and the thickness of the processes as checkpoints to avoid axonal segments in the analysis. Then, the number of intersections with spheres of increasing radius centered in the soma were analyzed.

The density of *en passant* axonal boutons from EGFP-expressing neurons was studied using stacks of confocal images (Z-step size of 0.38 µm), obtained with a 63x oil-immersion objective in the superficial layer I of the V1. Then, at least twelve axonal fragments of at least 25 µm length were traced per animal and filled using the Simple Neurite Tracer plugin. Afterwards, traces were processed as described above and a customized macro was used to discriminate and measure the area and fluorescence intensity of axonal boutons based on the increased fluorescence intensity of axonal boutons in relation to the adjacent shaft, using the 2% top brightest pixels as a threshold. We established a size filter up to 0.5 μm^2 based on previous manual quantification of a small subset of experimental images.

For the spine density study, six dendrites from 6 different interneurons within the V1 region, including layers II-V, were analyzed per animal. Dendrites were randomly chosen, but they had to meet different criteria to be included in the study: 1) They should measure at least 150 µm from the soma and 2) no other dendrites should be found crossing their trajectory. Stacks of confocal images (Z-step size of 0.38 µm) were obtained with a 63x objective and an additional 3.5 digital zoom. The spines were manually counted in three dendritic fragments (50 µm each) expanding until 150 µm from the soma. The classification of the spines was realized according to the length of the protrusion and the relative diameter of their head and neck. Three different categories were established: 1) stubby when the length of the protrusion was <1 µm; 2) mushroom when a clear head could be observed in relation with the neck (maximum diameter of the head at least 2 times larger than the diameter of the neck) and the total length of the protrusion was <2 µm and 3) thin when the length of the protrusion was >2 µm. Overall spine density, densities per segment and typology values were expressed as number of spines/10 µm.

Estimation of the density of parvalbumin expressing interneurons and perineuronal nets

We estimated the density of PV+ cells, PNNs and the ratio of PV cells surrounded by perineuronal nets (PV+PNN+). We acquired images at 1360x1024 pixels using a digital camera (Olympus DP71) coupled with a fluorescence microscope (Olympus BX41) and using a 20x objective. Eight images per animal of layers II-V were obtained from the same coronal sections previously described. Positive cells were manually counted from the images obtained. Densities of cells immunoreactive for PV and/or surrounded by PNNs and percentages of co-localization were determined for each animal and mean ± SEM were calculated. The mean intensity of the fluorescence of WFA staining for PNNs and its area were calculated as follows: after transforming the image to 8-bit deep, background was subtracted (rolling value= 30) to obtain the mean intensity. The percentage of area covered by PNN was then calculated by applying a predetermined threshold (value = 5) and measuring the binarized area respect the total area of the image. WFA mean intensity and area were determined for each animal.

Analysis of the density of perisomatic immunoreactive puncta surrounding pyramidal neurons

We analyzed the density of puncta surrounding the cell body of pyramidal neurons in layer V of the V1 region. Single confocal planes, obtained with a confocal microscope (Olympus FV10i), were obtained using a 60x oil-immersion objective and an additional 2x digital zoom. Thirty pyramidal somata per animal were identified by CAMKII immunoreactivity. The profile of every soma was manually delimited and the selection was enlarged 0.5 µm. Then, the puncta immunopositive for PV, CB1r, SYN or PSA-NCAM inside the selection were manually counted.

Estimation of the total number of PSA-NCAM expressing cells

The number of neuronal somata expressing PSA-NCAM was estimated using a modified version of the fractionator method (West et al., 1991). This is, we counted all labeled cells found in all the extension of V1 within each 50 µm thick section. One from six systematic-random series of sections covering the whole rostral to caudal extension of V1 on an Olympus BX41 fluorescence microscope. Cell somata were identified and counted with a 40x objective. Cells appearing in the upper focal plane were omitted to prevent counting cell caps.

Optical densitometry

When the neuropil area was too limited to allow the sketch of squares in single confocal planes (LGN and SC areas), we performed a study of the optical density of the immunoreactive

labeling. From each immunostaining, 2 sections per animal were selected from the regions of interest (-2.10 mm and -2.40 mm from Bregma for the LGN study; -3.60 mm and -3.90 mm from Bregma for the SC study). The images were obtained using an Olympus DP71 camera coupled with an Olympus BX41 microscope and using a 20x objective. For the imaging, samples were taken randomly and imaged using the same exposure time (1/200s) and ISO (400). In both sets of images grey levels were converted to optical densities and analyzed using FIJI software.

Statistics

We calculated the mean value ± SEM for comparing all the parameters analyzed. Normality and homoscedasticity of data were evaluated in order to find an appropriate statistical analysis. When comparing two means and variances, the data allowed for a parametric test, data were subjected to unpaired Student's *t* test. The number of PSA-NCAM expressing cells did not follow a normal distribution and thus were subjected to a non-parametric Mann-Whitney U test. All the analyses were performed using the SPSS statistics software (IBM, version 22)

Experiment 2: Effects of the antidepressant fluoxetine on the somatostatin interneurons in the basolateral amygdala

Animals

Sixteen male GIN (EGFP-expressing inhibitory neurons, Tg(GadGFP)45704Swn) mice, three months old, were used in this study. They were maintained in standard conditions of light (12 h cycles) and temperature, with access to food or water *ad libitum*. Four mice were used to analyze the phenotype and distribution of EGFP expressing cells in the amygdala. The rest of the animals received daily i.p. injections of either the antidepressant fluoxetine (n = 6, 20 mg/kg), or the saline solution (n = 6), over 14 days (once daily at 10.00 am). The day after the last injection, mice were perfused transcardially under deep chloral hydrate anaesthesia (4%, 0.01 ml/g), first with saline and then with 4% paraformaldehyde in sodium phosphate buffer (PB 0.1 M, pH 7.4). After perfusion, the brains were extracted and stored in PB 0.1 M and sodium azide 0.05%. The two hemispheres were separated, then one hemisphere was cut into 50 μm thick sections, while the other was cut into 100 μm thick sections, both with a vibratome (Leica VT 1000E, Leica). The sections were collected in six and three subseries, respectively, and stored at 4°C in PB 0.1 M and sodium azide 0.05% until used. All animal experimentation was conducted in accordance with the Directive 2010/63/EU of the European Parliament and of the Council of 22 September 2010 on the protection of animals used for scientific purposes and was approved by the Committee on Bioethics of the Universitat de València.

Immunohistochemistry

Tissue was processed free-floating for fluorescence immunohistochemistry. Sections were washed in PBS, then slices were incubated in 10% normal donkey serum, 0.2% Triton-X100 (Sigma) in PBS for 1 h. Sections were then incubated for 48 h at 4°C with different primary antibody cocktails diluted in PBS – 0.2% Triton-X100 (see **Table 2**). After washing, sections were incubated for 2 h at room temperature with different secondary antibody cocktails also diluted in PBS 0.2% Triton-X100 (see **Table 2**). Finally, the sections were washed in PB 0.1 M, mounted on slides and coverslipped using fluorescence mounting medium (Dako).

Primary antibodies				
Anti	**Host**	**Isotype**	**Dilution**	**Company**
CAMKII	Mouse	Monoclonal IgG1	1:500	Abcam
FosB	Rabbit	Polyclonal IgG	1:500	Santa Cruz
GAD6	Mouse	Monoclonal IgG	1:500	DSHB
GFP	Chicken	Polyclonal IgY	1:1000	Abcam
PV	Guinea Pig	Polyclonal IgG	1:2000	Synaptic Systems
PSA-NCAM	Mouse	Monoclonal IgM	1:700	DSHB
SST	Goat	Polyclonal IgG	1:500	Santa Cruz
Secondary antibodies				
Anti	**Host**	**Label**	**Dilution**	**Company**
Chicken	Donkey	CF488	1:1000	Biotium
Goat IgG	Donkey	DL649	1:400	Jackson
Guinea Pig IgG	Goat	A555	1:400	Life Technologies
Mouse IgG	Donkey	DL649	1:400	Jackson
Mouse IgG1	Goat	A647	1:400	Life Technologies
Mouse IgM	Donkey	A555	1:400	Invitrogen
Rabbit IgG	Donkey	A555	1:400	Invitrogen

Table 2. List of primary and secondary antibodies used in the experiment 2.

Distribution and phenotype of EGFP expressing cells

In four animals, all brain sections containing parts of the amygdala were analysed together to specifically study the distribution of cells expressing EGFP through the BLA, and their co-localization with somatostatin.

Analysis of immunoreactive puncta

We analyzed the density of puncta expressing different markers in single confocal planes (Olympus FV10i), using customized macros. The analyses were performed in the BLA in

two different sections: those corresponding to Bregma -1,22 mm and Bregma -1,70 mm. Confocal z -stacks of the superficial layers of the slices, for optimal penetration levels for antibody recognition, were selected. On these planes, four small areas of the neuropil (505 μm^2) were selected for analysis, in order to avoid blood vessels and cell somata. Images were processed using ImageJ software. The background was subtracted with a rolling value of 50, converted to 8-bit deep images and binarized using a determined threshold value. This value depended on the marker and the area analyzed and was kept the same for all images with the same marker and area. The images were then processed with a blur filter to reduce noise and separate closely apposed puncta. Finally, the number of the resulting dots per region was counted.

Analysis of FosB expression

In order to evaluate sustained changes in basal neuronal activity, we quantified the fluorescence intensity of FosB in the soma of all PV+ cells in two different sections containing the BLA (Bregma -1,22 mm and Bregma -1,70 mm). The area analyzed in each section was of 0.3 mm^2 and the number of PV+ cells in that area varied from 10 to 40 per section. Stacks were obtained covering the whole thickness of each section, and then the images were processed at an optimal penetration depth in the tissue (5-7 µm from tissue surface). To properly compare the intensity between animals, the acquiring conditions were the same in all cases, including laser intensity, photomultiplier gain, offset and pinhole among others. These images were then automatically processed using ImageJ software in order to avoid any bias. The background was automatically subtracted from all images, then a binary mask was applied in order to obtain the profiles of the PV+ interneurons and the fluorescence intensity of FosB was analyzed within these profiles. Similarly, for the analysis of FosB in SST and CAMKII expressing subpopulations, z-stacks were obtained at the optimal depth of the tissue (3-5 µm from tissue surface), and the nuclear profile of FosB within CAMKII and SST expressing neurons was manually delineated to measure the fluorescence intensity of FosB.

Structural analysis of EGFP-expressing cells

For the analysis of the structure of the EGFP-expressing cells, stacks of confocal images (Leica TCS-SPE) were obtained with a 63x objective. The stacks were obtained from two different Bregma levels (-1,22 and -1,70) inside the BLA. For the analysis of the dendritic spines, six dendritic segments were analyzed per animal. The classification of the spines was

performed manually, according to the length of the protrusion and the relative diameter of its head and neck. Three different categories were established: 1) stubby, when the length of the protrusion was <1 µm; 2) mushroom, when a clear head could be observed relative to the neck (maximum diameter of the head at least 2 times larger than the diameter of the neck) and the total length of the protrusion was <2 µm; and 3) filopodia-thin, when the length of the protrusion was >2 µm. The relative fraction of every type of spine was analyzed. For the axonal *bouton* density analysis, 15 axonal segments of at least 35 µm long were analyzed using ImageJ software. The background was subtracted and then a binary mask was applied over the top 1% brightest part of the image. In previous assays, we made sure that this fraction of binarization erased all the signal corresponding to unwanted cellular fragments, but preserved the threshold corresponding to the axonal *bouton* area due to its higher intensity. This mask allowed us to automatically analyse the density of *en passant* axonal *boutons* and to measure their size. After estimating the total axonal *bouton* density, we filtered our results to study only those axonal *boutons* occupying an area larger than 0.5 μm^2 to single out large *boutons* representing the especially active *bouton* population.

Statistical analysis

The resulting values of the different analyses were evaluated in order to apply the adequate statistical analysis. Due to their adaptation to parametric analysis and because of having two experimental groups: treated and control mice, the data was subjected to unpaired Student's *t* test statistical analysis. All the analyses were performed using GraphPad software.

Experiment 3: Perineuronal nets regulate the inhibitory perisomatic input onto parvalbumin interneurons and gamma rhythms in the prelimbic area of the medial prefrontal cortex

Animals

Thirty male PV-TdT (C57BL/6-Tg(Pvalb-tdTomato)15Gfng/J) three-month-old mice were used in the study (**Figure 8**). Four animals were used for the descriptive study of PV+ cells. Twenty-six animals were used for the study of ChABC effects on the mPFC: 14 for histological analysis and 12 for electrophysiological recordings. Animals were housed in groups of 2 to 4 in a standard environment (12 h light/dark cycle) and with *ad libitum* access to food and water. All animal experimentation was conducted in accordance with the Directive 2010/63/EU of the European Parliament and of the Council of 22 September 2010 on the protection of animals used for scientific purposes and was approved by the Committee on Bioethics of the Universitat de València. Every effort was made to minimize the number of animals used and their suffering.

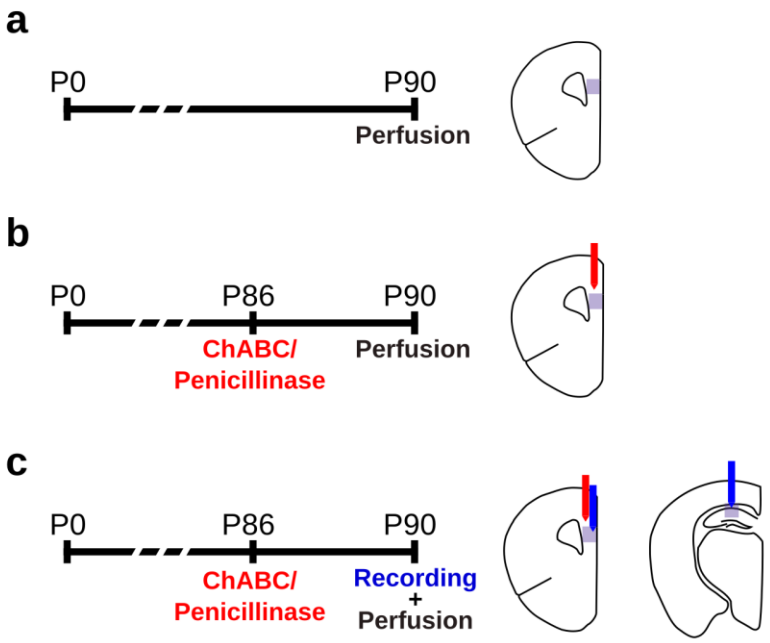

Figure 8. Scheme of the experimental design followed in the experiment 3. Experimental timeline used for the descriptive study **(a)**, the histological analysis of ChABC effects **(b)** and the impact of PNNs depletion on the physiology of PrL **(c)**.

Stereotaxic injection of ChABC

Mice were anesthetized with isoflurane (4% for induction, 2% for maintenance, both in 0.5ml O_2/min flow rate). Additionally, dexamethasone (0.6 mg/Kg) was intramuscularly injected to prevent inflammation. Animals were placed in a stereotaxic frame, then skin and periosteum were removed to expose the skull. Afterwards, 1 µl of the enzyme ChABC (n = 13, 50 U/ml in filtered PB; C3667, Sigma Aldrich) or the control enzyme penicillinase (n = 13, 1 µg/µl in filtered PB; P0389, Sigma Aldrich), were bilaterally injected using a Hamilton syringe with a 26G needle in the following coordinates relative to Bregma: anteroposterior +2.00; mediolateral ±0.25 and dorsoventral 1.00. The needle was left in position for 2 minutes before the injection and the flow rate during the injection was 100 nl/min. After the injection was completed, the needle was left in place for 5 minutes to reduce the reflux of the solution and then slowly withdrawn. Animals were left undisturbed for 4 days between the injection and the recording and/or perfusion.

Recording procedure

Mice were anesthetized with urethane (1.7 mg/kg i.p. in sterile saline solution; 94300, Sigma-Aldrich). Ten minutes after the urethane injection, a tracheotomy was performed in order to minimize respiratory pitfalls during the recording session, following a protocol previously described (Moldestad et al., 2009). Then, animals were placed in a stereotaxic frame (Narishige, Japan) and a midline sagittal incision was made. Lidocaine (2%, Normon) was administered and the skull surface was exposed and dried. We trephined the skull in the following coordinates from Bregma: anteroposterior +2.00, mediolateral + 0.25 and dorsoventral +1.20 to record the deep layers of the PrL and anteroposterior -3.00, mediolateral +1.00 and dorsoventral +1.20 to record the *Cornu Ammonis* 1 from the hippocampus (CA1) used as internal control.

LFPs were recorded using a formvar insulated stainless steel monopolar macroelectrode (120 um diameter, World Precision Instruments) placed in the PrL and CA1. The skin of the animal was used as a reference. Signals were recorded and filtered with a first differential AC pre-amplifier (Gress p551) with the settings x10, 0.3-300 Hz for the CA1 recording and x10, 0.3-10000 Hz for the PrL recording. Then, signal was subjected to another amplification (CIBERTEC Amplifier) of x100 between 0.3-300 Hz. Data were digitised with the Power 1401 plus A/D converter (Cambridge Electronic Design) and were digitally stored using the Spike2 software (Cambridge Electronic Design).

For the gamma oscillations induction, a tail-pinch protocol was used. After 30 minutes of basal recording, ten tail stimuli were performed. The pattern of stimulation used consisted in 15 seconds of tail stimulation by forceps pressure on the basal zone of the tail, followed of 3 minutes resting to recover the basal oscillations pattern. After the last stimulus, mice were perfused as explained in the histological procedure section.

Extracellular recording analysis

Data were imported into MATLAB environment (Mathworks, USA) for the off-line analysis using self-developed code. Recording sessions were divided into brain states of slow oscillations distinguished from theta periods in response to brief (30 s) sensory-induced (tail pinch) arousal. Firstly, the entire recording was band-pass filtered between 0.5 and 250 Hz (Butterworth filter, low-pass order 4, high-pass order 3) and band-stop filtered (49.5–50.5 Hz; 99.5–100.5 Hz) to remove residual 50 Hz power-line contamination and its harmonics.

Spectral analyses were implemented by Fast Fourier transform reporting the power distribution in the frequency domain. An estimation of the spectral normalized energy was done using Welch's method (50% overlapping 4s Hanning windows with an fft size of 2.56 Hz and an nfft value of 1024). The frequency bands defined in the spectral analysis were: delta (0.5–3 Hz), low-theta (3–6 Hz), high-theta (6-10 Hz), beta (10–30 Hz), low-gamma (30–70 Hz), high-gamma (70–100 Hz) and fast-gamma (> 100 Hz).

Cross-frequency interactions between different frequencies of the signals were assessed by the modulation index (MI) (Tort et al., 2010), which quantifies the deviation of the phase-amplitude distribution from the uniform distribution through Kullback-Leibler divergence. Briefly, raw time-series were filtered in the two frequency bands of interest (theta and gamma). MI is a normalized measure that reflects how well the instantaneous amplitude of a faster oscillation (amplitude modulated) is phase-locked to an underlying lower cycle (phase modulating). First, the raw signal was filtered at the two frequency ranges under analysis (two-way Butterworth filter with order 2). We then applied the Hilbert transform to extract the phase and the instantaneous amplitude (envelope) of both processed signals.

Histological procedures

Four days after injection (or immediately after the recording session for mice destined to electrophysiological analyses), animals were sacrificed. Deep anesthesia was induced by

sodium pentobarbital (300 mg/kg i.p., diluted in distilled water). Animals were perfused transcardially, first with saline and then with PFA 4% in PB 0.1 M for 20 minutes. After perfusion, brains were extracted and stored in PB 0.1 M with sodium azide 0.05%. Then, brains were cut into 50 microns sections using a vibratome (VT 1000E, Leica). Sections were collected in 6 subseries and stored at 4ºC in PB 0.1 M with sodium azide.

Sections were processed for fluorescence immunohistochemistry as follows. Slices were washed in PBS, then they were incubated for 1h in 10% normal donkey serum (Gibco), 0.2% Triton-X100 in PBS to block nonspecific binding. After that, sections were incubated for 48 h at 4 ºC with different primary antibodies cocktails (see **Table 3**) diluted in PBS 0.2% Triton-X100, and a 1:200 diluted biotinylated WFA for PNNs staining (Sigma-Aldrich L-1516). For confocal microscopy, sections were washed and incubated for 2 hours at room temperature with secondary antibody cocktails (see **Table 3**) diluted in PBS 0.2% Triton-X100. Finally, sections were washed in PB 0.1 M, mounted and coverslipped using fluorescence mounting medium (Dako).

For the PNNs digestion study in bright field microscopy, sections were washed and incubated for 1 hour with avidin-biotin-peroxidase complex (Vector Laboratories; PK-4000). Then, the sections were incubated for 3 minutes with 3,3'-diamino-benzidine tetrahydrochloride (Sigma Aldrich; D5637) and 0.033% H_2O_2 for staining. Sections were finally mounted on slides, dried for 12 hours at room temperature, dehydrated with ascending alcohols and rinsed in xylene before being coverslipped using Eukitt mounting medium (Sigma Aldrich; 03989).

Confocal imaging and image analysis

Sections were analyzed under a confocal microscope (Leica SPE). Stacks were obtained from deep layers of the PrL at an optimal penetration depth in the tissue (up to 6 µm deep). We used a 63x objective plus 2x digital zoom for the imaging of perisomatic puncta, neuropil puncta and axonal initial segment. A 20x objective was used for the quantification of cell somata. The acquiring conditions were maintained throughout all the imaging sessions to compare the fluorescence intensity between samples. For the image analysis of perisomatic puncta, we outlined manually the profile of the cell somata and we used a series of custom-made macros in Fiji (Schindelin et al., 2012). In order to evaluate sustained changes in basal neuronal activity, we quantified the fluorescence intensity of FosB in the soma of PV+ and CamKII+ cells in two different sections containing the PrL (Bregma -2.00 mm and Bregma -2.20

mm). Stacks were obtained covering the whole thickness of each section, and then the images were processed at an optimal penetration depth in the tissue (5-7 µm from tissue surface). To properly compare the intensity between animals, the acquiring conditions were the same in all cases, including laser intensity, photomultiplier gain, offset and pinhole among others. Then, the nuclear profile of FosB within CAMKII and PV expressing neurons was manually delineated to measure the fluorescence intensity of FosB.

Primary antibodies				
Anti	**Host**	**Isotype**	**Dilution**	**Company**
AnkG	Mouse	Monoclonal IgG1	1:500	Santa Cruz
CAMKII	Mouse	Monoclonal IgG1	1:500	Abcam
FosB	Mouse	Monoclonal IgG1	1:500	Santa Cruz
PV	Guinea Pig	Polyclonal	1:2000	Synaptic Systems
PV	Rabbit	Monoclonal	1:2000	Swant
SYN	Rabbit	Polyclonal	1:1000	Millipore
VGAT	Rabbit	Polyclonal	1:500	Synaptic Systems
VGLUT1	Guinea Pig	Polyclonal	1:2000	Millipore
VGLUT2	Guinea Pig	Polyclonal	1:2000	Millipore
Secondary Antibodies				
Anti	**Host**	**Label**	**Dilution**	**Company**
Biotin		A488	1:400	Invitrogen
Guinea Pig	Donkey	A647	1:400	Invitrogen
Guinea Pig	Donkey	A405	1:400	Invitrogen
Mouse IgG1	Donkey	DL549	1:400	Jackson
Mouse IgG1	Donkey	A488	1:400	Invitrogen
Mouse IgG	Donkey	DL649	1:400	Jackson
Mouse IgG	Donkey	A555	1:400	Molecular probes

Mouse IgM	Donkey	DL649	1:400	Jackson
Mouse IgM	Donkey	DL549	1:400	Jackson
Rabbit	Donkey	A405	1:400	Invitrogen
Rabbit	Donkey	A649	1:400	Invitrogen
Rabbit	Donkey	A555	1:400	Invitrogen
Rabbit IgG	Donkey	A555	1:400	Invitrogen

Table 3. List of primary and secondary antibodies used in the experiment 3

Statistics

The resulting values were evaluated in order to apply the adequate statistical analysis. The normality and homoscedasticity of data allowed us to perform parametric analysis on the data. The Pearson correlation coefficient (r) was calculated for correlation analyses. For the comparison in control animals between PV+PNN+ and PV+PNN- cells, we used a paired Student's t-test. For ChABC experiments, we used an unpaired Student's t-Test. All the results were expressed as the mean ± SEM. All the analysis and graphs were obtained using Graphpad software.

IV. RESULTS

Experiment 1. Dark exposure affects plasticity-related molecules and interneurons throughout the visual system during adulthood

Visual deprivation alters the expression of different synaptic markers in the neuropil of the primary visual cortex

We have studied whether the visual deprivation may affect the expression of inhibitory, as well as general and excitatory, synaptic markers in the adult V1 (**Figure 9**). In order to implement an automatic and accurate methodology to quantify immunoreactive puncta, we set up customized macros. We used a small subset of experimental images to adjust the binarization threshold of single confocal planes, obtaining comparable results to manual counting with a 2% threshold (**Figure 10**). After deprivation, we found a decrease in the density of synaptophysin (SYN)-expressing puncta (Figure 9a, 9b and 9e, $p = 0.042$). Moreover, we found a decrease in the density of vesicular glutamate transporter 1 (VGLUT1)-expressing puncta (Figure 9c, 9d and 9e, $p = 0.019$), but not in the vesicular GABA transporter (VGAT) puncta density ($p = 0.947$). This specific decrease in excitatory puncta suggested a decrease of the excitation/inhibition balance in V1 (Figure 9f, $p = 0.018$). Then, we analyzed the fluorescence intensity of synaptic puncta (Figure 9g). We found that visual deprivation produced a decrease in the fluorescence intensity of both VGAT ($p = 0.018$) and VGLUT1 ($p = 0.0019$) immunoreactive puncta, whereas the intensity of those expressing SYN was significantly increased ($p = 0.002$).

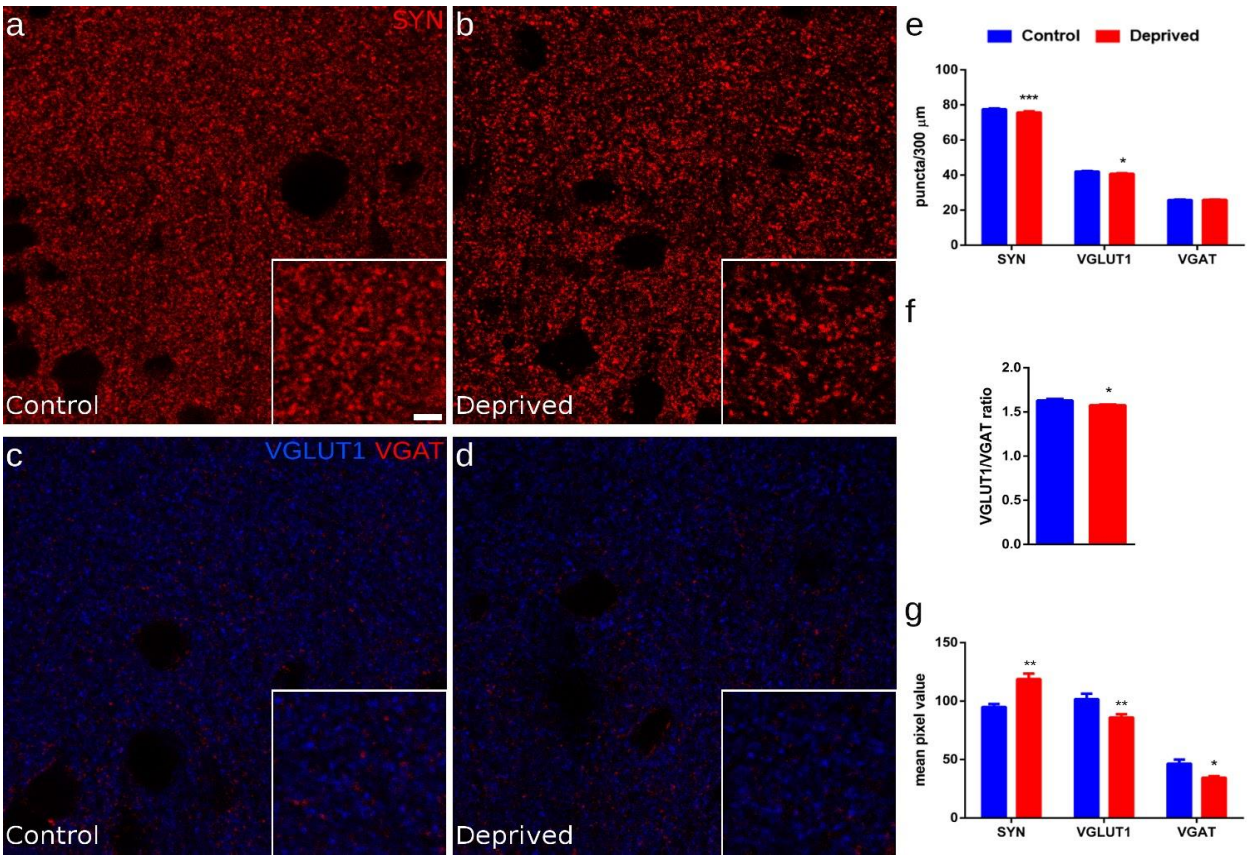

Figure 9. Effects of visual deprivation on the expression of synaptic molecules in the mouse V1. Single confocal planes showing the expression of synaptophysin **a)** and **b)** and the vesicular transporters of glutamate (VGLUT1) and GABA (VGAT) (**c** and **d**) in control and deprived animal. Insets in the lower right corner of the microphotographs are enlarged views of the neuropil. Graphs showing the density of SYN, VGLUT1 and VGAT **(e)** immunoreactive puncta, the ratio of VGLUT1/VGAT puncta **(f)** and the fluorescence intensity of SYN, VGLUT1 and VGAT **(g)** immunoreactive puncta. P-values *<0.05, **<0.01, *** <0.001. Scale bar: 12 µm, 3 µm for the insets**.**

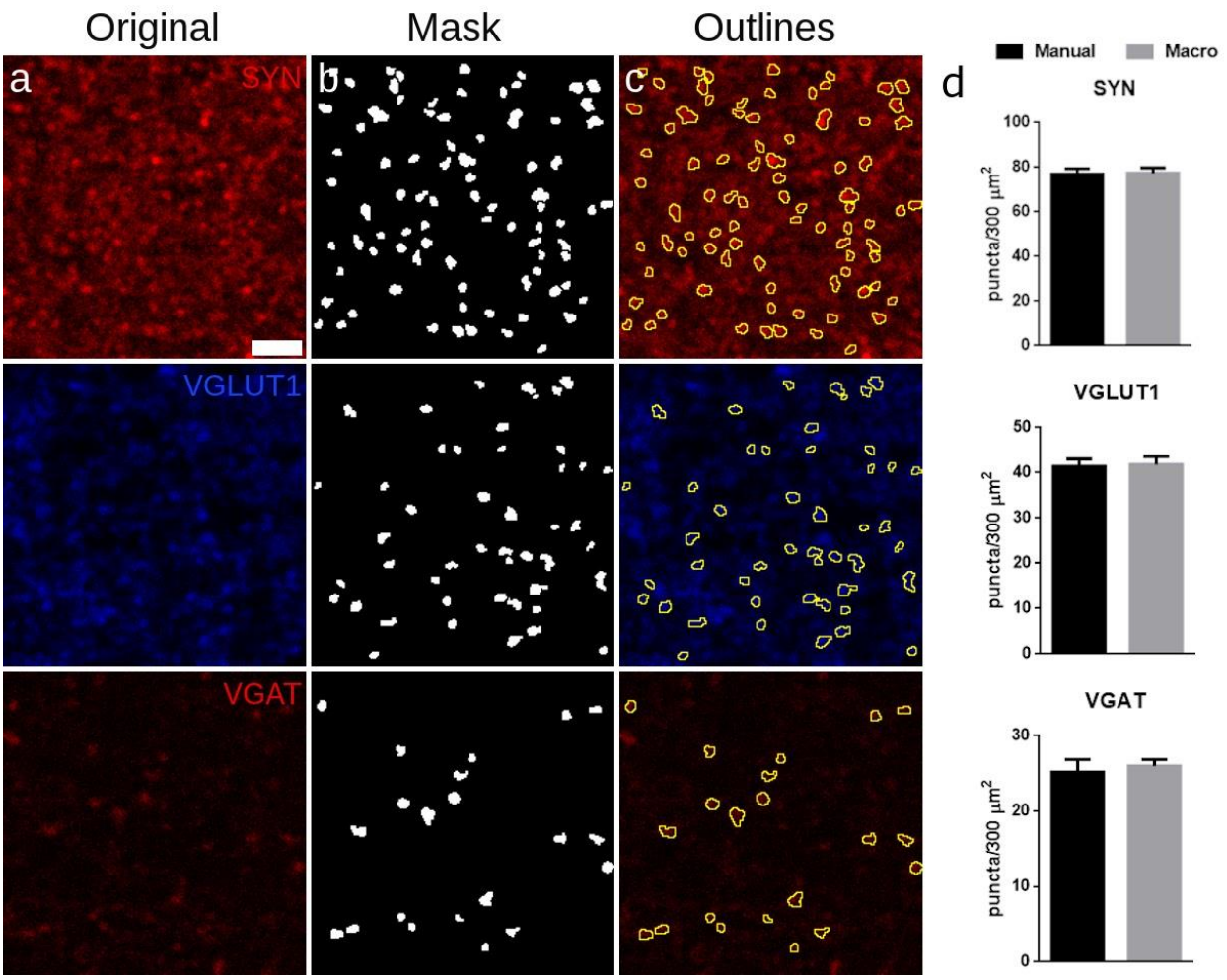

Figure 10. Validation of automatic immunoreactive puncta quantification. **(a)** Single confocal planes of SYN, VGLUT1 and VGAT. **(b)** Masks from the original images after macro processing using the top 2% pixel values as a threshold. **(c)** Outlines from masks overlapped on the original images. **(d)** Graphs showing the density of immunoreactive puncta of SYN, VGLUT1 and VGAT quantified by manual counting or macro processing. Scale bar: 3 µm.

Visual deprivation reduces the dendritic arborization, the density of mature dendritic spines and the size of axonal boutons of GAD67-EGFP expressing interneurons in the primary visual cortex

In order to analyze the impact of visual deprivation on the structure of interneurons on the V1 of GIN mice, we first determined the neurochemical phenotype of GAD67-EGFP expressing neurons in this cortical region (**Figure 11**) in order to confirm whether, as in other cortical regions, they were mainly Martinotti cells. We found that none of them expressed PV

(Figure 11a), excluding the possibility that they were PV+ basket or chandelier cells, but some of them expressed CR (52,92±3,45 **%**; Figure 11b) and CB (26,18±8,59%; Figure 11c). The vast majority of these interneurons expressed SST (88,63±8,34%; Figure 11d), but they expressed neither CCK (Figure 11e) nor PSA-NCAM (Figure 11f), confirming that they were mainly Martinotti cells. The other regions of the visual system pathway analyzed in this study, such as the LGN and the SC did not display GAD67-EGFP expressing somata, although an intense GAD67-EGFP positive axonal innervation could be observed in both structures.

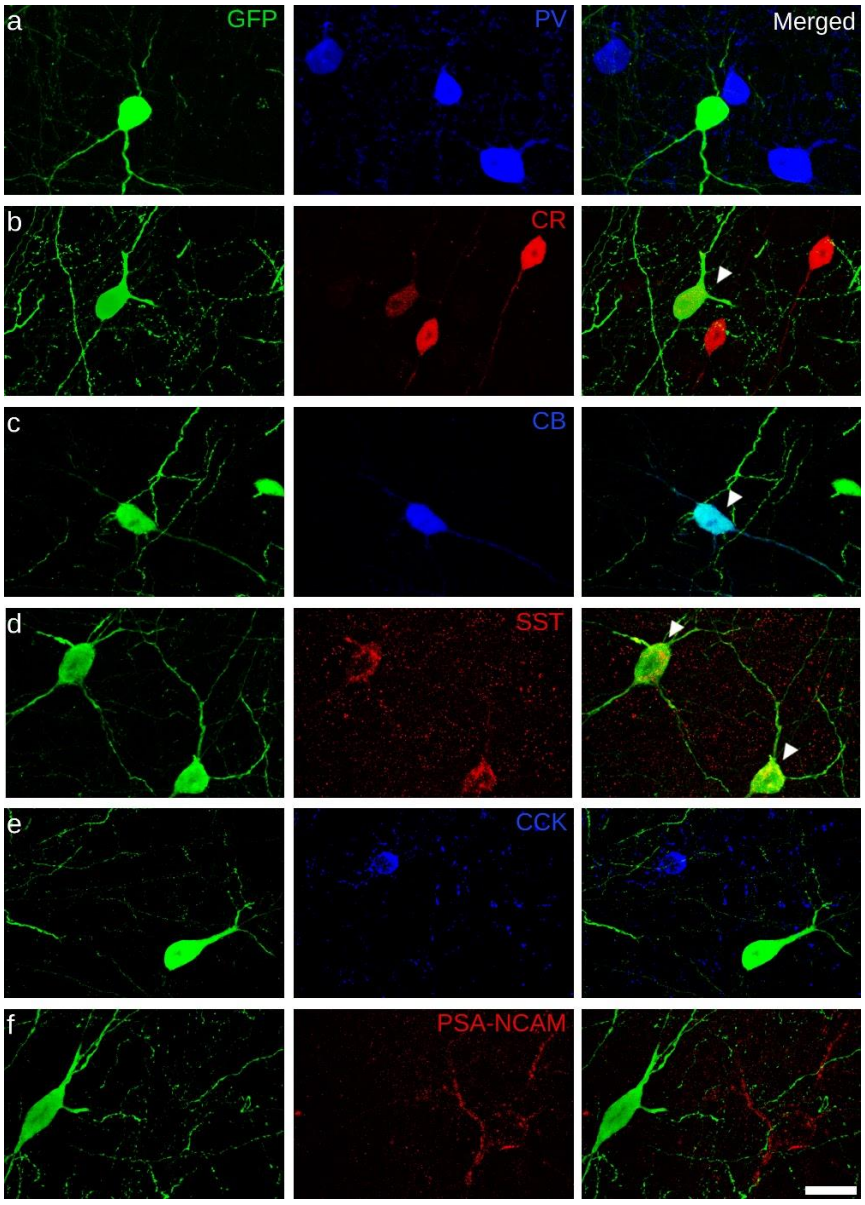

Figure 11. Neurochemical phenotype of EGFP-expressing cells in the V1. Double immunofluorescence against GFP and parvalbumin **(a)**, calretinin **(b)**, calbindin **(c)**, somatostatin **(d)**, cholecystokinin **(e)**, the polysialylated form of the neural cell adhesion molecule (PSA-NCAM) **(f)**. Arrowheads point to coexpressing cells. Scale bar: 20 µm.

To study the effects of visual deprivation on the structure of Martinotti cells (**Figure 12**), we used the Sholl method to analyze 3D reconstructions of their dendritic arborization (Figures 12a and 12b). The statistical analysis of data (Figure 12c) revealed specific and statistically significant changes in four of the spherical intersections (located every 20-µm from the center of the soma) analyzed. The 100 µm ($p = 0.01$), 120 µm ($p = 0.004$), 140 µm ($p = 0.007$) and 160 µm ($p = 0.009$) spheres showed a decrease in the number of intersections in interneurons of deprived animals when compared to controls, which indicates a decrease in dendritic complexity induced by visual deprivation.

We also analyzed the dendritic spine density in EGFP-expressing interneurons (Figure 12d and 12e), considering the different morphological types of spines. We did not observe differences in the total dendritic spine density (Figure 12f). Nevertheless, the analysis of the specific spine types revealed an increase in the density of stubby spines (Figure 12g) in the medial ($p = 0.002$) and distal dendritic segments of deprived animals ($p = 0.027$) and a decrease in mushroom spines in their distal segment (Figure 12h, $p = 0.031$). Moreover, we found a decrease in the density of thin spines in the distal portion of the dendrites of deprived animals (Figure 12i, $p = 0.025$).

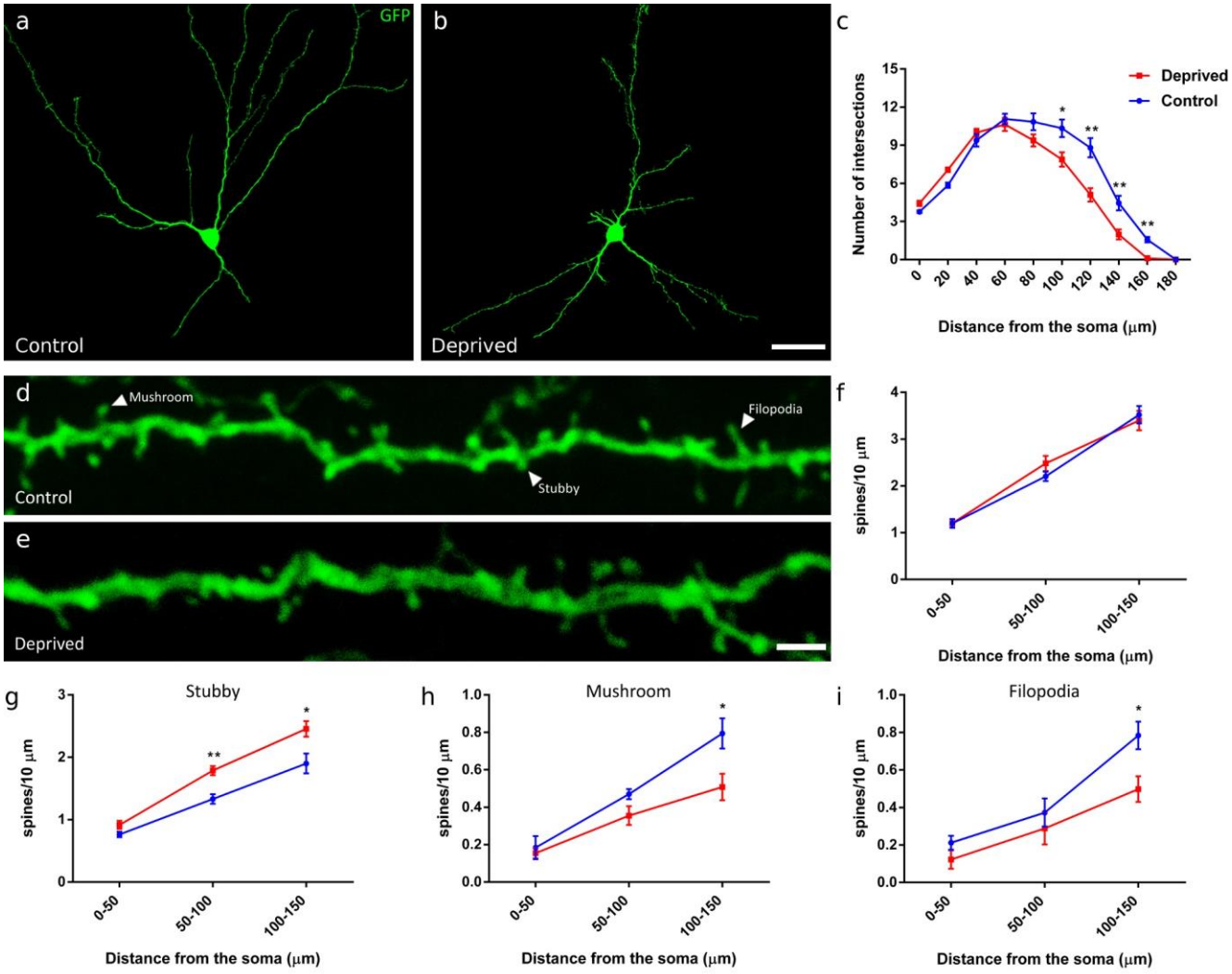

Figure 12. Effects of visual deprivation on the dendritic arborization and spine density of EGFP-expressing interneurons in the V1. Reconstruction of EGFP-expressing interneurons in the V1 of control **(a)** and deprived animals **(b)** and graph showing the results of the Sholl analysis **(c)** on the interneuronal reconstructions. Reconstruction of confocal planes showing a representative dendrite carrying spines of a EGFP-expressing interneuron of control **(d)** and deprived animals **(e)**. The arrowheads in d indicate the three types of spines considered in the study. Graphs showing the dendritic spine density per 50 µm segments **(f)** and the specific dendritic spine densities of stubby **(g)**, mushroom **(h)** and thin spines **(i)**. P-values *<0.05, **<0.01. Scale bar: 30 µm for A1 & A2 and 6 µm in B1 & B2.

In order to study whether there were also changes in the output of GAD67-EGFP neurons (**Figure 13**), we quantified the density of *en passant* boutons in EGFP-expressing axons in the layer I of V1 (Figure 13a and 13b), the major projection field of these interneuronal

subpopulation. Moreover, we also quantified the fluorescence intensity and size of axonal boutons, structural readouts of cortical reorganization by experience-dependent plasticity. No significant differences were found when comparing the deprived animals with their controls regarding the axonal boutons density (Figure 13c, p = 0.657). However, the fluorescence intensity of these boutons (Figure 13d, p = 0.0011) and their mean size (Figure 13e, p = 0.014) were significantly decreased as a consequence of visual deprivation.

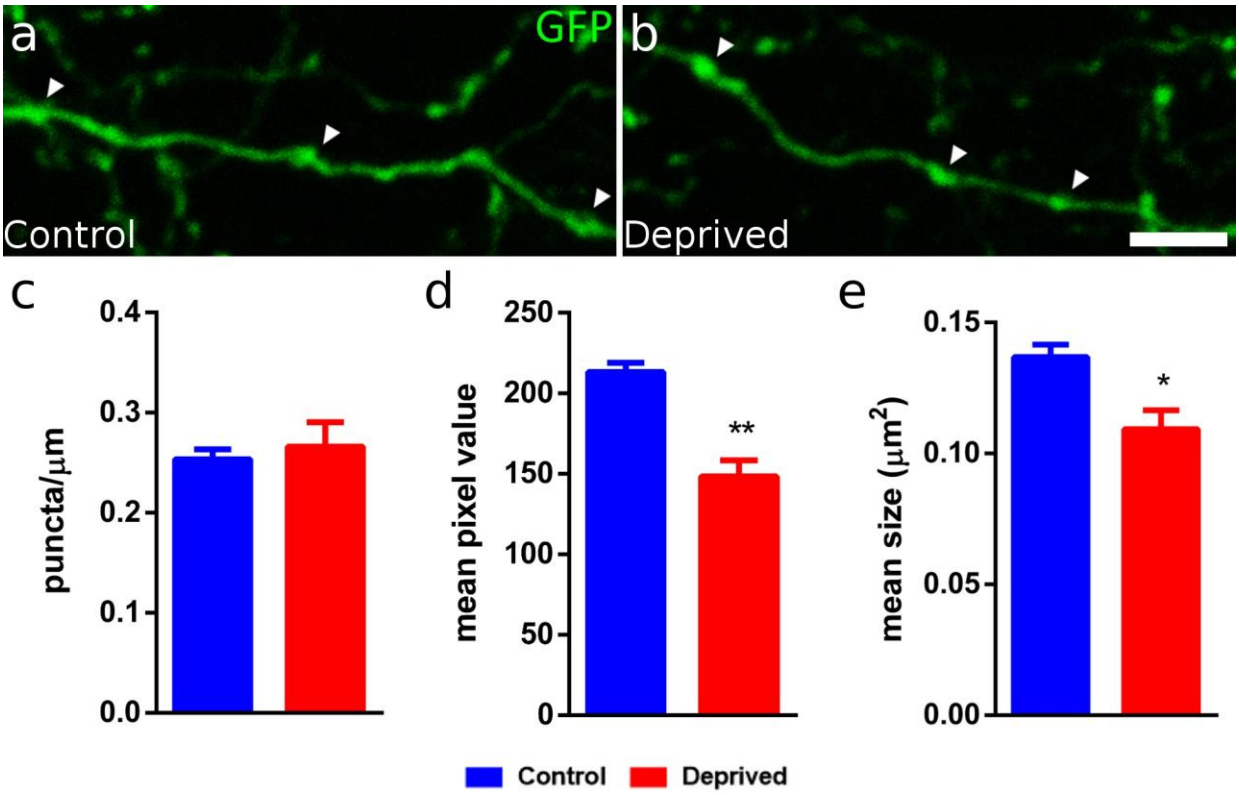

Figure 13. Effects of visual deprivation on *en passant* axonal boutons of EGFP-expressing cells in the layer I of the V1. Reconstruction of a EGFP-expressing interneuronal axonal fragment in the layer I of the V1 of control **(a)** and deprived **(b)** animal. Arrowheads point to axonal *en passant* boutons. Histogram showing the effects of visual deprivation on the density **(c)**, the fluorescence intensity **(d)** and the mean size **(e)** of *en passant* boutons. Scale bar: 2.5 µm.

Visual deprivation reduces the expression of PSA-NCAM and alters the PNNs in the primary visual cortex

Considering most of PSA-NCAM expressing cells in the adult rodent neocortex as SST+ interneurons, we investigated whether the structural plasticity observed in Martinotti cells could be mediated by PSA-NCAM (**Figure 14**). Therefore,we analyzed the expression of PSA-NCAM in V1, analyzing both the number of PSA-NCAM positive cells (Figure 14a) and the density of positive puncta of the neuropil (Figure 14b and 14c). We found a significant decrease in both the number of PSA-NCAM immunoreactive cells (Figure 14d, $p = 0.046$) and the density of puncta (Figure 14e, $p = 0.005$). However, the fluorescence intensity of these puncta was not altered by visual deprivation. We also analyzed the density of PV-expressing interneurons in V1 (Figure 14g and 14h) and found a significant decrease in the deprived animals ($p = 0.018$, Figure 14i) when compared with their controls. These changes were not accompanied by significant changes in the density of PNNs or the ratio of PV-expressing interneurons surrounded by PNNs. In order to explore whether there were changes in the expression of PNNs, we studied the area covered by these structures and their mean fluorescence intensity. Although we did not find changes in the area covered by PNNs (Figure 14j), we found a significant increase in their fluorescence intensity ($p=0.022$) in the deprived group (Figure 14k).

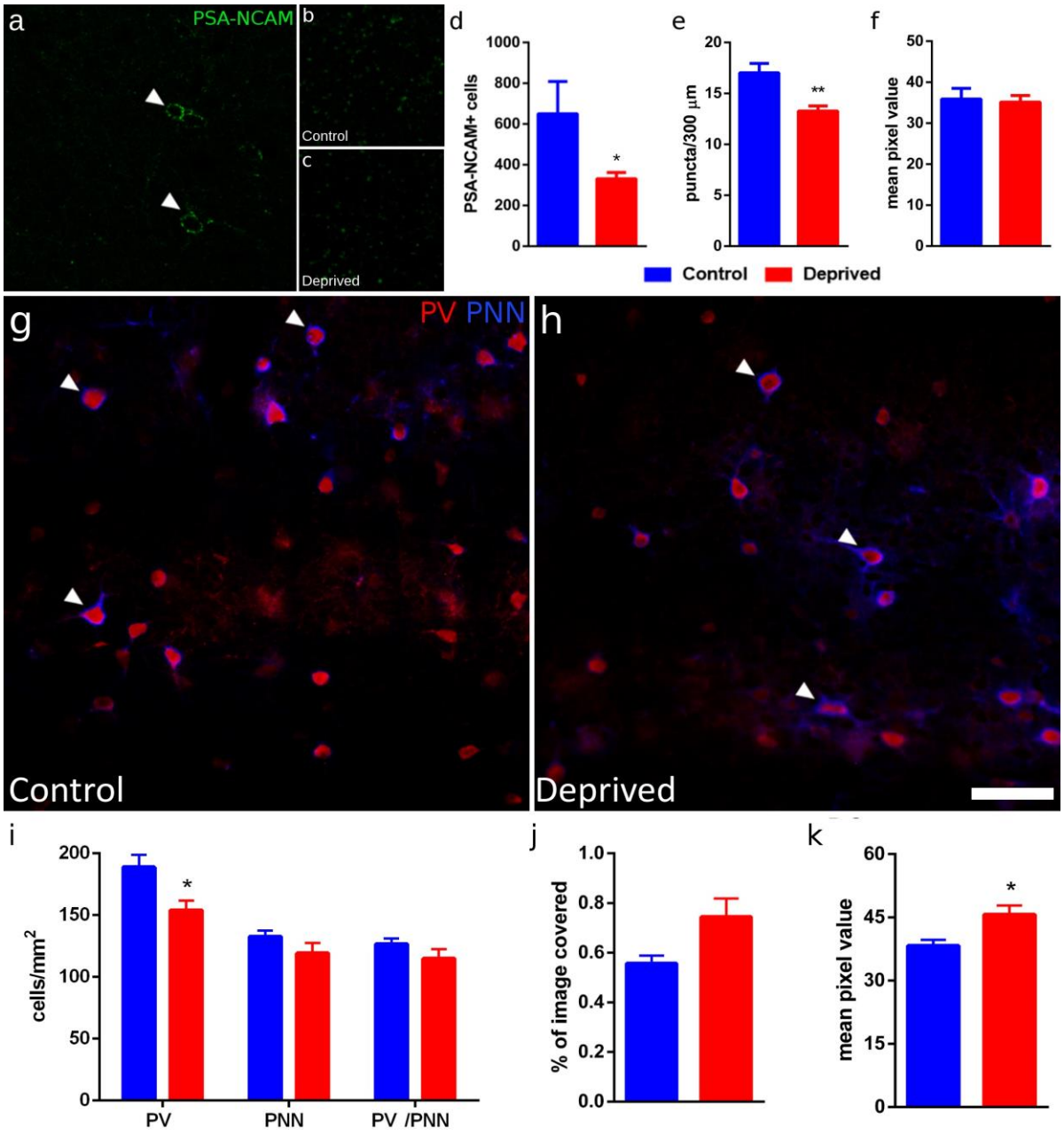

Figure 14. Expression of PSA-NCAM and PNNs in the mouse visual cortex and effects of visual deprivation. Representative confocal reconstruction showing the expression of PSA-NCAM in the V1 **(a)**. White arrowheads point to PSA-NCAM expressing cells. The insets displays a higher magnification of the neuropil of control **(b)** and deprived **(c)** animals. Graphs showing the total number of PSA-NCAM expressing cells **(d)**, the density of PSA-NCAM puncta **(e)** and the mean fluorescence intensity **(f)** in the neuropil. Confocal reconstructions of the V1 showing PV expressing interneurons and PNNs in the control **(g)** and deprived **(h)** animals. White arrowheads point to PV+/PNN+ cells. Graphs showing the density of cells expressing each marker **(i)**, the area of the image covered by PNNs **(j)** and their optical density **(k)**. P-values *<0.05. Scale bar: 50 µm and 5 µm for insets.

Visual deprivation does not change the density of inhibitory perisomatic puncta on pyramidal neurons in the primary visual cortex

As the main target of most PV-expressing interneurons is the perisomatic region of pyramidal cells, we carefully studied the inhibitory connectivity around the cell body of pyramidal neurons in the V1 (**Figure 15**). We studied the density of inhibitory puncta immunoreactive for PV (Figure 15a) and CB1r (Figure 15b) in the perisomatic region of pyramidal neurons (Figure 15c). No changes in their densities were observed in V1 after visual deprivation (Figure 15d). In order to analyze the characteristics of the inhibitory input from PV+ basket cells, we analyzed the density of perisomatic puncta expressing PV (Figure 15e) and their co-expression with the active synapse marker SYN (Figure 15f) and the plasticity-related molecule PSA-NCAM (Figure 15g) on pyramidal neurons (Figure 15h). However, we did not find any alteration in these parameters due to the visual deprivation (Figure 15i and 15j).

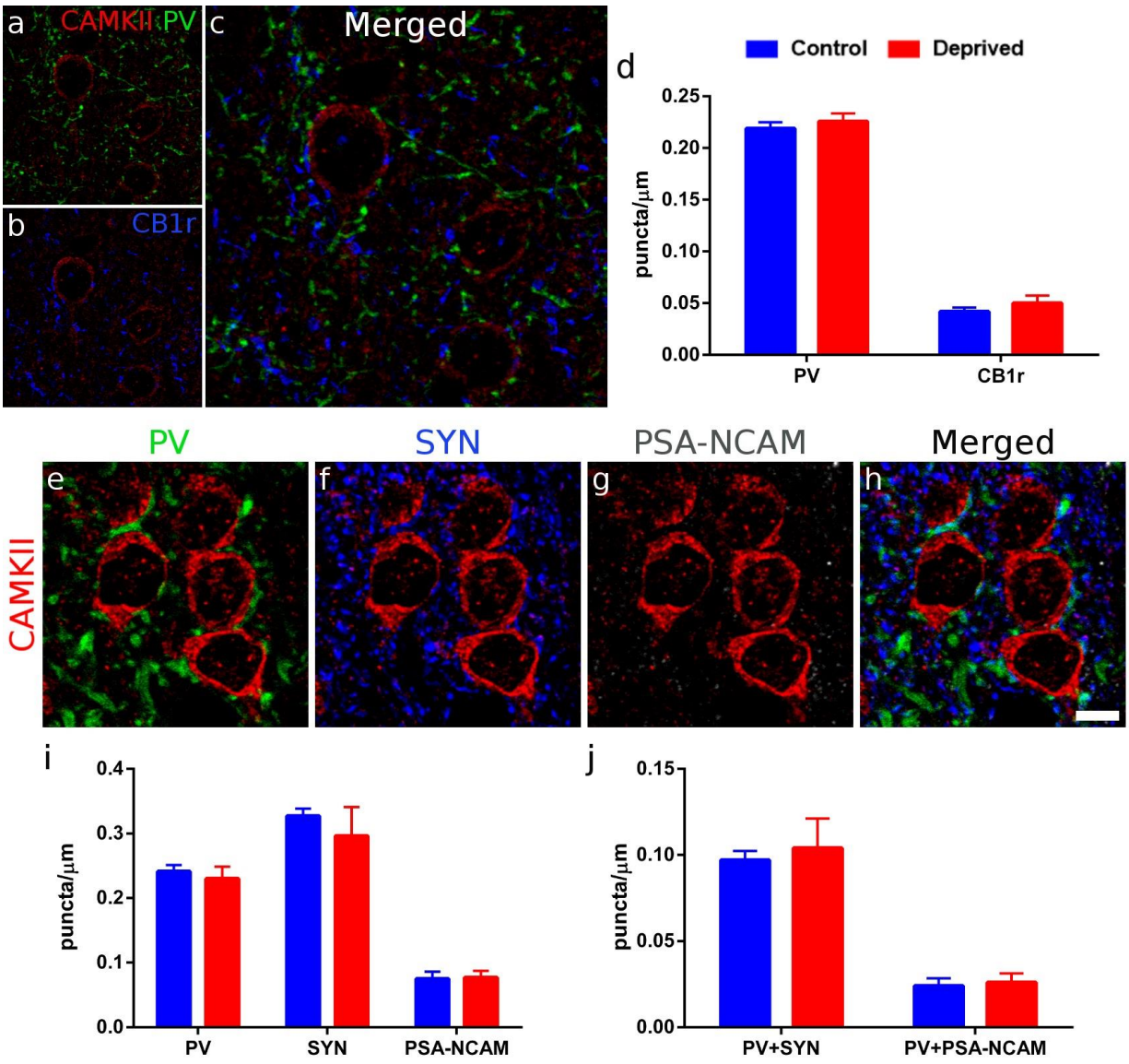

Figure 15. Effects of visual deprivation on the perisomatic innervation of pyramidal cells in the V1. Confocal reconstruction of representative perisomatic PV **(a)** and CB1r **(b)** inhibitory puncta on pyramidal cells marked with CAMKII **(c)**. Graph showing the density of PV and CB1r immunoreactive perisomatic puncta and the effect of the visual deprivation **(d)**. Reconstruction of representative parvalbumin **(e)**, synaptophysin **(f)** and PSA-NCAM **(g)** perisomatic puncta on pyramidal cells **(h)**. Graphs showing the density of PV, SYN and PSA-NCAM immunoreactive perisomatic puncta and the effect of the visual deprivation **(i)** and the colocalization of PV with SYN and PSA-NCAM **(j)**. Scale bar: 3 µm.

Visual deprivation alters the expression of different synaptic markers in the visual pathway

Similar to what we have described in V1, in the LGN (**Figure 16**), the analysis of the effect of visual deprivation revealed an increase in the optical density of SYN expression (Figure 16a and 16b), both in the dLGN ($p = 0.013$) and the vLGN ($p = 0.025$). It also produced an increase VGAT optical density (Figures 16c and 16d) in the vLGN ($p = 0.009$). However, we did not find any change in the expression of VGLUT1 after visual deprivation (Figures 16e and 16f). Similar to the effect of dark exposure in V1, the ratio between VGLUT1 and VGAT was significantly decreased in the vLGN ($p = 0.033$) (Figure 16g).

In the superior colliculus, we studied the synaptic markers SYN, VGLUT1 and VGAT in the superficial gray layer (SGL) and the zonal layer (ZL), those receiving visual input directly from the retina and indirectly from the dLGN. The analysis revealed an increase in the deprived animals of the SYN expression (Figures 16h and 16k) ($p = 0.0057$). However, the expression of VGLUT1 (Figure 16i) and VGAT (Figures 16j), as well as the ratio between them, were not altered by the visual deprivation.

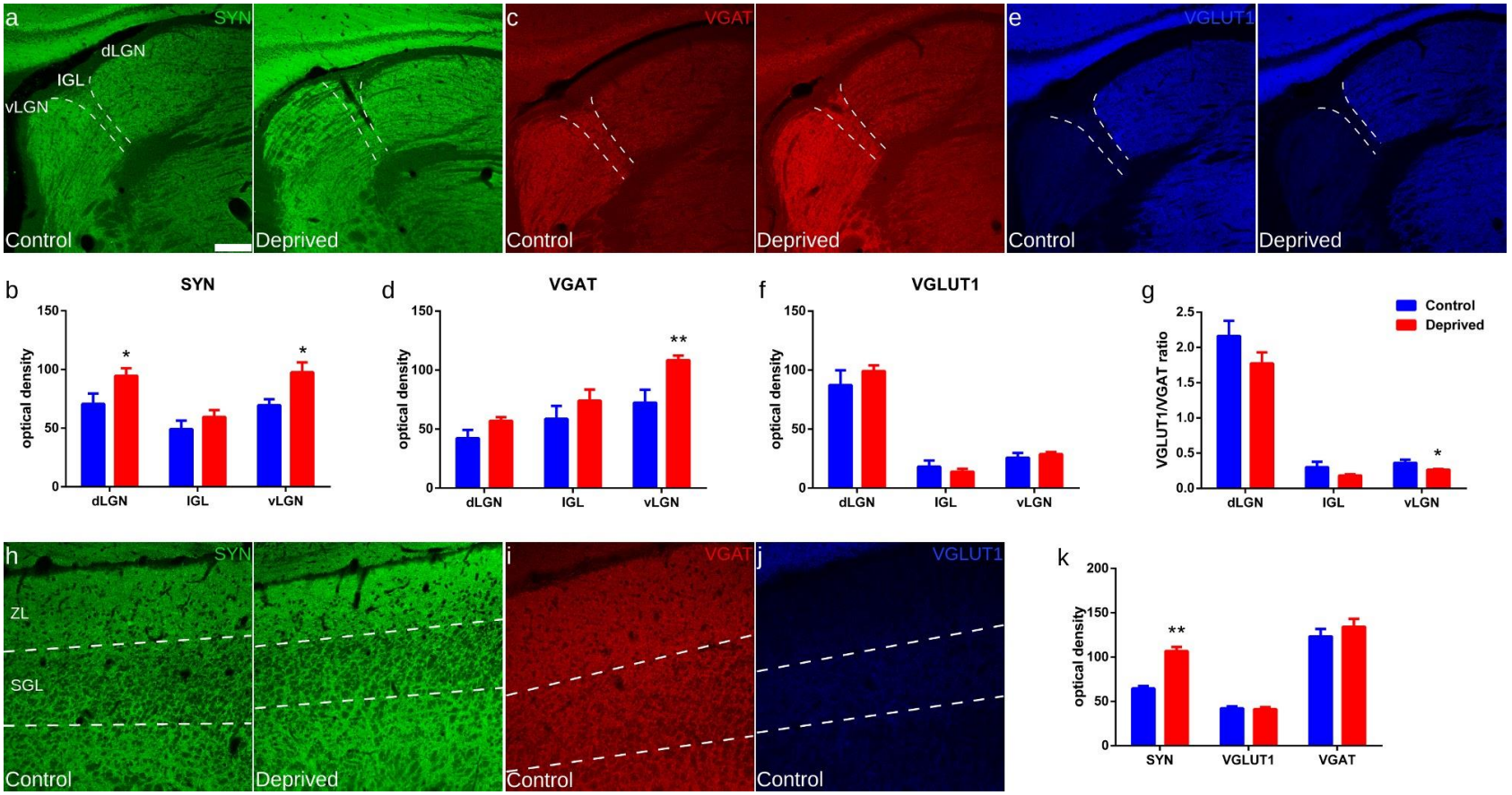

Figure 16. Expression of synaptic molecules in the extracortical nuclei of the visual system and the effects of visual deprivation. Lateral geniculate nucleus: Representative single confocal planes showing the expression of synaptophysin **(a)**, VGAT **(c)** and VGLUT1 **(e)**. The different areas of LGN are separated by dotted lines. Graphs showing the level of the expression of synaptophysin **(b)**, VGAT **(d)**, VGLUT1 **(f)** and the ratio VGLUT1/VGAT **(g)** in the lateral geniculate complex. Single confocal planes showing the expression of synaptophysin **(h)**, VGLUT1 **(i)** and VGAT **(j)** in the superior colliculus. Graphs showing the expression levels of synaptophysin, VGLUT1 and VGAT **(k)**. P-values *<0.05, ** <0.01. Scale bar: 100 µm for a, c and e; 50 µm for h, i and j.

Visual deprivation does not alter the distribution and the expression of plasticity-related molecules/structures in extracortical nuclei

We addressed the question of how plasticity-related molecules were distributed in the extracortical nuclei of the visual system and whether they were affected by visual deprivation. Therefore, we studied the expression of PSA-NCAM and the distribution of PV cells surrounded by PNNs in these nuclei (**Figure 17**).

Lateral Geniculate Complex

The distribution of PSA-NCAM in the LGN followed a clear pattern. The dLGN region showed a very low expression, while there was a high expression of this molecule in the IGL and the vLGN (Figure 17a). Regarding the distribution of PV expressing cells and PNNs, we found a dense axonal plexus expressing PV in the dLGN, but neither PV expressing cells nor PNNs were found in this region. This axonal plexus was markedly less dense in the IGL and vLGN, but we found PV expressing somata in the vLGN (Figure 17b and 17c). These PV expressing somata had a remarkable characteristic: those in the ventral part of vLGN were surrounded by both PNNs and PSA-NCAM (Figure 17b). On the other hand, those PV+ cells in the cluster of the dorsal part lack PNN coating while the PSA-NCAM expression was maintained (Figure 17c). Then, we analyzed the effects of visual deprivation on the expression of PSA-NCAM in the IGL and vLGN, but failed to find significant changes (Figure 17d).

Superior Colliculus

We found a wide distribution of PSA-NCAM expression in the sSC, observing immunoreactivity surrounding cell bodies and in the neuropil (Figure 17e). In the IGL, we found PSA-NCAM expression segregated in hubs. Regarding the presence of PV expressing cells and PNNs (Figure 17f), we found a spatial pattern similar to that described in the vLGN. The PV+ somata in the SGL were not surrounded by PNNs (Figure 17g), whereas in the IGL we found the vast majority of PV expressing cells surrounded by PNNs (Figure 17h). The visual deprivation had no effect on the expression of PSA-NCAM in the superficial layers of the SC (Figure 17i).

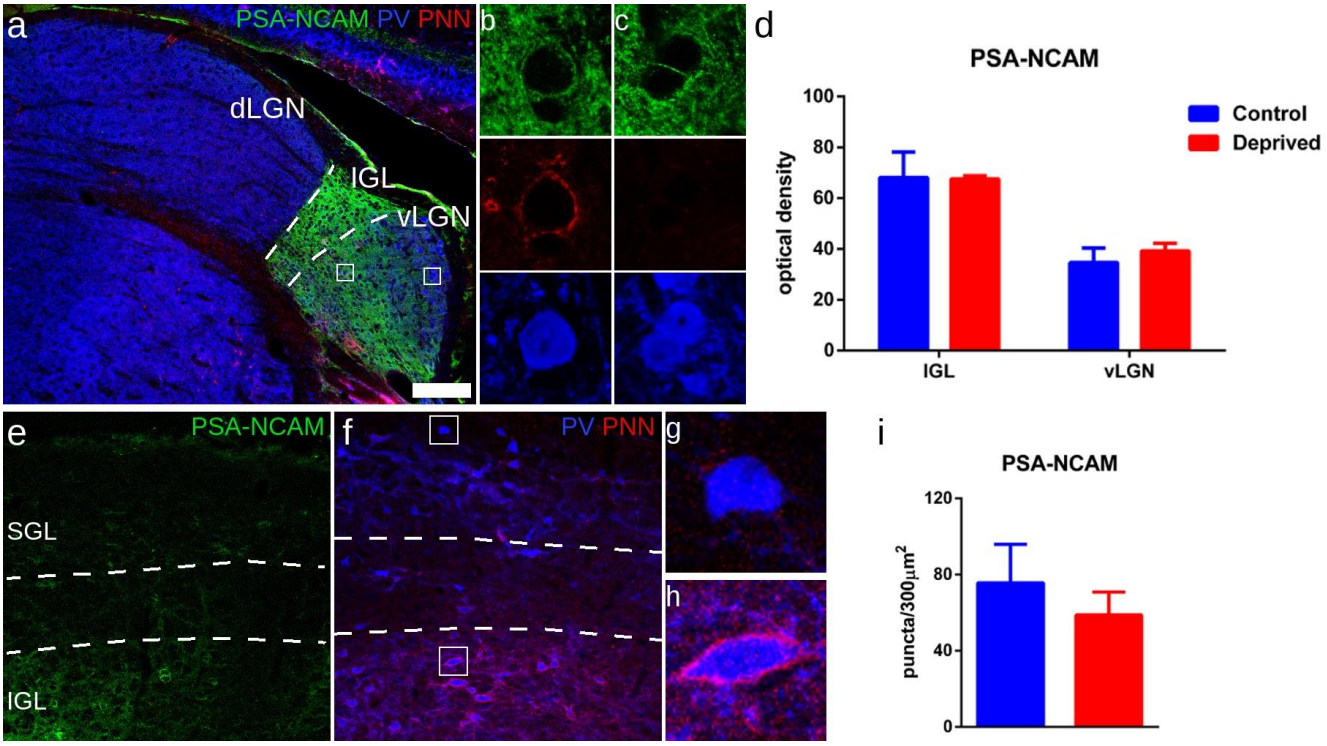

Figure 17. Effects of visual deprivation on PSA-NCAM expression and the presence of PNNs in the extracortical nuclei of the visual system. Lateral geniculate nucleus: Representative confocal reconstruction of the expression of PSA-NCAM, PV and PNNs **(a)** in the lateral geniculate complex. Insets showing higher magnification reconstructions displaying a parvalbumin expressing interneuron surrounded by PNN in the ventral region of the vLGN **(b)** and an example of a neuron in the dorsal region expressing PSA-NCAM but lacking PNNs surrounding it **(c)**. Graph showing the optical density of PSA-NCAM in the IGL and vLGN **(d)** Superior colliculus: Representative confocal reconstruction of the expression of PSA-NCAM **(e)** and a representative inset showing the area used for the analysis of the PSA-NCAM expression in the neuropil. Confocal reconstruction of the expression of PV and PNNs nets in the superior colliculus **(f)**. Insets show a SGL PV immunoreactive cell not surrounded by PNNs **(g)** whereas the PV expressing cell of the IGL express PNNs **(h)**. The dotted line indicates the limit between the superficial and intermediate gray layers of the superior colliculus. Graphs showing the density of the expression of PSA-NCAM in the lateral geniculate nucleus **(i)** and in the superior colliculus. Scale bars: 100 µm for 9, 50 µm for e and 10 µm for the insets b, c, g and h.

Experiment 2: Effects of the antidepressant fluoxetine on the somatostatin expressing interneurons in the basolateral amygdala

Expression of PSA-NCAM and GAD65/67

To study the effects of the chronic treatment with fluoxetine on the inhibitory circuitry of the BLA, we analyzed the expression of GAD 65/67 enzyme, the plasticity-related molecule PSA-NCAM, and the colocalization of both molecules (**Figure 18**): neuropil puncta expressing GAD65/67 and PSA-NCAM (Figure 18a and 18b). We found that animals treated with fluoxetine display a significant increase in the density of PSA-NCAM expressing puncta (p=0.008), but there were no significant changes in the density of GAD65/67 expressing puncta (Figure 18c). We also found that, in fluoxetine treated animals, the colocalization between PSA-NCAM and GAD65/67 was significantly increased (p=0.027), indicating that the increased expression of PSA-NCAM was associated to inhibitory neuropil elements (Figure 18c).

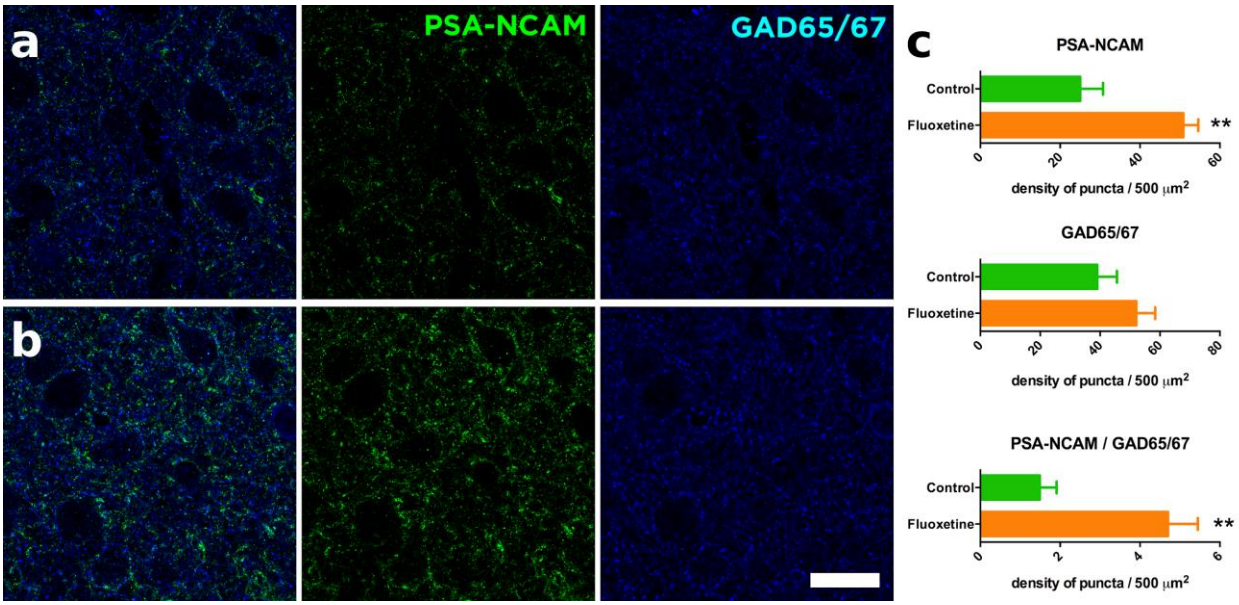

Figure 18. Fluoxetine increases the ratio of interneuronal neuropil surrounded by PSA-NCAM. Single confocal planes showing the expression of the polysialylated form of the neural cell adhesion molecule (PSA-NCAM) and Glutamic acid decarboxylase (GAD65/67) in both control animals **(a)** and treated with fluoxetine **(b)**. **(c)** Histograms showing the quantification of neuropil elements expressing PSA-NCAM, GAD65/67 and both molecules. *p-value < 0.05, **p-value < 0.01. Scale bar = 25 μm.

Distribution and neurochemical phenotype of the EGFP expressing cells

To better understand the effects of fluoxetine in the inhibitory networks of the BLA, we used a commercial transgenic mice expressing EGFP under the GAD promoter (**Figure 19**). This strain is characterized by restricted expression of EGFP in a subset of GABAergic neurons expressing SST. In the BLA, we found a scarce but well distributed population of EGFP interneurons. These cells were located mainly in the BLA and also in the boundaries between the basolateral and both the lateral and the basomedial amygdaloid nuclei (see asterisks in Figure 19a). We have analysed all EGFP interneurons in the BLA of 4 animals, and we have found that all these interneurons co-express SST (Figure 19b). Nevertheless, these EGFP cells only represent a fraction of all SST-expressing cells in the BLA.

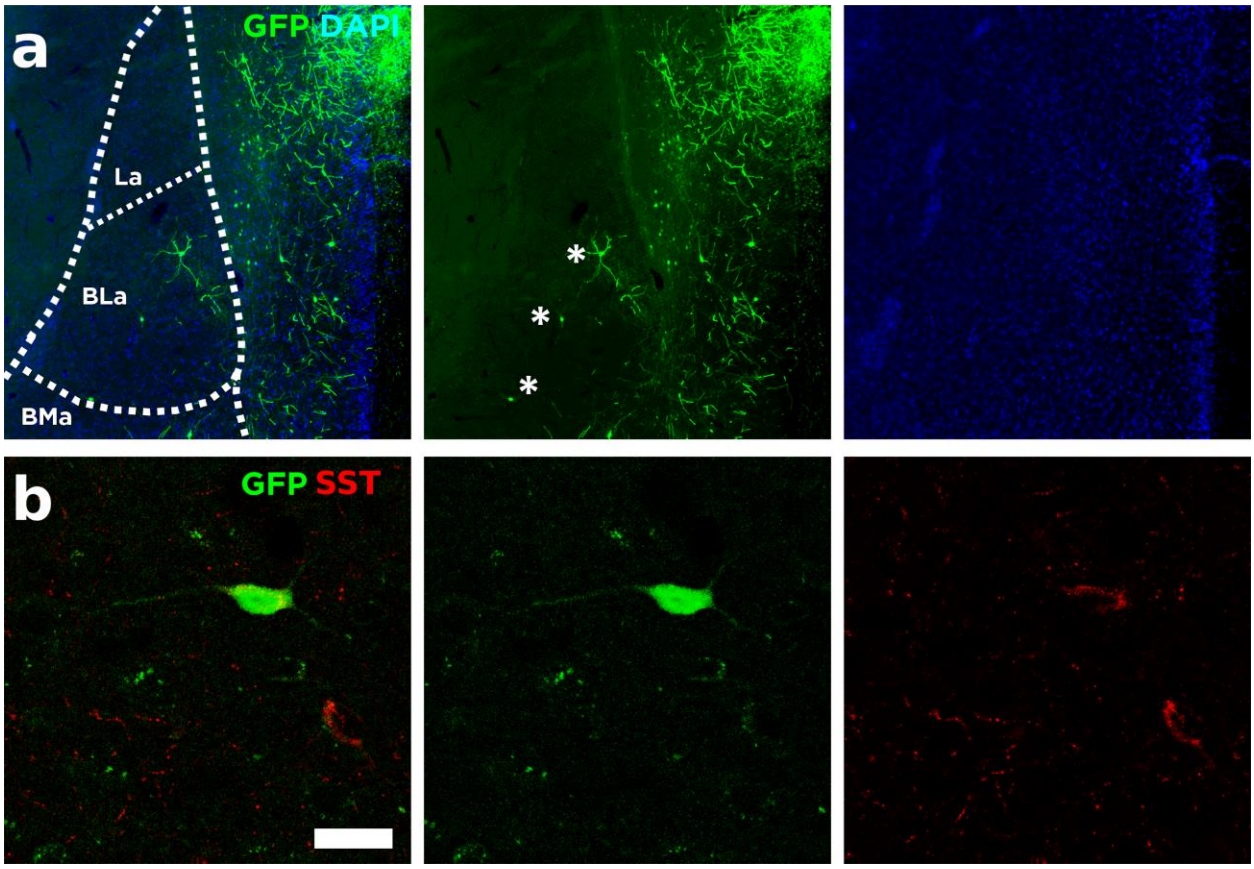

Figure 19. Neurochemical phenotype of EGFP neurons in the BLA. **(a)** Fluorescence microscope image showing the location of enhanced form of the green fluorescence protein (EGFP) neuron in green within the BLA and 4',6-diamidino-2-phenylindole (DAPI) in blue. **(b)**

Confocal plane showing an EGFP neuron expressing SST. Scale bar = 440 *μ*m in a and 30 *μ*m in b.

Effects of fluoxetine on the structure of EGFP expressing cells

We then analyzed the structural effects of fluoxetine on the EGFP expressing cells (**Figure 20**) by studying the morphology of dendritic spines and the density of axonal *en passant boutons* of these interneurons (Figure 20a and 20b). We found that fluoxetine produced an increase in the fraction of the stubby dendritic spines (p=0.029) and a decrease in the mushroom dendritic spines (p=0.019), whereas the fraction of thin dendritic spines remained unaltered (Figure 20c). Regarding the study of the axonal *en passant boutons*, we found a general decrease in their density in the animals treated with fluoxetine (p=0.010), as well as a decrease in the density of the larger axonal *boutons* (p=0.020) (Figure 20d).

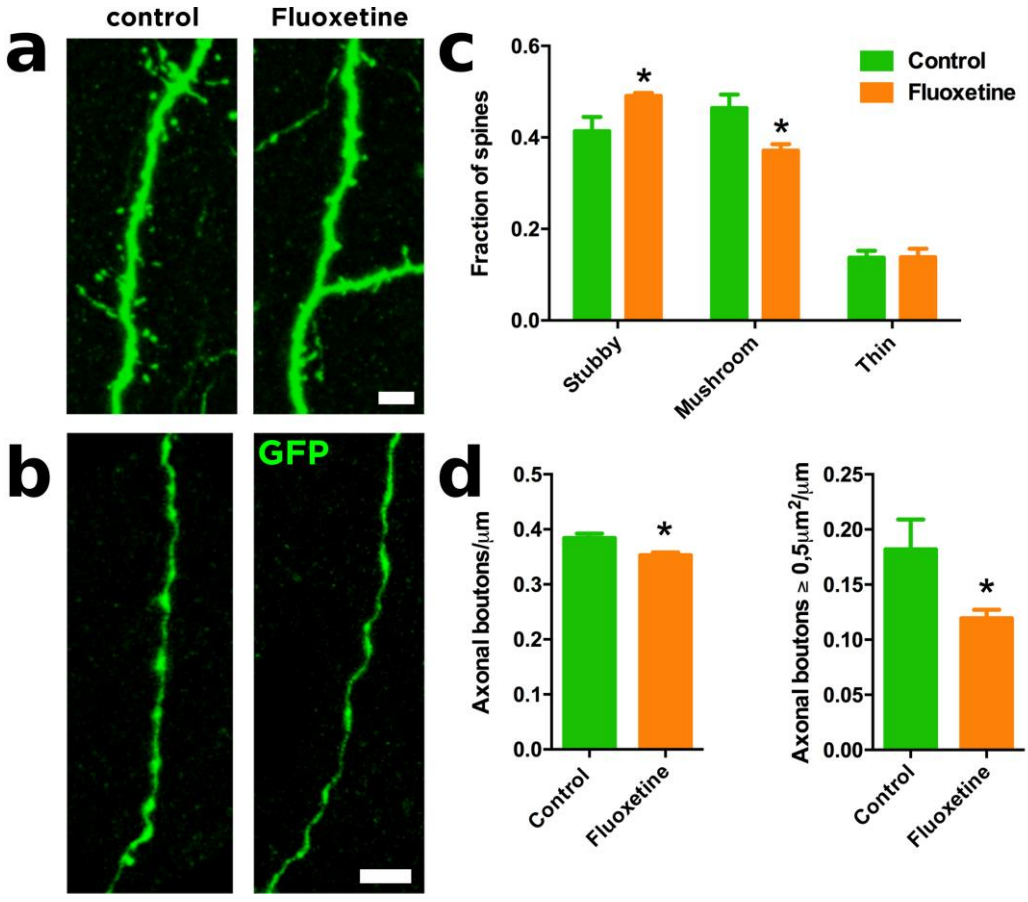

Figure 20. Structural remodeling in somatostatin interneurons produced by fluoxetine. **(a)** Confocal reconstructions of a dendritic segment showing spines of different morphology in control animals and treated with fluoxetine. **(b)** Confocal reconstructions of an axonal segment showing axonal *boutons* in both experimental groups. **(c)** Histograms showing the quantification

of the different dendritic spine morphologies. **(d)** Histograms showing the quantification of all axonal *boutons* and those with a total area greater than 0.5 microns2. *p-value < 0.05, **p-value < 0.01. Scale bars = 4 μm.

FosB expression

Finally, we analysed the effects of fluoxetine on the basal expression of the activity marker FosB (**Figure 21**). We studied the expression of FosB not only in the SST expressing interneurons (Figure 21g and 21h), but also in PV expressing interneurons (Figure 21e and 21f) and principal (CAMKII expressing) neurons of the BLA (Figure 21c and 21d). We found an increase in the expression of FosB within CAMKII+ (p=0.004) and PV+ neurons (p=0.029; Figure 21i). On the other hand, when we studied the SST expressing interneurons we found a significant decrease in fluoxetine treated animals (p<0.001*;* Figure 21i).

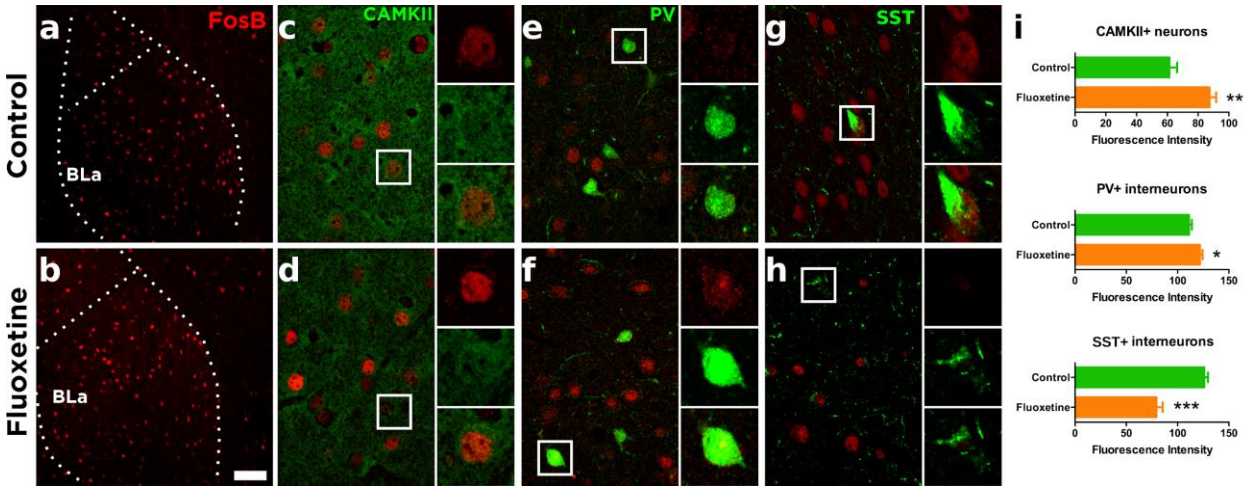

Figure 21. FosB expression in the BLA microcircuitry. Single confocal planes showing the expression of FosB in the BLA of **(a)** control animals and **(b)** treated with fluoxetine. Single confocal planes showing the expression of FosB in different neuronal subpopulations, such as excitatory neurons expressing CAMKII **(c** and **d)**, and interneurons expressing either PV **(e** and **f)** or somatostatin **(g** and **h)**. Histograms showing the quantification of FosB fluorescence intensity within these different neuronal subpopulations **(i)**. *p-value < 0.05, **p-value < 0.01, ***p-value < 0.001. Scale bar = 75 μm in **(a)** and **(b)**, 24 μm in the rest of the images and 10 μm in all the insets.

Experiment 3: Perineuronal nets regulate the inhibitory perisomatic input onto parvalbumin interneurons and gamma rhythms in the prelimbic area of the medial prefrontal cortex

The presence of PNNs influences the structure, immunoreactivity and connectivity of PV+ cells in the PrL

Considering the important role of PNNs in the maturation of the connectivity of PV+ interneurons, we wondered whether the presence of these specialized structures may influence their perisomatic input, PV expression and some structural characteristics. We compared PV expressing cells enwrapped by PNNs (PV+PNN+) with those that were not surrounded by this specialized region of the extracellular matrix (PV+PNN-) (**Figure 22** and **Figure 23**). All analyses were performed in PV+ cells located in deep layers (V and VI) of the PrL, where these interneurons were most abundant. We first studied the intensity of PV immunofluorescence as a readout of the expression of this calcium binding protein, finding PV+PNN+ cells more intense than PV+PNN- cells (Figure 22b, p= 0.0310). We also analyzed the intensity of WFA fluorescence in the PV+PNN+ cells and found a significant positive correlation between PV intensity and WFA intensity (Figure 22c, r= 0.5585, p< 0.0001). Then, we analyzed in detail the density of perisomatic synaptic puncta onto PV expressing cells. Regarding the puncta expressing markers of inhibitory synapses, we studied PV, VGAT (Figure 22d) and CB1r (Figure 23a). We found a significantly lower density of VGAT+ puncta (p= 0.046) and of puncta coexpressing VGAT/PV (p= 0.008, Figure 21e) but not of CB1r+ puncta (p= 0.980, Figure 23b). We also found a positive correlation between PV intensity and the density of VGAT+ inhibitory perisomatic puncta (Figure 22f, r= 0.3864, p= 0.0073). Regarding the study of perisomatic puncta expressing markers of excitatory synapses (Figure 22g), we did not find significant differences neither in the density of puncta from cortical origin (VGLUT1+, Figure 22h, p= 0.061) nor in that of puncta from extracortical origin (VGLUT2+, Figure 23c and 23d, p= 0.887). We then calculated the ratio between excitatory and inhibitory puncta (VGLUT1/VGAT) and we found an imbalance towards VGLUT1 in PV+PNN- cells when compared to PV+PNN+ cells (Figure 22i, p= 0.012). As a structural characteristic of their maturational stage, we studied the length of the AIS using Ankyrin G immunohistochemistry (Figure 22j) and found that it was significantly shorter in the PV+PNN- cells (P= 0.021, Figure 22k). Summarizing, PV expressing interneurons enwrapped by PNNs displayed a higher expression of PV in their somata, have a higher density of perisomatic inhibitory puncta and a longer AIS. We wondered then whether

any of these parameters could be also altered when PNNs were digested by ChABC in the adult mPFC.

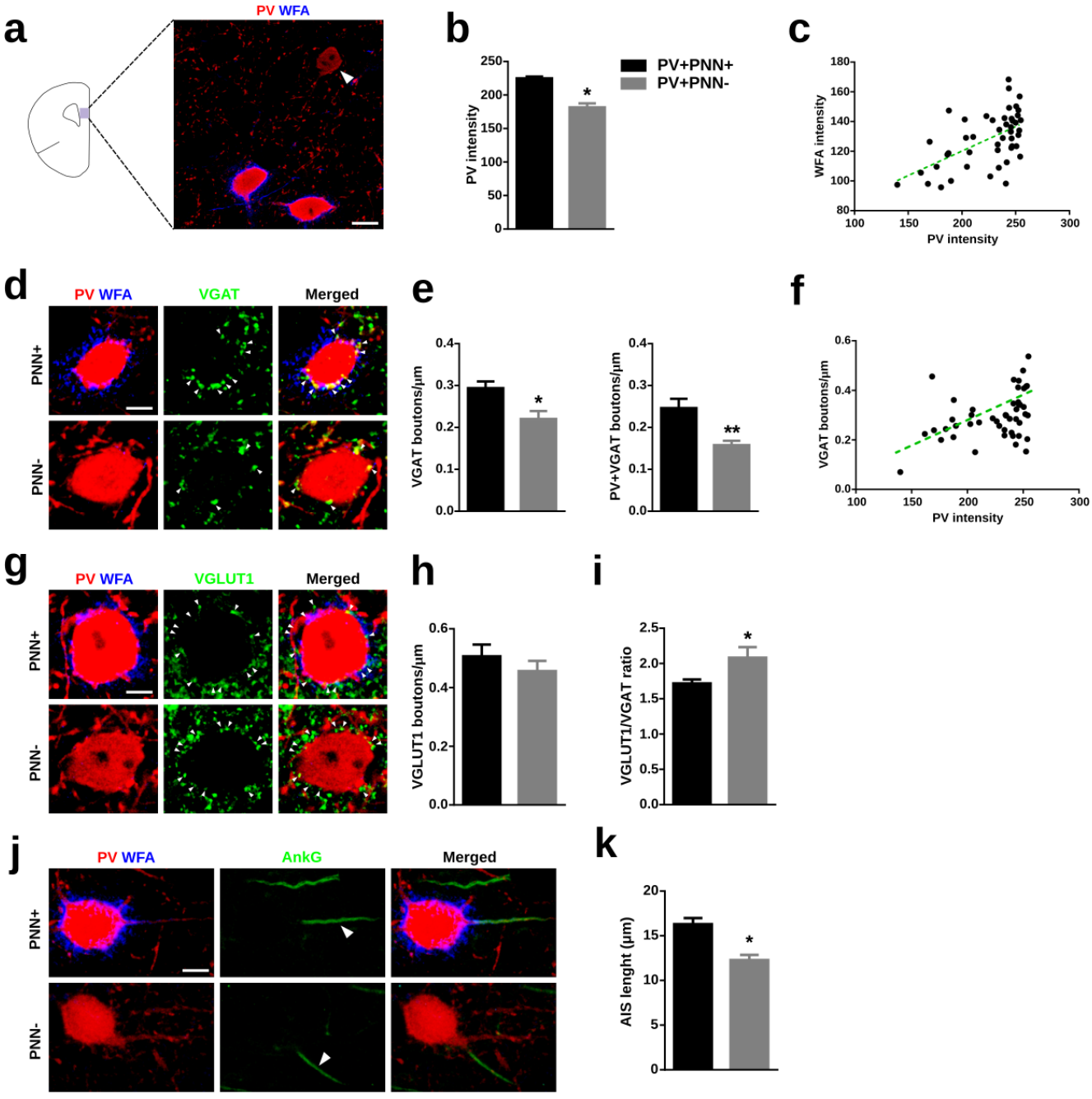

Figure 22. The presence or absence of PNNs surrounding PV+ interneurons influences PV expression in their somata and their perisomatic innervation. **(a)** Schematic drawing of a coronal slide, highlighting the area analyzed and a representative immunostaining of the expression of PV and WFA in PrL. The white arrowhead points to a PV+ cell lacking PNN. Scale bar, 10 µm.

(b) Graph showing the expression of PV in PV+ cells surrounded vs not surrounded by PNNs. **(c)** Distribution graph showing the positive correlation of PV fluorescence intensity and WFA fluorescence intensity. **(d)** High magnification single confocal planes comparing the inhibitory perisomatic innervation on PV+ cells depending on the presence or absence of PNNs. White arrowheads point to representative puncta. Scale bar, 4 µm. **(e)** Graphs showing the lower density of perisomatic puncta expressing inhibitory markers on PNN- PV cells. **(f)** Distribution graph showing the positive correlation of PV fluorescence intensity and density of inhibitory perisomatic puncta. **(g)** Single confocal planes of VGLUT1 expressing perisomatic puncta on PV+ cells. Scale bar, 4 µm. **(h**) Graph showing the density of VGLUT1+ puncta on the perisomatic region of PV+ cells. **(i)** Graph comparing the ratio of excitatory/inhibitory perisomatic puncta on PV+ cells. **(j)** Representative images of the AIS from PV+ cells. White arrowheads point to the AIS. Scale bar, 6 µm. **(k)** Graph comparing the length of the AIS in PV+ cells surrounded vs not surrounded by PNNs.

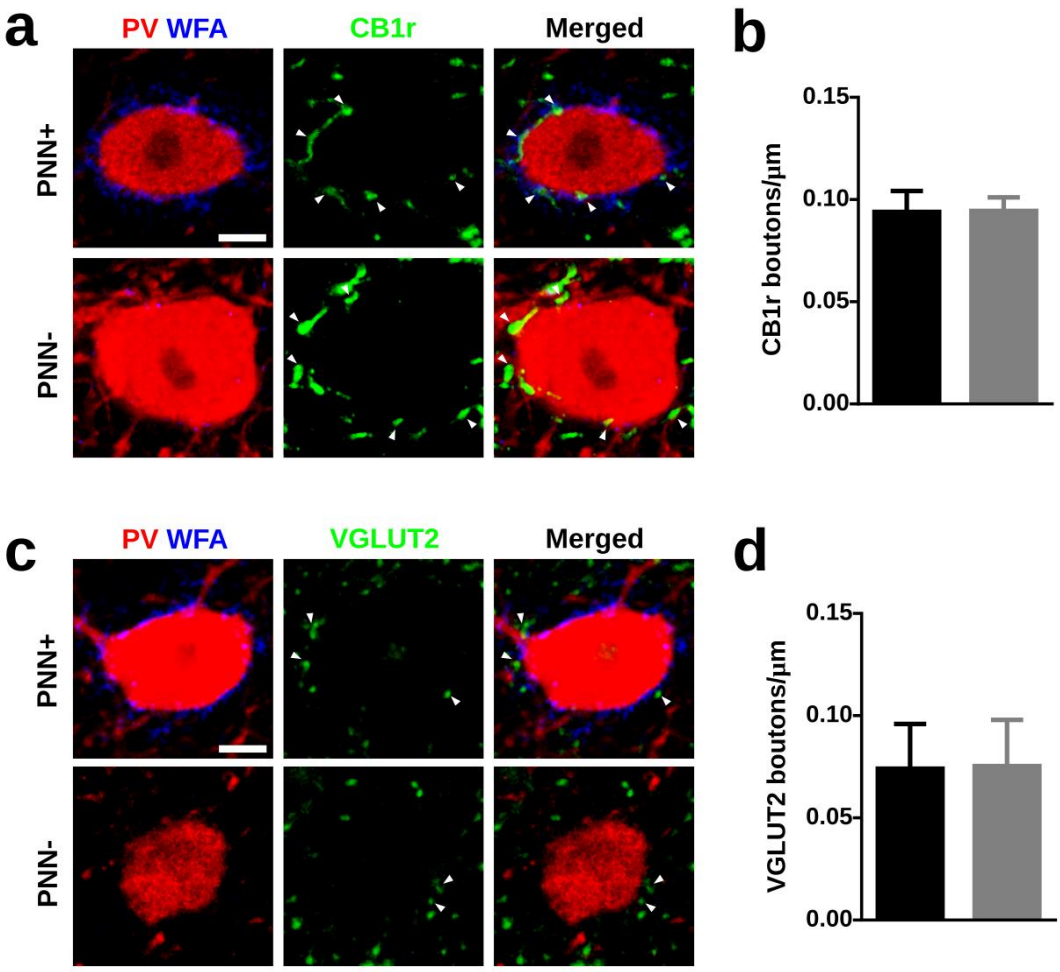

Figure 23. The presence of PNNs does not influence the density of perisomatic puncta coming from CCK+ basket cells or extracortical origin on PV+ interneurons. **(a)** Representative confocal planes showing CB1r immunoreactive perisomatic puncta on PV+ cells. Scale bar, 4 µm. **(b)** Graph comparing the density of CB1r expressing puncta on PV+ enwrapped by vs lacking PNNs **(c)** Single confocal planes showing the density of VGLUT2 expressing puncta on the perisomatic region of PV+ cells. Scale bar, 4 µm. **(d)** Graph showing the density of VGLUT2+ perisomatic puncta on PV+ cells, comparing those surrounded by PNNs vs those lacking these ECM structures.

Chondroitinase ABC depletes efficient, but transiently, the perineuronal nets in the medial prefrontal cortex

We analyzed the temporal progress of the depletion of PNNs after the intracerebral injection of ChABC (**Figure 24**), comparing it with the effects of the penicillinase injection (Figure 24a). Two days after the ChABC injection, we found a complete absence of WFA labeling in a large area covering all the mPFC extension (Figure 24b). This depletion was still evident 4 days after the ChABC injection. Nevertheless, after 6 days we found a slight recovery of WFA labeling in the perisomatic region of some cells. As our goal was to analyze alterations in the neuronal connectivity prior to the reappearance of PNNs, we set the histological and electrophysiological analyses 4 days after the injection of ChABC.

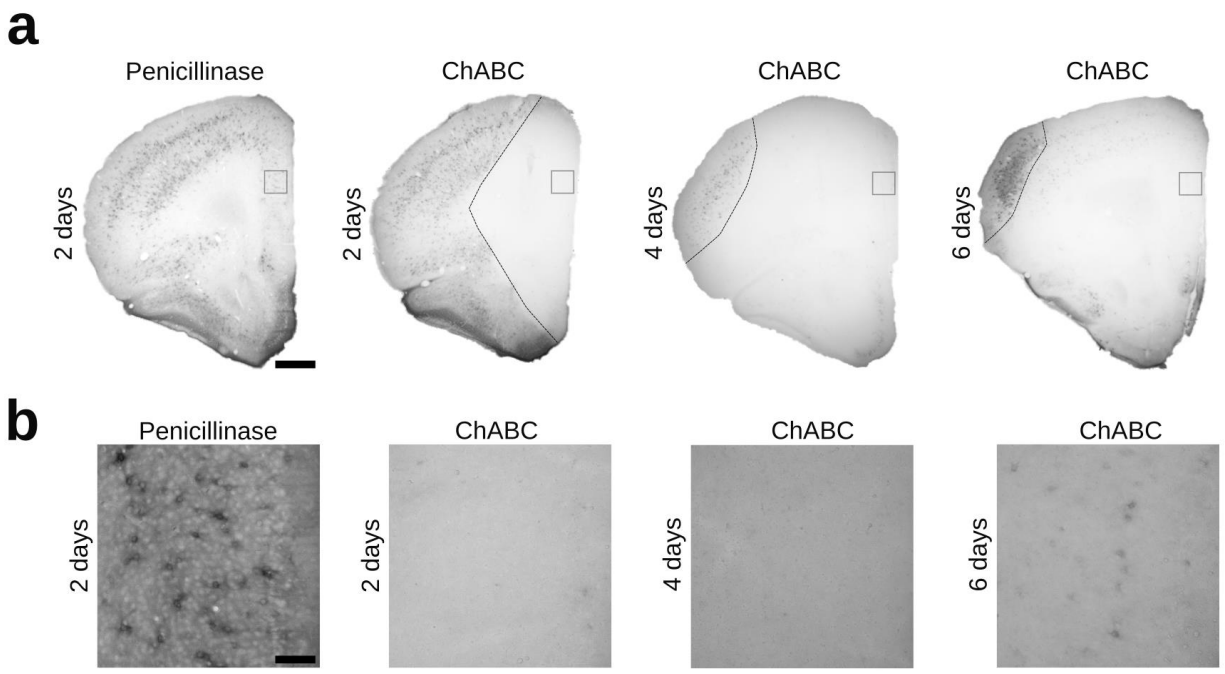

Figure 24. Timeline of PNNs digestion after the intracranial injection of ChABC revealed by WFA labeling. **(a)** Microphotographs showing labeled PNNs in the mPFC of control and ChABC injected mice. Dashed lines indicate the limits of ChABC effects. Scale bar, 300 µm. **(b)** Insets from the squares in PrL of figure **(a)** showing the digestion and the subsequent partial recovery of PNNs. Scale bar, 80 µm.

Effects of Chondroitinase ABC on PV expression and on the density of perisomatic puncta on parvalbumin expressing cells and pyramidal neurons

We studied the effects of ChABC on PV+ cells in the PrL (**Figure 25**). We quantified the intensity of PV fluorescence (Figure 25b) and we did not find differences in the ChABC treated animals when compared to controls (Figure 25c, p= 0.694).

Then, we studied the density of perisomatic synaptic puncta surrounding PV+ cells (Figure 25d). First, we studied the density of puncta expressing the general presynaptic marker SYN (Figure 25e) and we found a significant decrease in ChABC treated animals (Figure 25f, p= 0.0080). To better understand the origin of this decrease in synaptic puncta, we quantified the density of perisomatic puncta expressing excitatory (VGLUT1) and inhibitory (VGAT) presynaptic markers (Figure 25g). We found that ChABC produced a significant decrease in the density of VGAT+ puncta (p= 0.0162) but not in that of VGLUT1+ puncta (Figure 25h, p= 0.7700). We also found that this decreased density of inhibitory puncta most likely corresponded to those coming from from PV+ cells, since the density of perisomatic puncta coexpressing PV and VGAT was also decreased (Figure 25i, p= 0.0083). We analyzed the ratio of VGLUT1+/VGAT+ puncta and found an imbalance towards VGLUT1 in the perisomatic region of PV+ interneurons after ChABC injection (Figure 25j, p= 0.0181).

Next, we analyzed the synaptic puncta on the perisomatic region of CaMKII expressing pyramidal neurons (Figure 25k), in order to detect changes induced by ChABC treatment in the efferent connectivity of PV+ basket interneurons. We analyzed the effect of ChABC on the density of PV+ puncta (Figure 25l) and found that it remained unaltered after the treatment (Figure 25m, p= 0.3023). We analyzed CAMKII expression through the quantification of its fluorescence intensity in the cell body of pyramidal neuron somata. However, we did not find changes in this parameter (Figure 25n, p= 0.7269).

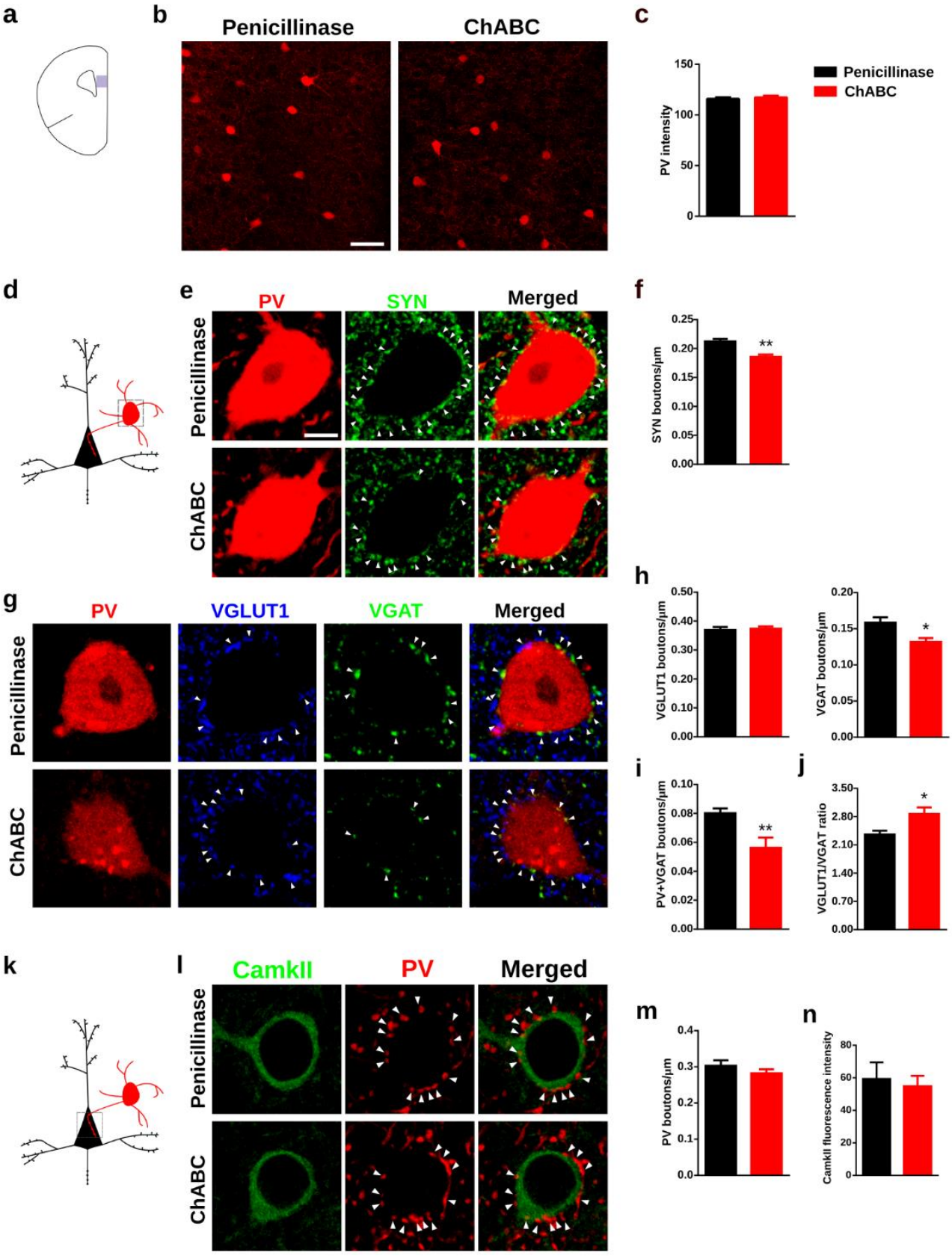
a
b
Penicillinase
ChABC
c
PV intensity
150
100
50
0
Penicillinase
ChABC
d
e
PV
SYN
Merged
Penicillinase
ChABC
f
SYN boutons/µm
0.25
0.20
0.15
0.10
0.05
0.00
**
g
PV
VGLUT1
VGAT
Merged
Penicillinase
ChABC
h
VGLUT1 boutons/µm
0.50
0.40
0.30
0.20
0.10
0.00
VGAT boutons/µm
0.20
0.15
0.10
0.05
0.00
*
i
PV+VGAT boutons/µm
0.10
0.08
0.06
0.04
0.02
0.00
**
j
VGLUT1/VGAT ratio
3.50
2.80
2.10
1.40
0.70
0.00
*
k
l
CamkII
PV
Merged
Penicillinase
ChABC
m
PV boutons/µm
0.4
0.3
0.2
0.1
0.0
n
CamkII fluorescence intensity
80
60
40
20
0

Figure 25. Effects of ChABC on PV expression and perisomatic puncta in the PrL. **(a)** Schematic drawing of a coronal slide, highlighting the area analyzed in **(b)**. **(b)** Representative confocal stacks of PV immunostaining in the PrL. Scale bar, 45 µm **(c)** Graphs showing that ChABC treatment does not alter the PV fluorescence intensity in the PrL. **(d)** Schematic drawing showing the area of analysis highlighted by a grey square. **(e)** Single confocal planes showing SYN expressing puncta (white arrowheads) surrounding the soma of a PV+ cell. Scale bar, 5 µm. **(f)** Graphs showing that ChABC treatment induces a decrease in the density of SYN expressing puncta on the perisomatic region of PV+ cells **(g)** Single confocal planes showing the density of excitatory (VGLUT1+) and inhibitory (VGAT+) perisomatic puncta (white arrowheads) on PV+ cells. Scale bar, 5 µm. **(h)** Graphs showing the ChABC induced decrease in the density of inhibitory but not excitatory puncta on the perisomatic region of PV+ cells. **(i)** Graph showing the significant decrease induced by ChABC on the density of puncta coexpresssing VGAT and PV in the perisomatic region of PV+ cells. **(j)** Graphs showing the ratio between the densities of VGLUT1/VGAT expressing puncta. **(k)** Schematic drawing showing the area of analysis highlighted by a grey square. **(l)** Single confocal planes showing PV expressing puncta (white arrowheads) on the perisomatic region of pyramidal neurons. Scale bar, 5 µm. **(m)** Graph showing the effects of ChABC treatment on the density of PV+ perisomatic puncta on pyramidal neurons. **(n)** Graph showing intensity of CamkII fluorescence in the cell body of pyramidal neurons.

We also analyzed the density of puncta expressing different synaptic markers in the neuropil of the PrL (**Figure 26**), in order to understand whether the effects observed in the perisomatic area were also extended to other regions (Figure 26a). We first studied the density of SYN+ puncta and did not find significant changes (Figures 26b and 26c, p= 0.7573). Likewise, the densities of VGLUT1+ and VGAT+ puncta were not altered by ChABC (Figures 26d and 26e, p= 0.482 and p= 0.221 respectively).

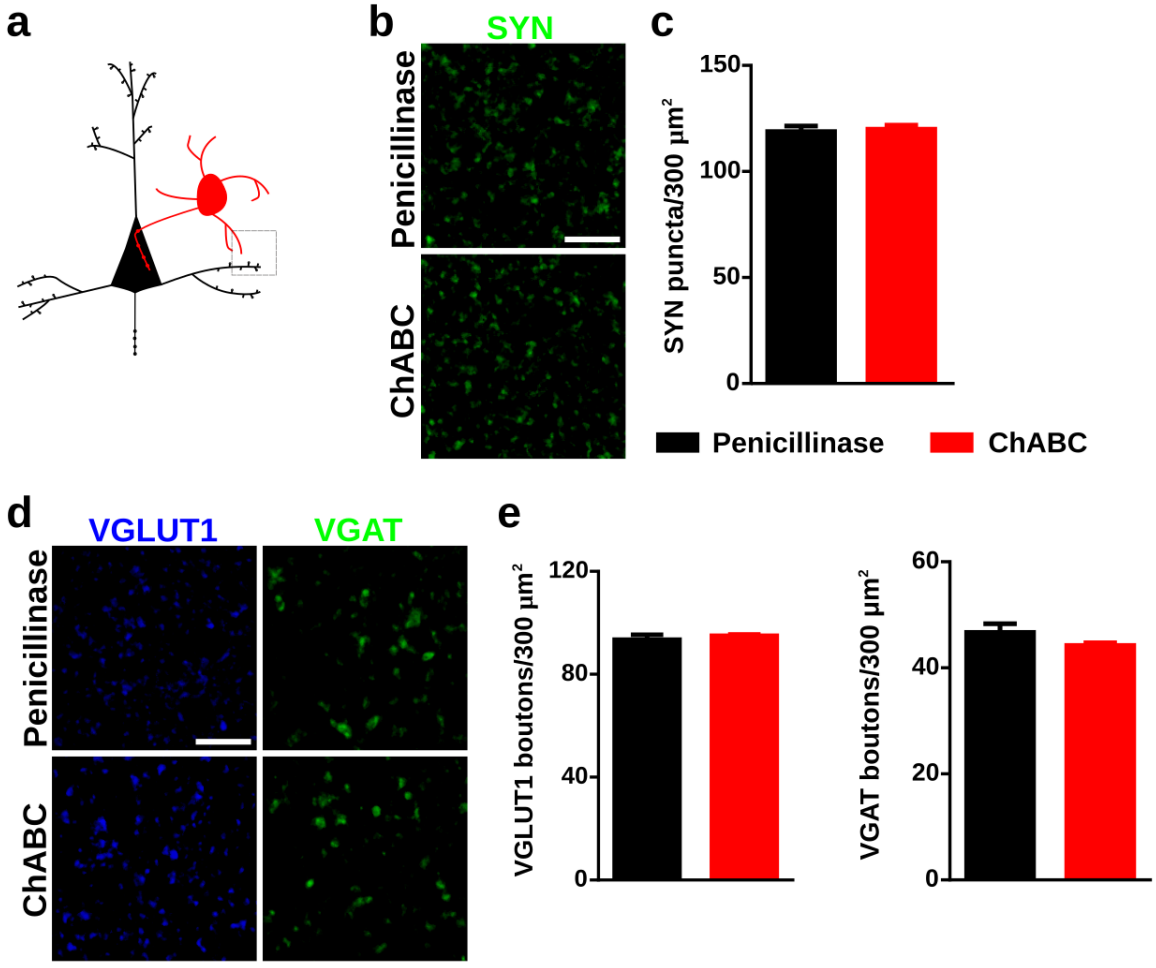

Figure 26. ChABC effects on the neuropil of the PrL. **(a)** Schematic drawing of the area imaged. **(b)** Representative confocal planes showing SYN expressing puncta in the neuropil. Scale bar, 6 µm. **(c)** Graph showing the effects of ChABC on the density of SYN+ puncta in the neuropil. **(d)** Representative confocal planes of VGLUT1+ and VGAT+ puncta. Scale bar, 6 µm. **(e)** Graphs showing the effects of ChABC on the density of VGLUT1+ and VGAT+ puncta.

ChondroitinaseABC affects the expression of the basal activity molecule FosB

We hypothesized that the effects of ChABC on the density of synaptic puncta described above may in turn affect the physiology of PrL circuits. Therefore, as an initial approach we analyzed the expression of the basal activity marker FosB (**Figure 27**) in PV+ cells and pyramidal neurons (Figure 27a). The injection of ChABC produced a significant decrease in of FosB expression (measured as the intensity of FosB immunofluorescence in the nuclei) in both PV+ cells ($P < 0.0001$) and pyramidal cells ($P < 0.0001$) when compared to that of penicillinase (Figures 27b and 27c).

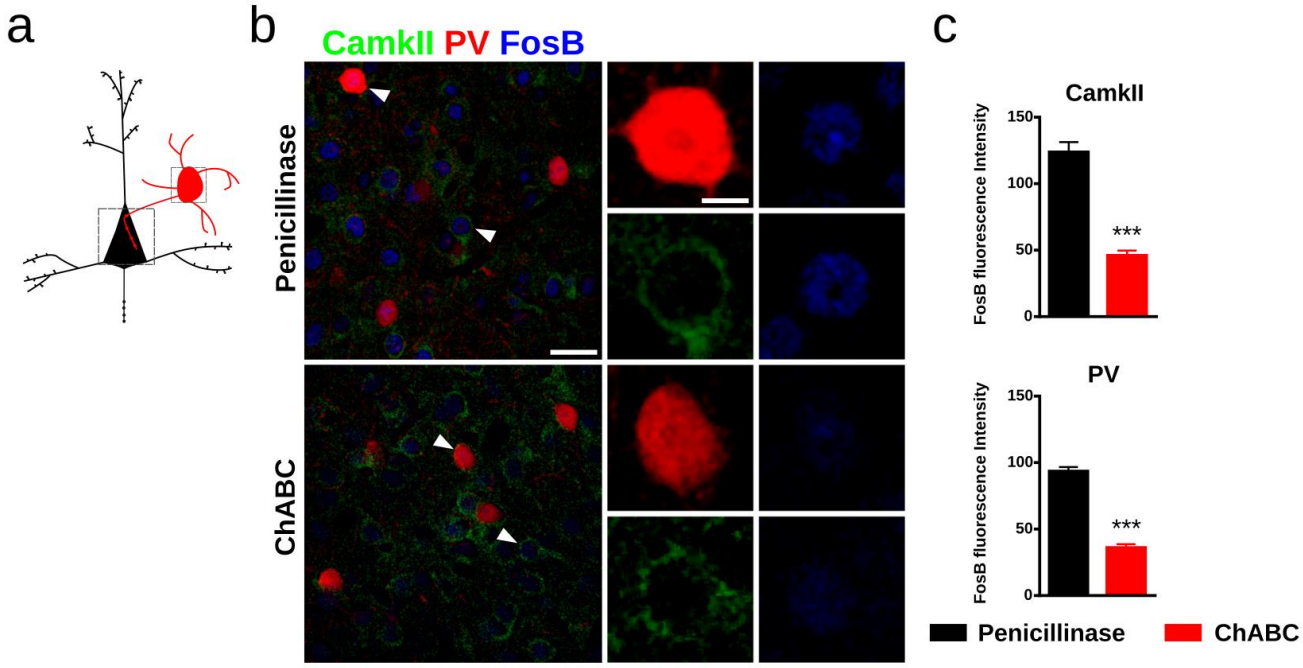

Figure 27. ChABC effects on FosB expression. **(a)** Schematic drawing of the area imaged: squares indicate the somata of PV+ (red) and pyramidal (black) cells. **(b)** 2D projection of a confocal stack (3 confocal planes) of the PrL, showing the expression of PV, CamkII and FosB. White arrowheads point to the somata shown in the higher magnification microphotographs on the right of the figure. **(c)** Graph showing the decrease of the FosB expression in PV cells and CamkII cells in the ChABC animals.

Chondroitinase ABC treatment decreases the gamma oscillations induced by tail-pinch

We examined whether the changes described in the density of perisomatic synaptic puncta on PV+ cells might affect the response of the local neuronal network under theta-elicited stimuli (**Figure 28**). Extracellular recordings were performed in PrL to register the response to a tail-pinch stimulation protocol. The tail-pinch was able to evoke theta rhythmicity, a distinctive oscillation representing the online state of the PrL (Figure 28a). The *grand average* (*n* = 5*)* of the power spectra of this stimulated epoch revealed a prominent differential peak in the high-theta range (Figure 28b). While the low-theta waves showed no significant changes under the effect of ChABC (*t* = 1.63, *p* = 0.11), the high-theta oscillations exhibited a significant increase (*t* = -2.68, *p* = 0.009) in the spectral power of the PrL recordings.

However, the most significant change in PrL activity was the decrease in gamma oscillations (Figure 28c, left), both in the high (*t* = 3.04, *p* = 0.003) and fast (t = 4.35, *p* = 6´10^{-5}) ranges (Figure 28c, middle), without significant changes in low gamma waves (t = -0.46, *p* = 0.65). To verify that the differences were not due to aberrant activity, the modulation index was calculated as a measure of theta-gamma coupling. No differences were found in control and experimental conditions (Figure 28c, right), indicating the presence of a decreased pattern between theta and gamma oscillations (*t* = 1.12, *p* = 0.26).

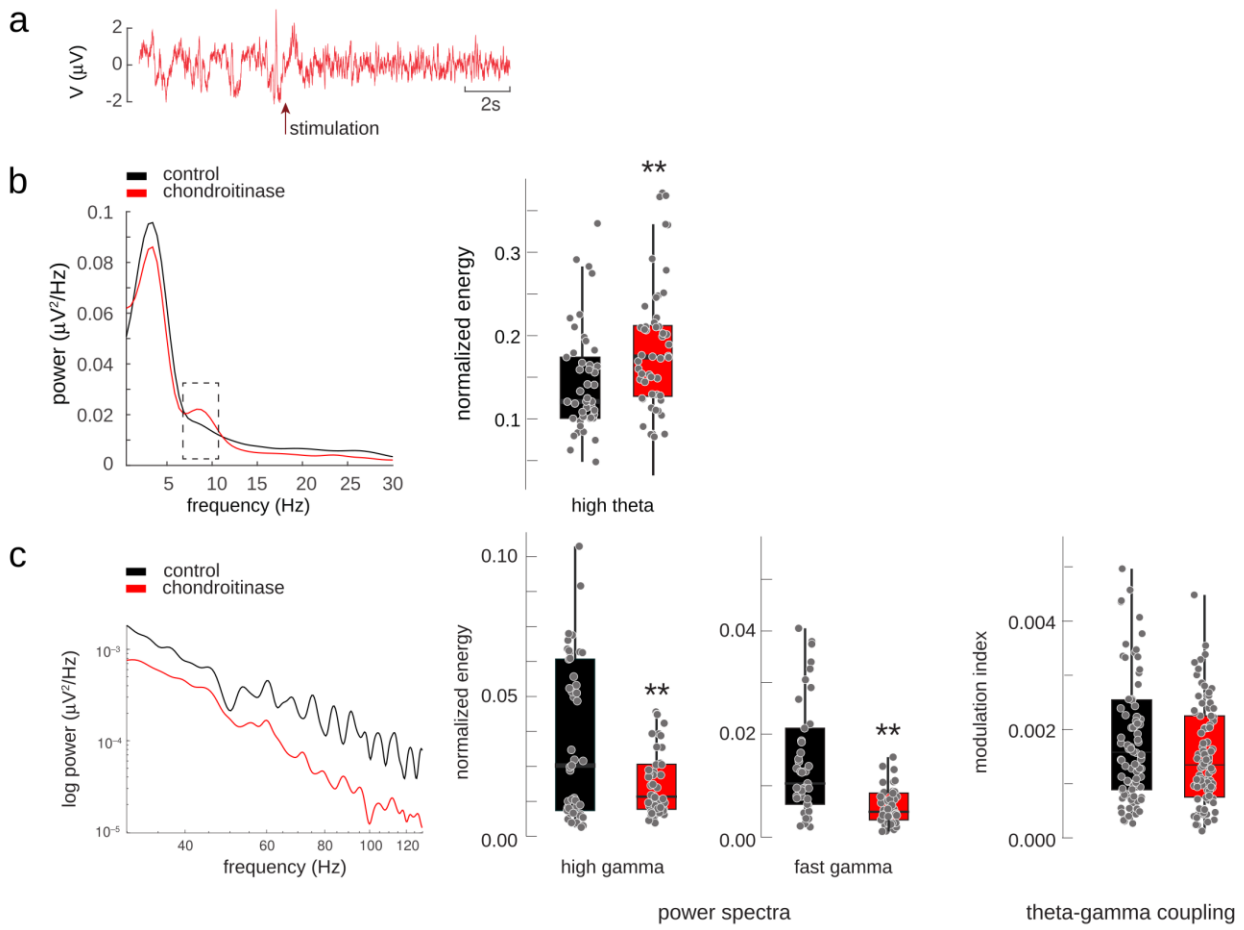

Figure 28. The enzymatic depletion of PNNs affects local field potential (LFP) oscillations in the PrL after tail-pinch stimulation. **(a)** Representative case of LFP recording in the PrL. The red arrow indicates the tail-pinch activation. A clear change is evidenced after the stimulation, with the presence of the theta rhythmicity as an activation pattern. **(b)** Grand average of the power spectra (left plot) in the low range of frequencies (0 -30 Hz). Both profiles maintain a similar pattern in the range of delta oscillations (0-3Hz), while the high theta oscillatory range (6-10Hz) shows a differential peak between the control and chondroitinase groups. This characteristic is statistically assessed with the comparison between both groups, validating an increase in power (normalized energy) of the high theta waves for the experimental group. **(c)** Grand average of the power spectra (left plot) in the gamma frequencies (30-140 Hz). Both distributions mark a clear decrease of the gamma power over the high and fast gamma range (≥ 60Hz) in the experimental group. The statistical analysis (middle plot) shows a significant decrease in both high and fast gamma rhythms. The theta-gamma coupling (right plot) remains unaltered.

V. DISCUSSION

Experiment 1. Dark exposure affects plasticity-related molecules and interneurons throughout the visual system during adulthood

In the present thesis, we have used dark exposure as an environmental manipulation to study the structural and molecular plasticity of inhibitory networks in the visual cortex of adult mice. We provide evidence that visual deprivation alters the structure and connectivity of different interneuronal subpopulations, as well as the expression of synaptic molecules in the neuropil of the V1. We have also described alterations in the expression of these molecules in the subcortical nuclei of the visual pathway. Finally, we show changes in plasticity-related molecules such as the components of PNNs and PSA-NCAM, which are known to mediate changes in interneuronal structure and connectivity in the adult cerebral cortex and may also participate in mechanisms underlying visual plasticity .

Synaptic molecules

First, we investigated whether dark exposure produced any alteration in the expression of presynaptic molecules in the visual cortex. We studied the expression of vesicular neurotransmitter transporters and the general presynaptic marker synaptophysin (Masliah et al., 1990). We found a decrease in the density of excitatory puncta, whereas inhibitory puncta remained unaltered. This specific decrease in excitatory puncta suggests a decrease of the excitatory/inhibitory balance of the visual cortex. We observed a decrease in SYN puncta density, which suggests a general decrease in the number of active synapses in the visual cortex as a result of the visual deprivation. Nevertheless, the fluorescence intensity disclosed counterintuitive results: VGLUT1 and VGAT fluorescence intensity decreased, suggesting a

reduction in neurotransmitters transport to synaptic vesicles as a consequence of the expected reduction of cortical activity after visual deprivation (Huang et al., 2015). Nevertheless, SYN fluorescence intensity increased, not only in visual cortex but in all the structures of the visual pathway analyzed, arising questions about the role of this protein in synaptic transmission. Although the lack of SYN induces soft behavioural alterations (Schmitt et al., 2009), this protein is not necessary for the formation of synaptic vesicles or neurotransmitter release (Eshkind and Leube, 1995; McMahon et al., 1996), suggesting a highly subtle function. On the other hand, other plasticity-inducing paradigm, environmental enrichment (Greifzu et al., 2014), induces an increase in SYN expression (Saito et al., 1994), suggesting a role for this protein in the efficiency of neurotransmission. Our results point to a scenario of decreased synaptic activity, revealed by the density of synaptic puncta. Nonetheless, the efficiency of synaptic transmission may be increased as a consequence of visual deprivation. It is interesting to note that VGLUT1 is only present in the synapses of excitatory cortical neurons and not in those of thalamo-cortical axons, which express VGLUT2. Given the alterations that we have observed in extracortical regions after visual deprivation, it would be very interesting to analyze also the density of VGLUT2 expressing puncta in V1 in future studies.

Previous studies have shown that other plasticity-inducing treatments decrease synaptic activity in the visual cortex, mainly by affecting the structure and connectivity of inhibitory (Keck et al., 2011; van Versendaal et al., 2012; Kuhlman et al., 2013) but also excitatory neurons (Keck et al., 2008). In this line, other studies have described reduced levels of synaptic activity specifically after the induction of ocular dominance plasticity by dark exposure in adult mice (He et al., 2006; Stodieck et al., 2014; Erchova et al., 2017). Therefore, our results on the density of different synaptic puncta support these previous results and the hypothesis of a decreased connectivity as a requirement for plasticity in the adult cerebral cortex.

Structure of EGFP-expressing interneurons

To further investigate the decrease in the expression of synaptic markers produced by dark exposure, especially those involved in inhibitory neurotransmission, we analyzed the structural features of interneurons by using a strain of transgenic mice expressing GFP under the GAD promoter. First, we confirmed that in the visual cortex, as in the other cortical regions analyzed previously in this strain (Oliva et al., 2000; Gilabert-Juan et al., 2013), these EGFP-expressing cells correspond mainly to Martinotti cells. Then, we analyzed their dendritic arborization by Sholl analysis and found a decreased complexity, especially in the distal

segments. In a similar way, retractions of dendritic branch tips have been previously reported applying dark exposure after monocular deprivation, specifically in layer II/III interneurons (Chen et al., 2011). Nevertheless, our study focuses on the Martinotti subpopulation, which spreads from layers II to IV. Moreover, the study of the dendritic spines of these interneurons revealed a significant decrease in the density of mushroom spines, while there was an increase in the density of the stubby spines. This decreased ratio of mature and consolidated dendritic spines (Adrian et al., 2017) is also consistent with the hypothesis of reduced connectivity as a consequence of dark exposure in the visual cortex. The decrease in the density of thin spines also suggests a shift in spine dynamics induced by dark exposure. Other studies have shown a similar decrease in the spine density of NPY expressing interneurons following visual deprivation in adult mice (Keck et al., 2011) and interestingly, some of these interneurons might co-express SST (May, 2006). Moreover, this decrease in spine density is followed by an increase in the dynamics of dendritic spines in the apical dendrites of pyramidal neurons (Keck et al., 2008). This supports the idea that dendrite-targeting interneurons are key players in the visual plasticity during adulthood and that probably respond earlier than excitatory neurons to plastic changes (van Versendaal and Levelt, 2016). In contrast to these changes in the densities of postsynaptic elements of Martinotti cells, our results have not revealed changes in the density of their axonal boutons. This is apparently in contrast with previous results on V1 interneurons after visual deprivation, which described a parallel reduction in dendritic branches and the inhibitory inputs onto neighboring pyramidal cells (Chen et al., 2011). However, this study was not focused on Martinotti cells. It has to be noted also that in our present study we have observed reductions in the intensity of fluorescence and the mean size of the axonal boutons, which strongly suggests alterations in their synaptic input to the dendrites of pyramidal cells.

Plasticity-related molecules: PSA-NCAM and PNNs

PSA-NCAM has been previously linked to the remodeling of the structure and connectivity of Martinotti (Gómez-Climent et al., 2011; Guirado et al., 2014b) and PV+ basket interneurons (Di Cristo et al., 2007; Castillo-Gómez et al., 2011). We have characterized the pattern of expression of PSA-NCAM in the different regions of the visual circuit and analyzed the impact of dark exposure. We found a decrease in the expression of this molecule in V1, suggesting that PSA-NCAM not only plays a role in the enhanced plasticity elicited during the critical period (Di Cristo et al., 2007), but also in the plasticity induced by visual deprivation during adulthood. However, further research will be necessary to understand the role of PSA-NCAM in visual plasticity, since in a previous study we found that the presence of PSA-NCAM

was not necessary for the shifts in ocular dominance triggered by antidepressants (Guirado et al., 2016).

Other molecules involved in the plasticity of interneurons and shifts in ocular dominance are those constituting the PNNs surrounding PV+ interneurons (Pizzorusso et al., 2002). We did not find any alteration in the density of PNNs in V1, in contrast with previous reports that combined dark exposure and monocular deprivation (Stodieck et al., 2014; Erchova et al., 2017). However, we have found an increase in the fluorescence intensity of *Wisteria Floribunda* agglutinin histochemical staining in deprived animals. This result suggests that dark exposure may trigger a remodeling in the composition of PNNs surrounding PV+ interneurons, probably due to an increase in the expression of chondroitin sulfate proteoglycans. Whether this increase is accompanied by changes in other components of the PNNs still has to be explored.

Parvalbumin expressing neurons and perisomatic innervation of pyramidal neurons

We have found that visual deprivation induces a significant reduction in the density of PV+ interneurons. These results may indicate a decrease in PV protein expression rather than a disappearance of interneurons, because there is no evidence in the literature or in the present results for deprivation-induced loss of inhibitory neurons. Since a previous report showed that optogenetic inhibition of PV+ cells leads to ocular dominance plasticity in the adult visual cortex (Kuhlman et al., 2013), it arises the possibility of considering PV expression level as a readout of the activity of PV+ cells. Nevertheless, it remains unclear whether this change in PV expression is correlated with a reduced synaptic activity of these cells. In order to understand how these changes in the PV+ cells affect their input on excitatory neurons, we have studied the perisomatic inhibitory puncta of basket cells on pyramidal cells and have found that their density was not altered by the visual deprivation. This suggests that our paradigm alters mainly the structure and connectivity of dendrite targeting interneurons, as indicated by our results in Martinotti cells, rather than those targeting the perisomatic region.

Extracortical nuclei

To better understand the role of plasticity related molecules in the visual circuitry, we have expanded our study by describing the distribution of PSA-NCAM and PNNs in the extracortical nuclei of the visual pathway. In the LGN, we found a clear segregation in their expression between the different nuclei. On one hand, the dLGN had a very low expression of PSA-NCAM, whereas the IGL-vLGN complex, implicated in the tuning of the circadian rhythm

through the geniculo-hypothalamic pathway (Moore et al., 2000), showed an intense expression of PSA-NCAM, especially in the IGL. On the other hand, the dLGN presented an extensive PV positive axonal innervation, although it lacked cell bodies expressing this calcium binding protein, as previous studies have shown in rats (Lüth et al., 1993; Okoyama and Moriizumi, 2001) and guinea pigs (De Biasi et al., 1994). However, in the IGL-vLGN we found PV expressing cells that could be subdivided into two subpopulations: those found near the optic tract, which were never surrounded by PNNs and those found in the inner region of the vLGN, near the ventral posteriomedial nucleus of the thalamus, which always were surrounded by PNNs. In both cases these cells were also surrounded by PSA-NCAM, a feature that has never been observed in neocortical structures (Castillo-Gómez et al., 2011; Gómez-Climent et al., 2011; Gilabert-Juan et al., 2013). This feature may be related to the extraordinary plasticity induced by the circadian rhythm, which, at least in the suprachiasmatic nucleus, is known to be PSA-NCAM dependent (Prosser et al., 2003).

Regarding the study of the superior colliculus, it can be functionally subdivided in the superficial layers that participate in visual processing and the intermediate layers, implicated in the coordination of the visual stimuli and the motor effects (May, 2006). We have found that PSA-NCAM is present in the superficial retinal recipient layers, as previously described (Murphy et al., 2007), but its expression was not affected by the visual deprivation. Regarding the study of the distribution of PV+ cells, we found them concentrated in the superficial visuosensory layer and distributed sparsely and in patches in the intermediate layers, as previously described (González-Soriano et al., 2000; Villalobos et al., 2018). The PV+ expressing cells located in the superficial retinorecipient layers were not surrounded by PNNs, whereas most of those located in deeper layers were enwrapped by these structures. This differential pattern, together with the evidence supporting the role of PNNs as a neural plasticity brake in the visual system (Pizzorusso et al., 2002), allow us to hypothesize that PV expressing interneurons may be subdivided according to their association with PNNs, into different subpopulations with different levels of plasticity.

Altogether, our results suggest that visual deprivation enables plasticity levels as long as dark exposure continues, inducing a permissive context to stimulate a directed connectivity in the visual cortex through focused visual stimulation.

Summary

Summarizing, we have observed alterations in the inhibitory circuitry throughout the visual system after ten days of visual deprivation. Moreover, we have described changes in plasticity-related molecules such as PSA-NCAM and components of PNNs, which are likely related to these alterations in interneuronal circuits, especially those involving Martinotti and PV expressing interneurons. Further research directed to manipulate PSA-NCAM or molecules integrated in the PNNs will be necessary to further understand their impact on visual plasticity, not only in V1, but throughout the visual pathway.

Experiment 2: Effects of the antidepressant fluoxetine on the somatostatin expressing interneurons in the basolateral amygdala

In the present thesis, we have shown that chronic fluoxetine treatment triggers a series of changes in different neuronal plasticity features in the inhibitory circuits of the BLA of adult mice, including the PV and SST expressing subpopulations.

PSA-NCAM and GAD6 expression

We have found that fluoxetine produced a robust increase in the expression of PSA-NCAM in the BLA after chronic fluoxetine treatment. This is in agreement with our previous studies showing that chronic antidepressant treatment increases the expression of PSA-NCAM in the BLA (Karpova et al., 2011) as well as in the dorsal hippocampus (Guirado et al., 2014b) and the medial prefrontal cortex (Varea et al., 2007a). It also agrees with the decrease in PSA-NCAM expression reported in animal models of depression such as chronic stress in the amygdala of rats (Cordero et al., 2005), and in the BLA of human patients suffering from major depression (Varea et al., 2012). Conversely, our results in mice are in disagreement with a previous study that showed no alteration in the expression of PSA-NCAM in the BLA of adult rats after fluoxetine treatment (Varea et al., 2007b). Interestingly, the total number of neuropil elements expressing GAD65/67 does not change after fluoxetine treatment, while the density of neuropil expressing both PSA-NCAM and GAD65/67 is significantly increased. These results indicate that the total number of dendrites and axons of interneurons remains intact, but the ratio of these neuropil elements surrounded by PSA-NCAM is increased after fluoxetine, suggesting a reorganization of the amygdaloid inhibitory networks mediated by PSA-NCAM. Nevertheless, the role of PSA-NCAM in the BLA still remains unclear; since higher expression of this molecule seems to correlate with fear conditioning, and its removal in this region leads to increased fear extinction (Markram et al., 2007).

Structural remodeling of somatostatin expressing interneurons

Since the structural remodeling of somatostatin interneurons has been recently shown to be a key element in the mechanism of action of antidepressants (Wohleb et al., 2016), we have analyzed the effects of fluoxetine on different structural features of this interneuronal subpopulation in the BLA. Our results show that fluoxetine produced an increased fraction of stubby spines, but a decrease of mushroom spines.

It is important to remark that previous studies have shown that SST expressing interneurons of the BLA display spines on their dendritic arbour (Muller et al., 2007). Moreover, in a previous study from our laboratory, where we studied the ultrastructure features of these SST-EGFP interneurons, we found that the spines of these interneurons are structural postsynaptic specializations, which mainly receive excitatory inputs (Guirado et al., 2014a) similar to those of excitatory neurons (Colonnier, 1968; Peters and Kaiserman-Abramof, 1970). Thus, it is likely that different morphologies, as it happens in the spines of excitatory neurons, represent different developmental and functional stages: Filopodia protrusions seeking the presynaptic element to then become thin or stubby spines that eventually develop into mushroom spines as those synapses become stronger and more stable (Nimchinsky et al., 2002; Berry and Nedivi, 2017). Therefore, our results suggest that fluoxetine might be causing a decrease in the excitatory input of these interneurons. In fact, we also describe here that fluoxetine produces a decrease in the density of their axonal *boutons*, the presynaptic specializations of the axon, and an even greater decrease when considering the density of the large, more synaptically active, *en passant boutons*. In this line, we have recently shown that the excitatory input, through NMDA receptors, especially affects the axonal bouton density of these SST expressing interneurons and also their spine dynamics in the hippocampus of this same mice strain (Perez-Rando et al., 2017).

FosB expression

To better understand the effects of fluoxetine on the microcircuitry of the BLA, we analysed the expression of FosB, a Fos family member used as a long-term activity marker (Nestler et al., 2001; Robison and Nestler, 2011) in different neuronal subpopulations. It has been established that fluoxetine produces an overall increase in FosB expression throughout the brain, including different nuclei in the amygdala (Vialou et al., 2010), indicating an increased activity of glutamatergic neurons, which represent 85% of the neurons in the BLA (McDonald, 1992). We also found a specific increase in the expression of FosB within PV+ and CAMKII+ profiles, suggesting a homeostatic balance in inhibition and excitation. On the other hand, we found a decrease in FosB expression within the SST+ subpopulation, contrary to what has been shown in the mPFC after the action of the fast-acting antidepressant isoflurane (Antila et al., 2017). In fact, the reported increase in FosB in the somatostatin subpopulation of the mPFC is in line with the increased dendritic spine density we found after fluoxetine treatment in this same region (Guirado et al., 2014b). Our present results suggest an inhibition of SST+ interneurons

from the BLA, in line with decreased structural features in terms of both axonal boutons and mushroom dendritic spines.

Previous studies have, however, found contrasting patterns of c-fos expression in the SST+ interneurons of the BLA in anxiety paradigms: SST expressing interneurons show decreased c-fos expression soon after exposure to predator odor, but increased c-fos after being subjected to an elevated plus maze (Butler et al., 2012). Moreover, female human patients suffering from major depression display reduced SST gene expression and reduced density of SST clusters in the amygdala, with no effect in males (Guilloux et al., 2012; Douillard-Guilloux et al., 2017). The arborisation of SST+ interneurons in the BLA is also reduced in animal models of depression BLA (Gilabert-Juan et al., 2011).

Summary

Our results point to the importance of better understanding the role of these amygdaloid interneurons, and whether their structural and functional alterations might underlie the mechanism of action of fluoxetine on the limbic system. Since major depression is still a highly incapacitating disease without efficient treatment in many cases, SST expressing interneurons in the BLA might represent a successful target for developing new antidepressant strategies.

Experiment 3: Perineuronal nets regulate the inhibitory perisomatic input onto parvalbumin interneurons and gamma rhythms in the prelimbic area of the medial prefrontal cortex

In the present thesis, we describe differences in the expression of PV and the density of perisomatic synaptic puncta on prefrontocortical PV+ interneurons according to the presence of PNNs. We have found that PV+PNN+ cells express more PV and receive a higher density of inhibitory perisomatic puncta from other PV+ cells than PV+PNN- cells. Moreover, we show that the digestion of PNNs in PrL produces a reduction of the density of inhibitory puncta, specifically of those expressing PV on the perisomatic region of PV+ cells. In connection with this reduction in the perisomatic inhibition, the depletion of PNNs also leads to a reduction in both the gamma activity and the expression of the basal activity marker FosB in the mPFC.

The presence of perineuronal nets influences the phenotype of parvalbumin expressing interneurons

To address how the presence of PNNs may affect the connectivity and activity of PV+ cells in the PrL, we compared the density of perisomatic puncta expressing different synaptic markers, as well as other molecular and structural characteristics, such as the length of the AIS and the level of expression of PV. We observed that PV+PNN- cells display lower expression levels of parvalbumin when compared to PV+PNN+ cells. Our results are in agreement with previous work in the hippocampal CA3 (Donato et al., 2013), which proposes a biphasic PV circuitry, with high PV expression cells forming a consolidated circuitry and low PV expression cells sensitive to plastic changes. Considering that 60-70% of PV+ cells are surrounded by PNNs in the mPFC of mice (Guirado et al., 2014b; Ueno et al., 2018) it is plausible to consider that those PV+ cells that reach a determined threshold of inhibitory and excitatory input in their perisomatic region and proximal dendrites at the end of the CP, start to form PNNs around themselves.

Our results on the positive correlation of PV expression and the density of perisomatic inhibitory puncta onto PV+ cells are apparently in contrast with those obtained by Donato et al. (2013) in the CA3, which described that high PV expression cells receive less inhibitory input than low PV expression cells. We think that this discrepancy is mainly due to the fact that our quantification in the mPFC was performed exclusively in the perisomatic region, while in CA3 it

was performed in dendrites. It has to be taken into account that PNNs exclusively enwrap the soma and most proximal segment of dendrites (Celio et al., 1998; Fawcett et al., 2019).

We also describe a positive correlation between PNNs and PV expression, in agreement with the described activity-dependent formation of PNNs (Dityatev et al., 2007). Thus, we propose that the establishment of the inhibitory input on the perisomatic region and proximal neurites of PV+ cells at the end of the critical periods constitutes a critical event for the formation of PNNs. Specifically, our results suggest that the innervation of PV+ cells by other PV+ cells might represent a threshold necessary for the formation of PNNs. This is, only those PV+ cells with a certain degree of innervation from the PV circuitry may develop PNNs and fix their perisomatic connectivity. Supporting this idea, different studies have found an increased cortical plasticity after the induction of a decrease in inhibitory activity, in some cases involving the depletion of PNNs (Harauzov et al., 2010; Toyoizumi et al., 2013; Lensjø et al., 2017b). On the other hand, an experience-dependent accumulation of exogenous OTX2, a homeoprotein commonly bound to PNNs and PV+ cells in the mPFC (Cheong Lee et al., 2017), is necessary for the formation of PNNs and critical period closure in the visual cortex (Sugiyama et al., 2008). Therefore, the formation of PNNs may be the result of a combination of the reachment of certain thresholds in perisomatic inhibitory activity and OTX2 internalisation. We have also analyzed the AIS length and have found that PV+PNN+ cells had a longer AIS compared to PV+PNN- cells. Since the increase in the AIS length has been previously related to the maturation of pyramidal neurons and dentate granule cells (Sammons et al., 2018; Bolós et al., 2019), our data supports the hypothesis of the presence of PNNs as a feature of mature PV+ cells, which may have a different role in the PV circuitry from those without PNNs. Taken together, our results suggest the existence of 2 subpopulations of PV+ cells in the mPFC, defined by the presence or absence of PNNs, with differential PV expression and perisomatic connectivity. In order to test whether the digestion of PNNs was able to induce the transformation of most PV+ cells to a phenotype similar to the PV+PNN- cells in control animals, we tested the effects of ChABC injection in the PrL.

Chondroitinase ABC affects the perisomatic connectivity on parvalbumin expressing interneurons

We have found that ChABC treatment induces specifically a reduction in the density of inhibitory perisomatic puncta from PV+ cells onto PV+ cells, rendering a VGLUT1/VGAT ratio similar to that found in the PV+PNN- cells in control animals. A recent report has also found a

decrease in puncta expressing inhibitory markers after ChABC treatment in the V1 (Lensjø et al., 2017a). However, these puncta were quantified in the neuropil and our study focused only on those located in the perisomatic region of PV+ cells. Interestingly, we did not find changes in the density of perisomatic puncta on pyramidal neurons, which suggests that ChABC treatment, despite its impact on the perisomatic input received by PV+ cells, does not induce structural plasticity in the connections that these basket interneurons establish onto pyramidal neurons. However, it is possible that other forms of plasticity, such as the modification of the efficacy of the synapses, may be occurring in these circuits after ChABC, because we have observed alterations in gamma band oscillations, a rhythm inextricably tied to perisomatic inhibition (Buzsáki and Wang, 2012). It is interesting to note that, unlike (Lensjø et al., 2017a), we have not observed changes in the density of puncta expressing synaptic markers in the neuropil of PrL. This discrepancy may be due to the fact that we are analyzing a different neocortical region, although the percentage of PV+ cells surrounded by PNNs is similar in both regions; it can also be due to the different survival time after ChABC, 7 days in Lensjø et al. (2017a), 4 days in our study. The difference may also be due to the type of molecules analyzed, while (Lensjø et al., 2017a) analyzed gephyrin, a postsynaptic marker, we measured only presynaptic markers (SYN, VGAT and VGLUT1).

Chondroitinase ABC affects theta and gamma oscillations in the PrL

In order to study whether the ChABC treatment also affected the physiology of neurons in the mPFC, especially that of PV+ basket cells, we conducted electrophysiological studies and analyses of the expression of markers of cellular activity, such as c-Fos and FosB.

We used a sensory paradigm to induce a synchronous activated state in the prefrontocortical neuronal circuitry, and quantified then the theta and gamma coupling (Sohal et al., 2009), a characteristic functional profile depending on the synaptic inhibition onto PV-expressing cells (Buzsáki and Wang, 2012). Apart from external sources of rhythmicity, cortical local networks are prone to synchronize at theta frequency due to intrinsic oscillations on the substrate of various neuronal types. After ChABC treatment in the mPFC, our results showed: (i) a shift in the theta peak frequency to higher ranges; (ii) a decrease of the highest gamma oscillations; (iii) unchanged theta modulation of gamma. Based on these results, we hypothesize that theta waves are maintained, probably by an external input (Siapas et al., 2005; Sirota et al., 2008), while gamma oscillations reduce their presence by an unbalance of the excitatory-inhibitory activity as a consequence of the loss of perisomatic synapses on PV+ cells.

However, we performed our experiments in an associative cortical area by means of temporal stimulus. Thus, we suggest that PNNs digestion is capable to decrease perisomatic innervation on the circuitry of PV interneurons, which impairs PV+ cell synchrony producing a decrease in local gamma activity. Although we did not find changes after the depletion of PNNs in the expression of PV, we found a strong reduction in the expression of FosB, not only in PV+ interneurons but also in pyramidal neurons. Since FosB has been linked to long-term activity levels (Nestler, 2015), this data supports our electrophysiology results, indicating that the amount of active PV+ cells is reduced after ChABC treatment. Altogether, our results suggest that the disengagement of a portion of PV+ interneurons from the established connectivity patterns is a key mechanism underlying the plasticity observed after PNN removal.

Summary

In the present thesis, we use *in vivo* extracellular recordings and confocal microscopy to investigate the effects of PNNs on gamma and theta activity and the perisomatic innervation of PV+ cells in the mPFC. We show that the digestion of PNNs resets the perisomatic input of PV+ cells to that found in PV+ cells lacking PNNs in control animals. Moreover, we describe a reduction in the gamma activity, but an increase in theta oscillations as a consequence of the reduced innervation. Therefore, the enzymatic ablation of PNNs appears to reactivate plasticity through a decrease of the inhibitory input on PV+ interneurons.

VI. CONCLUSIONS

1. Visual deprivation reduces the density of puncta expressing synaptophysin and vesicular glutamate transporter 1, and increases the fluorescence intensity of synaptophysin and a reduction in both vesicular glutamate transporter 1 and vesicular GABA transporter in the primary visual cortex of adult mice.
2. The immunohistochemical analyses reveal that EGFP expressing cells in the primary visual cortex of GIN mice can be identified as Martinotti cells.
3. Visual deprivation reduces the dendritic complexity, alters the density of different types of dendritic spines and reduces the size and fluorescence intensity of axonal boutons of EGFP expressing cells in the primary visual cortex.
4. Visual deprivation causes a reduction in the number of PSA-NCAM expressing cells and PSA-NCAM positive puncta, a reduction in the density of parvalbumin expressing cells and an increase in the fluorescence intensity of perineuronal nets in the primary visual cortex.
5. PSA-NCAM is highly expressed in the intergeniculate leaflet and the ventral part of lateral geniculate leaflet, whereas it is barely expressed in the dorsal part of lateral geniculate leaflet of the adult mouse.
6. The somata of parvalbumin expressing interneurons are surrounded by perineuronal nets and PSA-NCAM in the ventral part of lateral geniculate leaflet.
7. Parvalbumin expressing interneurons in the superior colliculus are spatially segregated on the basis of the presence of perineuronal nets surrounding them.
8. Fluoxetine treatment increases the density of PSA-NCAM expressing puncta and the density of puncta expressing PSA-NCAM and GAD65/67, but not that expressing GAD65/67 in the basolateral amygdala of adult mice.
9. A scarce, but well distributed population of EGFP interneurons, all of which express somatostatin, can be found in the basolateral amygdala of adult GIN mice.

10. Fluoxetine treatment decreases the density of mature dendritic spines, the density and the average size of axonal *bout*ons, while it increases the density of immature dendritic spines in somatostatin expressing interneurons in the basolateral amygdala of adult GIN mice.

11. The expression of the activity marker FosB is increased in pyramidal neurons and parvalbumin expressing interneurons, but decreased in somatostatin expressing interneurons, of the basolateral amygdala of adult GIN mice after chronic fluoxetine treatment.

12. Parvalbumin expressing interneurons surrounded by perineuronal nets express more parvalbumin and receive a higher density of inhibitory perisomatic puncta from other parvalbumin expressing interneurons than parvalbumin expressing cells lacking perineuronal nets in the prelimbic cortex of adult mice.

13. Perineuronal nets in the medial prefrontal cortex of adult mice are completely depleted 4 days after intracerebral injection of Chondroitinase ABC , but they start to reappear 6 days after.

14. The digestion of perineuronal nets using the enzyme chondroitinase ABC in the prelimbic area of adult mice induces a significant reduction of the density of inhibitory puncta, specifically of those expressing parvalbumin, on the perisomatic region of parvalbumin expressing cells.

15. The injection of chondroitinase ABC in the prelimbic cortex does not affect the density of puncta expressing the synaptic markers vesicular glutamate transporter 1, vesicular GABA transporter and synaptophysin in the neuropil of this prefrontocortical region.

16. The depletion of perineuronal nets with chondroitinase ABC reduces the expression of the basal activity marker FosB in the prelimbic region prefrontal cortex, both in pyramidal neurons and in parvalbumin expressing interneurons.

17. The depletion of perineuronal nets with chondroitinase ABC leads to a reduction in gamma activity and an increase in theta activity in the prelimbic cortex after tail pinch stimulation.

VII. BIBLIOGRAPHY

Adell A. 2015. Revisiting the role of raphe and serotonin in neuropsychiatric disorders. J Gen Physiol 145:257–259.

Adrian M, Kusters R, Storm C, Hoogenraad CC, Kapitein LC. 2017. Probing the Interplay between Dendritic Spine Morphology and Membrane-Bound Diffusion. Biophys J 113:2261–2270.

Anon. 2012. The Mouse Nervous System. Elsevier. Anon. Paxinos and Franklin's the Mouse Brain in Stereotaxic Coordinates, Compact - 5th Edition.

Antila H, Ryazantseva M, Popova D, Sipilä P, Guirado R, Kohtala S, Yalcin I, Lindholm J, Vesa L, Sato V, Cordeira J, Autio H, Kislin M, Rios M, Joca S, Casarotto P, Khiroug L, Lauri S, Taira T, Castrén E, Rantamäki T. 2017. Isoflurane produces antidepressant effects and induces TrkB signaling in rodents. Sci Rep 7:7811.

Arcelli P, Frassoni C, Regondi MC, De Biasi S, Spreafico R. 1997. GABAergic neurons in mammalian thalamus: a marker of thalamic complexity? Brain Res Bull 42:27–37.

Barritt AW, Davies M, Marchand F, Hartley R, Grist J, Yip P, McMahon SB, Bradbury EJ. 2006. Chondroitinase ABC promotes sprouting of intact and injured spinal systems after spinal cord injury. J Neurosci Off J Soc Neurosci 26:10856–10867.

Bartos M, Vida I, Jonas P. 2007. Synaptic mechanisms of synchronized gamma oscillations in inhibitory interneuron networks. Nat Rev Neurosci 8:45–56.

Beliveau V, Ganz M, Feng L, Ozenne B, Højgaard L, Fisher PM, Svarer C, Greve DN, Knudsen GM. 2017. A High-Resolution *In Vivo* Atlas of the Human Brain's Serotonin System. J Neurosci 37:120–128.

Berry KP, Nedivi E. 2017. Spine Dynamics: Are They All the Same? Neuron 96:43–55.

Bolós M, Terreros-Roncal J, Perea JR, Pallas-Bazarra N, Ávila J, Llorens-Martín M. 2019. Maturation Dynamics of the Axon Initial Segment (AIS) of Newborn Dentate Granule Cells in Young Adult C57BL/6J Mice. J Neurosci 39:1605–1620.

Brown VJ, Bowman EM. 2002. Rodent models of prefrontal cortical function. Trends Neurosci 25:340–343.

Brückner G, Grosche J, Schmidt S, Härtig W, Margolis RU, Delpech B, Seidenbecher CI, Czaniera R, Schachner M. 2000. Postnatal development of perineuronal nets in wild-type mice and in a mutant deficient in tenascin-R. J Comp Neurol 428:616–629.

Bucher D, Marder E. 2013. SnapShot: Neuromodulation. Cell 155:482-482.e1.

Buddhala C, Hsu C-C, Wu J-Y. 2009. A novel mechanism for GABA synthesis and packaging into synaptic vesicles. Neurochem Int 55:9–12.

Bukalo O, Schachner M, Dityatev A. 2001. Modification of extracellular matrix by enzymatic removal of chondroitin sulfate and by lack of tenascin-R differentially affects several forms of synaptic plasticity in the hippocampus. Neuroscience 104:359–369.

Butler RK, White LC, Frederick-Duus D, Kaigler KF, Fadel JR, Wilson MA. 2012. Comparison of the activation of somatostatin- and neuropeptide Y-containing neuronal populations of the rat amygdala following two different anxiogenic stressors. Exp Neurol 238:52–63.

Buzsáki G. 2002. Theta Oscillations in the Hippocampus. Neuron 33:325–340.

Buzsáki G, Anastassiou CA, Koch C. 2012. The origin of extracellular fields and currents — EEG, ECoG, LFP and spikes. Nat Rev Neurosci 13:407–420.

Buzsáki G, Draguhn A. 2004. Neuronal oscillations in cortical networks. Science 304:1926–1929.

Buzsáki G, Wang X-J. 2012. Mechanisms of gamma oscillations. Annu Rev Neurosci 35:203–225.

Campeau S, Davis M. 1995. Involvement of the central nucleus and basolateral complex of the amygdala in fear conditioning measured with fear-potentiated startle in rats trained concurrently with auditory and visual conditioned stimuli. J Neurosci Off J Soc Neurosci 15:2301–2311.

Capogna M. 2014. GABAergic cell type diversity in the basolateral amygdala. Curr Opin Neurobiol 26:110–116.

Carulli D, Pizzorusso T, Kwok JCF, Putignano E, Poli A, Forostyak S, Andrews MR, Deepa SS, Glant TT, Fawcett JW. 2010. Animals lacking link protein have attenuated perineuronal nets and persistent plasticity. Brain J Neurol 133:2331–2347.

Castillo-Gómez E, Pérez-Rando M, Vidueira S, Nacher J. 2016. Polysialic Acid Acute Depletion Induces Structural Plasticity in Interneurons and Impairs the Excitation/Inhibition Balance in Medial Prefrontal Cortex Organotypic Cultures. Front Cell Neurosci 10:170.

Castillo-Gómez E, Varea E, Blasco-Ibáñez JM, Crespo C, Nacher J. 2011. Polysialic acid is

required for dopamine D2 receptor-mediated plasticity involving inhibitory circuits of the rat medial prefrontal cortex. PloS One 6:e29516.

Castrén E. 2005. Is mood chemistry? Nat Rev Neurosci 6:241–246.

Celio MR, Spreafico R, De Biasi S, Vitellaro-Zuccarello L. 1998. Perineuronal nets: past and present. Trends Neurosci 21:510–515.

Chen JL, Lin WC, Cha JW, So PT, Kubota Y, Nedivi E. 2011. Structural basis for the role of inhibition in facilitating adult brain plasticity. Nat Neurosci 14:587–594.

Chen JL, Villa KL, Cha JW, So PTC, Kubota Y, Nedivi E. 2012. Clustered dynamics of inhibitory synapses and dendritic spines in the adult neocortex. Neuron 74:361–373.

Choi DW. 1988. Glutamate neurotoxicity and diseases of the nervous system. Neuron 1:623–634.

Colonnier M. 1968. Synaptic patterns on different cell types in the different laminae of the cat visual cortex. An electron microscope study. Brain Res 9:268–287.

Conel JLR. 1939. The postnatal development of the human cerebral cortex. Vol. 1. The cortex of the newborn. Oxford, England: Harvard Univ. Press.

Cordero MI, Rodríguez JJ, Davies HA, Peddie CJ, Sandi C, Stewart MG. 2005. Chronic restraint stress down-regulates amygdaloid expression of polysialylated neural cell adhesion molecule. Neuroscience 133:903–910.

Curto Y, Garcia-Mompo C, Bueno-Fernandez C, Nacher J. 2016. Chronic benzodiazepine treatment decreases spine density in cortical pyramidal neurons. Neurosci Lett 613:41–46.

Dalley JW, Cardinal RN, Robbins TW. 2004. Prefrontal executive and cognitive functions in rodents: neural and neurochemical substrates. Neurosci Biobehav Rev 28:771–784.

Dauth S, Grevesse T, Pantazopoulos H, Campbell PH, Maoz BM, Berretta S, Parker KK. 2016. Extracellular matrix protein expression is brain region dependent. J Comp Neurol 524:1309–1336.

De Biasi S, Arcelli P, Spreafico R. 1994. Parvalbumin immunoreactivity in the thalamus of guinea pig: light and electron microscopic correlation with gamma-aminobutyric acid immunoreactivity. J Comp Neurol 348:556–569.

Di Cristo G, Chattopadhyaya B, Kuhlman SJ, Fu Y, Bélanger M-C, Wu CZ, Rutishauser U, Maffei L, Huang ZJ. 2007. Activity-dependent PSA expression regulates inhibitory maturation and onset of critical period plasticity. Nat Neurosci 10:1569–1577.

Dityatev A, Brückner G, Dityateva G, Grosche J, Kleene R, Schachner M. 2007. Activity-dependent formation and functions of chondroitin sulfate-rich extracellular matrix of

perineuronal nets. Dev Neurobiol 67:570–588.

Divito CB, Underhill SM. 2014. Excitatory amino acid transporters: roles in glutamatergic neurotransmission. Neurochem Int 73:172–180.

Donato F, Rompani SB, Caroni P. 2013. Parvalbumin-expressing basket-cell network plasticity induced by experience regulates adult learning. Nature 504:272–276.

Douillard-Guilloux G, Lewis D, Seney ML, Sibille E. 2017. Decrease in somatostatin-positive cell density in the amygdala of females with major depression. Depress Anxiety 34:68–78.

Dräger UC, Olsen JF. 1980. Origins of crossed and uncrossed retinal projections in pigmented and albino mice. J Comp Neurol 191:383–412.

Duvarci S, Pare D. 2014. Amygdala microcircuits controlling learned fear. Neuron 82:966–980.

Ehrlich I, Humeau Y, Grenier F, Ciocchi S, Herry C, Lüthi A. 2009. Amygdala inhibitory circuits and the control of fear memory. Neuron 62:757–771.

Ellis EM, Gauvain G, Sivyer B, Murphy GJ. 2016. Shared and distinct retinal input to the mouse superior colliculus and dorsal lateral geniculate nucleus. J Neurophysiol 116:602–610.

Elston GN. 2003. Cortex, cognition and the cell: new insights into the pyramidal neuron and prefrontal function. Cereb Cortex N Y N 1991 13:1124–1138.

Erchova I, Vasalauskaite A, Longo V, Sengpiel F. 2017. Enhancement of visual cortex plasticity by dark exposure. Philos Trans R Soc B Biol Sci 372.

Erecińska M, Silver IA. 1990. Metabolism and role of glutamate in mammalian brain. Prog Neurobiol 35:245–296.

Eshkind LG, Leube RE. 1995. Mice lacking synaptophysin reproduce and form typical synaptic vesicles. Cell Tissue Res 282:423–433.

Fagiolini M, Hensch TK. 2000. Inhibitory threshold for critical-period activation in primary visual cortex. Nature 404:183–186.

Fagiolini M, Pizzorusso T, Berardi N, Domenici L, Maffei L. 1994. Functional postnatal development of the rat primary visual cortex and the role of visual experience: Dark rearing and monocular deprivation. Vision Res 34:709–720.

Favuzzi E, Marques-Smith A, Deogracias R, Winterflood CM, Sánchez-Aguilera A, Mantoan L, Maeso P, Fernandes C, Ewers H, Rico B. 2017. Activity-Dependent Gating of Parvalbumin Interneuron Function by the Perineuronal Net Protein Brevican. Neuron 95:639-655.e10.

Fawcett JW, Oohashi T, Pizzorusso T. 2019. The roles of perineuronal nets and the perinodal extracellular matrix in neuronal function. Nat Rev Neurosci 20:451.

Freund TF, Katona I. 2007. Perisomatic Inhibition. Neuron 56:33–42.

Frischknecht R, Heine M, Perrais D, Seidenbecher CI, Choquet D, Gundelfinger ED. 2009. Brain extracellular matrix affects AMPA receptor lateral mobility and short-term synaptic plasticity. Nat Neurosci 12:897–904.

Fuster JM. 2001. The prefrontal cortex--an update: time is of the essence. Neuron 30:319–333.

Genç E, Schölvinck ML, Bergmann J, Singer W, Kohler A. 2016. Functional Connectivity Patterns of Visual Cortex Reflect its Anatomical Organization. Cereb Cortex 26:3719–3731.

Gilabert-Juan J, Castillo-Gomez E, Guirado R, Moltó MD, Nacher J. 2013. Chronic stress alters inhibitory networks in the medial prefrontal cortex of adult mice. Brain Struct Funct 218:1591–1605.

Gilabert-Juan J, Castillo-Gomez E, Pérez-Rando M, Moltó MD, Nacher J. 2011. Chronic stress induces changes in the structure of interneurons and in the expression of molecules related to neuronal structural plasticity and inhibitory neurotransmission in the amygdala of adult mice. Exp Neurol 232:33–40.

Goel A, Lee H-K. 2007. Persistence of Experience-Induced Homeostatic Synaptic Plasticity through Adulthood in Superficial Layers of Mouse Visual Cortex. J Neurosci Off J Soc Neurosci 27:6692–6700.

Golgi C. 1873. Sulla struttura della sostanza grigia del cervello.

Gómez-Climent MÁ, Guirado R, Castillo-Gómez E, Varea E, Gutierrez-Mecinas M, Gilabert-Juan J, García-Mompó C, Vidueira S, Sanchez-Mataredona D, Hernández S, Blasco-Ibáñez JM, Crespo C, Rutishauser U, Schachner M, Nacher J. 2011. The polysialylated form of the neural cell adhesion molecule (PSA-NCAM) is expressed in a subpopulation of mature cortical interneurons characterized by reduced structural features and connectivity. Cereb Cortex N Y N 1991 21:1028–1041.

González-Soriano J, González-Flores ML, Contreras-Rodríguez J, Rodríguez-Veiga E, Martínez-Sainz P. 2000. Calbindin D28k and parvalbumin immunoreactivity in the rabbit superior colliculus: an anatomical study. Anat Rec 259:334–346.

Greifzu F, Pielecka-Fortuna J, Kalogeraki E, Krempler K, Favaro PD, Schluter OM, Lowel S. 2014. Environmental enrichment extends ocular dominance plasticity into adulthood and protects from stroke-induced impairments of plasticity. Proc Natl Acad Sci 111:1150–1155.

Gu Y, Tran T, Murase S, Borrell A, Kirkwood A, Quinlan EM. 2016. Neuregulin-Dependent Regulation of Fast-Spiking Interneuron Excitability Controls the Timing of the Critical Period. J Neurosci 36:10285–10295.

Guilloux J-P, Douillard-Guilloux G, Kota R, Wang X, Gardier AM, Martinowich K, Tseng GC, Lewis DA, Sibille E. 2012. Molecular evidence for BDNF- and GABA-related dysfunctions in the amygdala of female subjects with major depression. Mol Psychiatry 17:1130–1142.

Guirado R, La Terra D, Bourguignon M, Carceller H, Umemori J, Sipilä P, Nacher J, Castrén E. 2016. Effects of PSA Removal from NCAM on the Critical Period Plasticity Triggered by the Antidepressant Fluoxetine in the Visual Cortex. Front Cell Neurosci 10:22.

Guirado R, Perez-Rando M, Sanchez-Matarredona D, Castillo-Gómez E, Liberia T, Rovira-Esteban L, Varea E, Crespo C, Blasco-Ibáñez JM, Nacher J. 2014a. The dendritic spines of interneurons are dynamic structures influenced by PSA-NCAM expression. Cereb Cortex N Y N 1991 24:3014–3024.

Guirado R, Perez-Rando M, Sanchez-Matarredona D, Castrén E, Nacher J. 2014b. Chronic fluoxetine treatment alters the structure, connectivity and plasticity of cortical interneurons. Int J Neuropsychopharmacol 17:1635–1646.

Guirado R, Varea E, Castillo-Gómez E, Gómez-Climent MA, Rovira-Esteban L, Blasco-Ibáñez JM, Crespo C, Martínez-Guijarro FJ, Nàcher J. 2009. Effects of chronic fluoxetine treatment on the rat somatosensory cortex: activation and induction of neuronal structural plasticity. Neurosci Lett 457:12–15.

Harauzov A, Spolidoro M, DiCristo G, De Pasquale R, Cancedda L, Pizzorusso T, Viegi A, Berardi N, Maffei L. 2010. Reducing intracortical inhibition in the adult visual cortex promotes ocular dominance plasticity. J Neurosci Off J Soc Neurosci 30:361–371.

Harrington ME. 1997. The ventral lateral geniculate nucleus and the intergeniculate leaflet: interrelated structures in the visual and circadian systems. Neurosci Biobehav Rev 21:705–727.

Hattar S, Kumar M, Park A, Tong P, Tung J, Yau K-W, Berson DM. 2006. Central projections of melanopsin-expressing retinal ganglion cells in the mouse. J Comp Neurol 497:326–349.

He H-Y, Hodos W, Quinlan EM. 2006. Visual deprivation reactivates rapid ocular dominance plasticity in adult visual cortex. J Neurosci Off J Soc Neurosci 26:2951–2955.

He H-Y, Ray B, Dennis K, Quinlan EM. 2007. Experience-dependent recovery of vision following chronic deprivation amblyopia. Nat Neurosci 10:1134–1136.

Hensch TK. 2005. Critical period plasticity in local cortical circuits. Nat Rev Neurosci 6:877.

Herzog E, Gilchrist J, Gras C, Muzerelle A, Ravassard P, Giros B, Gaspar P, El Mestikawy S. 2004. Localization of VGLUT3, the vesicular glutamate transporter type 3, in the rat brain. Neuroscience 123:983–1002.

Hoover WB, Vertes RP. 2007. Anatomical analysis of afferent projections to the medial prefrontal cortex in the rat. Brain Struct Funct 212:149–179.

Huang S, Hokenson K, Bandyopadhyay S, Russek SJ, Kirkwood A. 2015. Brief Dark Exposure Reduces Tonic Inhibition in Visual Cortex. J Neurosci 35:15916.

Hubel DH, Wiesel TN. 1970. The period of susceptibility to the physiological effects of unilateral eye closure in kittens. J Physiol 206:419–436.

Jembrek MJ, Vlainic J. 2015. GABA Receptors: Pharmacological Potential and Pitfalls. Curr Pharm Des 21:4943–4959.

Jermakowicz WJ, Casagrande VivienA. 2007. Neural Networks a Century after Cajal. Brain Res Rev 55:264–284.

Ji X, Zingg B, Mesik L, Xiao Z, Zhang LI, Tao HW. 2016. Thalamocortical Innervation Pattern in Mouse Auditory and Visual Cortex: Laminar and Cell-Type Specificity. Cereb Cortex N Y NY 26:2612–2625.

Jiao Y, Zhang C, Yanagawa Y, Sun Q-Q. 2006. Major effects of sensory experiences on the neocortical inhibitory circuits. J Neurosci Off J Soc Neurosci 26:8691–8701.

Kaiser T, Ting JT, Monteiro P, Feng G. 2016. Transgenic labeling of parvalbumin-expressing neurons with tdTomato. Neuroscience 321:236–245.

Kandel ER, Schwartz JH, Jessell TM, Siegelbaum SA, Hudspeth AJ eds. 2012. Principles of Neural Science, Fifth Edition. 5th edition. New York: McGraw-Hill Education / Medical.

Karpova NN, Pickenhagen A, Lindholm J, Tiraboschi E, Kulesskaya N, Agústsdóttir A, Antila H, Popova D, Akamine Y, Bahi A, Sullivan R, Hen R, Drew LJ, Castrén E. 2011. Fear erasure in mice requires synergy between antidepressant drugs and extinction training. Science 334:1731–1734.

Kasper EM, Larkman AU, Lübke J, Blakemore C. 1994. Pyramidal neurons in layer 5 of the rat visual cortex. I. Correlation among cell morphology, intrinsic electrophysiological properties, and axon targets. J Comp Neurol 339:459–474.

Keck T, Mrsic-Flogel TD, Vaz Afonso M, Eysel UT, Bonhoeffer T, Hübener M. 2008. Massive restructuring of neuronal circuits during functional reorganization of adult visual cortex. Nat Neurosci 11:1162–1167.

Keck T, Scheuss V, Jacobsen RI, Wierenga CJ, Eysel UT, Bonhoeffer T, Hübener M. 2011. Loss of sensory input causes rapid structural changes of inhibitory neurons in adult mouse visual cortex. Neuron 71:869–882.

Kerschensteiner D, Guido W. 2017. Organization of the dorsal lateral geniculate nucleus in the mouse. Vis Neurosci 34:E008.

Koch C, Zador A. 1993. The function of dendritic spines: devices subserving biochemical rather than electrical compartmentalization. J Neurosci Off J Soc Neurosci 13:413–422.

Kolmac C, Mitrofanis J. 2000. Organization of brain stem afferents to the ventral lateral geniculate nucleus of rats. Vis Neurosci 17:313–318.

Krauzlis RJ, Lovejoy LP, Zénon A. 2013. Superior colliculus and visual spatial attention. Annu Rev Neurosci 36:165–182.

Kubota Y. 2014. Untangling GABAergic wiring in the cortical microcircuit. Curr Opin Neurobiol 26:7–14.

Kuhlman SJ, Olivas ND, Tring E, Ikrar T, Xu X, Trachtenberg JT. 2013. A disinhibitory microcircuit initiates critical-period plasticity in the visual cortex. Nature 501:543–546.

Lee T-S, Bjørnsen LP, Paz C, Kim JH, Spencer SS, Spencer DD, Eid T, de Lanerolle NC. 2006. GAT1 and GAT3 expression are differently localized in the human epileptogenic hippocampus. Acta Neuropathol (Berl) 111:351–363.

Lensjø KK, Christensen AC, Tennøe S, Fyhn M, Hafting T. 2017a. Differential Expression and Cell-Type Specificity of Perineuronal Nets in Hippocampus, Medial Entorhinal Cortex, and Visual Cortex Examined in the Rat and Mouse. eNeuro 4.

Lensjø KK, Lepperød ME, Dick G, Hafting T, Fyhn M. 2017b. Removal of Perineuronal Nets Unlocks Juvenile Plasticity Through Network Mechanisms of Decreased Inhibition and Increased Gamma Activity. J Neurosci Off J Soc Neurosci 37:1269–1283.

Levelt CN, Hübener M. 2012. Critical-period plasticity in the visual cortex. Annu Rev Neurosci 35:309–330.

Longair MH, Baker DA, Armstrong JD. 2011. Simple Neurite Tracer: open source software for reconstruction, visualization and analysis of neuronal processes. Bioinforma Oxf Engl 27:2453–2454.

Lüth HJ, Winkelmann E, Celio MR. 1993. Light- and electron microscopic localization of parvalbumin, calbindin D-28k and calretinin in the dorsal lateral geniculate nucleus of the rat. J Hirnforsch 34:47–56.

Marik SA, Yamahachi H, McManus JNJ, Szabo G, Gilbert CD. 2010. Axonal dynamics of excitatory and inhibitory neurons in somatosensory cortex. PLoS Biol 8:e1000395.

Markram H, Toledo-Rodriguez M, Wang Y, Gupta A, Silberberg G, Wu C. 2004. Interneurons of the neocortical inhibitory system. Nat Rev Neurosci 5:793–807.

Markram K, Lopez Fernandez MA, Abrous DN, Sandi C. 2007. Amygdala upregulation of NCAM polysialylation induced by auditory fear conditioning is not required for memory formation, but plays a role in fear extinction. Neurobiol Learn Mem 87:573–582.

Martin DL, Rimvall K. 1993. Regulation of gamma-aminobutyric acid synthesis in the brain. J Neurochem 60:395–407.

Masliah E, Terry RD, Alford M, DeTeresa R. 1990. Quantitative immunohistochemistry of synaptophysin in human neocortex: an alternative method to estimate density of presynaptic terminals in paraffin sections. J Histochem Cytochem Off J Histochem Soc 38:837–844.

Matthews RT, Kelly GM, Zerillo CA, Gray G, Tiemeyer M, Hockfield S. 2002. Aggrecan glycoforms contribute to the molecular heterogeneity of perineuronal nets. J Neurosci Off J Soc Neurosci 22:7536–7547.

May PJ. 2006. The mammalian superior colliculus: laminar structure and connections. Prog Brain Res 151:321–378.

Maya Vetencourt JF, Sale A, Viegi A, Baroncelli L, De Pasquale R, O'Leary OF, Castrén E, Maffei L. 2008. The antidepressant fluoxetine restores plasticity in the adult visual cortex. Science 320:385–388.

McDonald AJ. 1982. Neurons of the lateral and basolateral amygdaloid nuclei: a Golgi study in the rat. J Comp Neurol 212:293–312.

McDonald AJ. 1992. Projection neurons of the basolateral amygdala: a correlative Golgi and retrograde tract tracing study. Brain Res Bull 28:179–185.

McDonald AJ. 1998. Cortical pathways to the mammalian amygdala. Prog Neurobiol 55:257–332.

McDonald AJ, Mascagni F. 2001. Colocalization of calcium-binding proteins and GABA in neurons of the rat basolateral amygdala. Neuroscience 105:681–693.

McDonald AJ, Mascagni F. 2002. Immunohistochemical characterization of somatostatin containing interneurons in the rat basolateral amygdala. Brain Res 943:237–244.

McEwen BS. 1999. Stress and hippocampal plasticity. Annu Rev Neurosci 22:105–122.

McMahon HT, Bolshakov VY, Janz R, Hammer RE, Siegelbaum SA, Südhof TC. 1996. Synaptophysin, a major synaptic vesicle protein, is not essential for neurotransmitter release. Proc Natl Acad Sci 93:4760–4764.

Méndez P, Bacci A. 2011. Assortment of GABAergic plasticity in the cortical interneuron melting pot. Neural Plast 2011:976856.

Mikics É, Guirado R, Umemori J, Tóth M, Biró L, Miskolczi C, Balázsfi D, Zelena D, Castrén E, Haller J, Karpova NN. 2018. Social Learning Requires Plasticity Enhanced by Fluoxetine Through Prefrontal Bdnf-TrkB Signaling to Limit Aggression Induced by Post-Weaning Social Isolation. Neuropsychopharmacol Off Publ Am Coll Neuropsychopharmacol

43:235–245.

Mitchell DE, MacNeill K, Crowder NA, Holman K, Duffy KR. 2016. Recovery of visual functions in amblyopic animals following brief exposure to total darkness. J Physiol 594:149–167.

Moldestad O, Karlsen P, Molden S, Storm JF. 2009. Tracheotomy improves experiment success rate in mice during urethane anesthesia and stereotaxic surgery. J Neurosci Methods 176:57–62.

Montey KL, Quinlan EM. 2011. Reactivation of thalamocortical plasticity by dark exposure during recovery from chronic monocular deprivation. Nat Commun 2:317.

Moore RY, Card JP. 1994. Intergeniculate leaflet: an anatomically and functionally distinct subdivision of the lateral geniculate complex. J Comp Neurol 344:403–430.

Moore RY, Weis R, Moga MM. 2000. Efferent projections of the intergeniculate leaflet and the ventral lateral geniculate nucleus in the rat. J Comp Neurol 420:398–418.

Morellini F, Sivukhina E, Stoenica L, Oulianova E, Bukalo O, Jakovcevski I, Dityatev A, Irintchev A, Schachner M. 2010. Improved reversal learning and working memory and enhanced reactivity to novelty in mice with enhanced GABAergic innervation in the dentate gyrus. Cereb Cortex N Y N 1991 20:2712–2727.

Morikawa S, Ikegaya Y, Narita M, Tamura H. 2017. Activation of perineuronal net-expressing excitatory neurons during associative memory encoding and retrieval. Sci Rep 7.

Morin LP, Allen CN. 2006. The circadian visual system, 2005. Brain Res Rev 51:1–60.

Muller JF, Mascagni F, McDonald AJ. 2007. Postsynaptic targets of somatostatin-containing interneurons in the rat basolateral amygdala. J Comp Neurol 500:513–529.

Murphy JA, Nickerson PEB, Clarke DB. 2007. Injury to retinal ganglion cell axons increases polysialylated neural cell adhesion molecule (PSA-NCAM) in the adult rodent superior colliculus. Brain Res 1163:21–32.

Nacher J, Guirado R, Castillo-Gómez E. 2013. Structural plasticity of interneurons in the adult brain: role of PSA-NCAM and implications for psychiatric disorders. Neurochem Res 38:1122–1133.

Nacher J, Lanuza E, McEwen BS. 2002. Distribution of PSA-NCAM expression in the amygdala of the adult rat. Neuroscience 113:479–484.

Nestler EJ. 2015. ΔFosB: a transcriptional regulator of stress and antidepressant responses. Eur J Pharmacol 753:66–72.

Nestler EJ, Barrot M, Self DW. 2001. DeltaFosB: a sustained molecular switch for addiction. Proc Natl Acad Sci U S A 98:11042–11046.

Nimchinsky EA, Sabatini BL, Svoboda K. 2002. Structure and function of dendritic spines. Annu Rev Physiol 64:313–353.

Okoyama S, Moriizumi T. 2001. Onset of calbindin-D 28K and parvalbumin expression in the lateral geniculate complex and olivary pretectal nucleus during postnatal development of the rat. Int J Dev Neurosci Off J Int Soc Dev Neurosci 19:655–661.

Oliva AA, Jiang M, Lam T, Smith KL, Swann JW. 2000. Novel hippocampal interneuronal subtypes identified using transgenic mice that express green fluorescent protein in GABAergic interneurons. J Neurosci Off J Soc Neurosci 20:3354–3368.

Orrego F, Villanueva S. 1993. The chemical nature of the main central excitatory transmitter: a critical appraisal based upon release studies and synaptic vesicle localization. Neuroscience 56:539–555.

Padival MA, Blume SR, Rosenkranz JA. 2013. Repeated restraint stress exerts different impact on structure of neurons in the lateral and basal nuclei of the amygdala. Neuroscience 246:230–242.

Pape H-C, Pare D. 2010. Plastic synaptic networks of the amygdala for the acquisition, expression, and extinction of conditioned fear. Physiol Rev 90:419–463.

Peng J, Kim MJ, Cheng D, Duong DM, Gygi SP, Sheng M. 2004. Semiquantitative proteomic analysis of rat forebrain postsynaptic density fractions by mass spectrometry. J Biol Chem 279:21003–21011.

Perez-Rando M, Castillo-Gómez E, Guirado R, Blasco-Ibañez JM, Crespo C, Varea E, Nacher J. 2017. NMDA Receptors Regulate the Structural Plasticity of Spines and Axonal Boutons in Hippocampal Interneurons. Front Cell Neurosci 11:166.

Peters A, Kaiserman-Abramof IR. 1970. The small pyramidal neuron of the rat cerebral cortex. The perikaryon, dendrites and spines. Am J Anat 127:321–355.

Pfeffer CK, Xue M, He M, Huang ZJ, Scanziani M. 2013. Inhibition of inhibition in visual cortex: the logic of connections between molecularly distinct interneurons. Nat Neurosci 16:1068–1076.

Pinal CS, Tobin AJ. 1998. Uniqueness and redundancy in GABA production. Perspect Dev Neurobiol 5:109–118.

Pitkänen A, Pikkarainen M, Nurminen N, Ylinen A. 2000. Reciprocal connections between the amygdala and the hippocampal formation, perirhinal cortex, and postrhinal cortex in rat. A review. Ann N Y Acad Sci 911:369–391.

Pizzorusso T, Medini P, Berardi N, Chierzi S, Fawcett JW, Maffei L. 2002. Reactivation of ocular dominance plasticity in the adult visual cortex. Science 298:1248–1251.

Pollak Dorocic I, Fürth D, Xuan Y, Johansson Y, Pozzi L, Silberberg G, Carlén M, Meletis K. 2014. A whole-brain atlas of inputs to serotonergic neurons of the dorsal and median raphe nuclei. Neuron 83:663–678.

Poulin J-F, Tasic B, Hjerling-Leffler J, Trimarchi JM, Awatramani R. 2016. Disentangling neural cell diversity using single-cell transcriptomics. Nat Neurosci 19:1131–1141.

Prosser RA, Rutishauser U, Ungers G, Fedorkova L, Glass JD. 2003. Intrinsic role of polysialylated neural cell adhesion molecule in photic phase resetting of the Mammalian circadian clock. J Neurosci Off J Soc Neurosci 23:652–658.

Riga D, Kramvis I, Koskinen MK, van Bokhoven P, van der Harst JE, Heistek TS, Jaap Timmerman A, van Nierop P, van der Schors RC, Pieneman AW, de Weger A, van Mourik Y, Schoffelmeer ANM, Mansvelder HD, Meredith RM, Hoogendijk WJG, Smit AB, Spijker S. 2017. Hippocampal extracellular matrix alterations contribute to cognitive impairment associated with a chronic depressive-like state in rats. Sci Transl Med 9.

Robison AJ, Nestler EJ. 2011. Transcriptional and Epigenetic Mechanisms of Addiction. Nat Rev Neurosci 12:623–637.

Rowlands D, Lensjø KK, Dinh T, Yang S, Andrews MR, Hafting T, Fyhn M, Fawcett JW, Dick G. 2018. Aggrecan Directs Extracellular Matrix-Mediated Neuronal Plasticity. J Neurosci 38:10102–10113.

Rudy B, Fishell G, Lee S, Hjerling-Leffler J. 2011. Three groups of interneurons account for nearly 100% of neocortical GABAergic neurons. Dev Neurobiol 71:45–61.

Rutishauser U. 2008. Polysialic acid in the plasticity of the developing and adult vertebrate nervous system. Nat Rev Neurosci 9:26–35.

Sah P, Faber ESL, Lopez De Armentia M, Power J. 2003. The amygdaloid complex: anatomy and physiology. Physiol Rev 83:803–834.

Saito S, Kobayashi S, Ohashi Y, Igarashi M, Komiya Y, Ando S. 1994. Decreased synaptic density in aged brains and its prevention by rearing under enriched environment as revealed by synaptophysin contents. J Neurosci Res 39:57–62.

Sammons RP, Clopath C, Barnes SJ. 2018. Size-Dependent Axonal Bouton Dynamics following Visual Deprivation In Vivo. Cell Rep 22:576–584.

Schindelin J, Arganda-Carreras I, Frise E, Kaynig V, Longair M, Pietzsch T, Preibisch S, Rueden C, Saalfeld S, Schmid B, Tinevez J-Y, White DJ, Hartenstein V, Eliceiri K, Tomancak P, Cardona A. 2012. Fiji: an open-source platform for biological-image analysis. Nat Methods 9:676–682.

Schmitt U, Tanimoto N, Seeliger M, Schaeffel F, Leube RE. 2009. Detection of behavioral

alterations and learning deficits in mice lacking synaptophysin. Neuroscience 162:234–243.

Shatz CJ, Stryker MP. 1978. Ocular dominance in layer IV of the cat's visual cortex and the effects of monocular deprivation. J Physiol 281:267–283.

Shepherd GM, Rowe TB. 2017. Neocortical Lamination: Insights from Neuron Types and Evolutionary Precursors. Front Neuroanat 11.

Sholl DA. 1953. Dendritic organization in the neurons of the visual and motor cortices of the cat. J Anat 87:387-406.1.

Siapas AG, Lubenov EV, Wilson MA. 2005. Prefrontal phase locking to hippocampal theta oscillations. Neuron 46:141–151.

Sirota A, Montgomery S, Fujisawa S, Isomura Y, Zugaro M, Buzsáki G. 2008. Entrainment of neocortical neurons and gamma oscillations by the hippocampal theta rhythm. Neuron 60:683–697.

Smith QR. 2000. Transport of glutamate and other amino acids at the blood-brain barrier. J Nutr 130:1016S–22S.

Sohal VS, Zhang F, Yizhar O, Deisseroth K. 2009. Parvalbumin neurons and gamma rhythms enhance cortical circuit performance. Nature 459:698–702.

Spruston N. 2008. Pyramidal neurons: dendritic structure and synaptic integration. Nat Rev Neurosci 9:206–221.

Stodieck SK, Greifzu F, Goetze B, Schmidt K-F, Löwel S. 2014. Brief dark exposure restored ocular dominance plasticity in aging mice and after a cortical stroke. Exp Gerontol 60:1–11.

STRYKER MP, LÖWEL S. 2018. Amblyopia: New molecular/pharmacological and environmental approaches. Vis Neurosci 35:E018.

Sugiyama S, Di Nardo AA, Aizawa S, Matsuo I, Volovitch M, Prochiantz A, Hensch TK. 2008. Experience-Dependent Transfer of Otx2 Homeoprotein into the Visual Cortex Activates Postnatal Plasticity. Cell 134:508–520.

Sullivan CS, Gotthard I, Wyatt EV, Bongu S, Mohan V, Weinberg RJ, Maness PF. 2018. Perineuronal Net Protein Neurocan Inhibits NCAM/EphA3 Repellent Signaling in GABAergic Interneurons. Sci Rep 8:6143.

Sultan KT, Brown KN, Shi S-H. 2013. Production and organization of neocortical interneurons. Front Cell Neurosci [Internet] 7. Available from: https://www.frontiersin.org/articles/10.3389/fncel.2013.00221/full

Thompson EH, Lensjø KK, Wigestrand MB, Malthe-Sørenssen A, Hafting T, Fyhn M. 2018.

Removal of perineuronal nets disrupts recall of a remote fear memory. Proc Natl Acad Sci U S A 115:607–612.

Tort ABL, Komorowski R, Eichenbaum H, Kopell N. 2010. Measuring Phase-Amplitude Coupling Between Neuronal Oscillations of Different Frequencies. J Neurophysiol 104:1195–1210.

Toyoizumi T, Miyamoto H, Yazaki-Sugiyama Y, Atapour N, Hensch TK, Miller KD. 2013. A theory of the transition to critical period plasticity: inhibition selectively suppresses spontaneous activity. Neuron 80:51–63.

Traynelis SF, Wollmuth LP, McBain CJ, Menniti FS, Vance KM, Ogden KK, Hansen KB, Yuan H, Myers SJ, Dingledine R. 2010. Glutamate Receptor Ion Channels: Structure, Regulation, and Function. Pharmacol Rev 62:405–496.

Tremblay R, Lee S, Rudy B. 2016. GABAergic Interneurons in the Neocortex: From Cellular Properties to Circuits. Neuron 91:260–292.

Tropea D, Majewska AK, Garcia R, Sur M. 2010. Structural dynamics of synapses in vivo correlate with functional changes during experience-dependent plasticity in visual cortex. J Neurosci Off J Soc Neurosci 30:11086–11095.

Ueno H, Takao K, Suemitsu S, Murakami S, Kitamura N, Wani K, Okamoto M, Aoki S, Ishihara T. 2018. Age-dependent and region-specific alteration of parvalbumin neurons and perineuronal nets in the mouse cerebral cortex. Neurochem Int 112:59–70.

Van den Oever MC, Lubbers BR, Goriounova NA, Li KW, Van der Schors RC, Loos M, Riga D, Wiskerke J, Binnekade R, Stegeman M, Schoffelmeer ANM, Mansvelder HD, Smit AB, De Vries TJ, Spijker S. 2010. Extracellular matrix plasticity and GABAergic inhibition of prefrontal cortex pyramidal cells facilitates relapse to heroin seeking. Neuropsychopharmacol Off Publ Am Coll Neuropsychopharmacol 35:2120–2133.

Varea E, Blasco-Ibáñez JM, Gómez-Climent MA, Castillo-Gómez E, Crespo C, Martínez-Guijarro FJ, Nácher J. 2007a. Chronic fluoxetine treatment increases the expression of PSA-NCAM in the medial prefrontal cortex. Neuropsychopharmacol Off Publ Am Coll Neuropsychopharmacol 32:803–812.

Varea E, Castillo-Gómez E, Gómez-Climent MA, Blasco-Ibáñez JM, Crespo C, Martínez-Guijarro FJ, Nàcher J. 2007b. Chronic antidepressant treatment induces contrasting patterns of synaptophysin and PSA-NCAM expression in different regions of the adult rat telencephalon. Eur Neuropsychopharmacol J Eur Coll Neuropsychopharmacol 17:546–557.

Varea E, Guirado R, Gilabert-Juan J, Martí U, Castillo-Gomez E, Blasco-Ibáñez JM, Crespo C, Nacher J. 2012. Expression of PSA-NCAM and synaptic proteins in the amygdala of

psychiatric disorder patients. J Psychiatr Res 46:189–197.

Varea E, Nácher J, Blasco-Ibáñez JM, Gómez-Climent MA, Castillo-Gómez E, Crespo C, Martínez-Guijarro FJ. 2005. PSA-NCAM expression in the rat medial prefrontal cortex. Neuroscience 136:435–443.

Varoqui H, Schäfer MKH, Zhu H, Weihe E, Erickson JD. 2002. Identification of the differentiation-associated Na+/PI transporter as a novel vesicular glutamate transporter expressed in a distinct set of glutamatergic synapses. J Neurosci Off J Soc Neurosci 22:142–155.

van Versendaal D, Levelt CN. 2016. Inhibitory interneurons in visual cortical plasticity. Cell Mol Life Sci 73:3677–3691.

van Versendaal D, Rajendran R, Saiepour MH, Klooster J, Smit-Rigter L, Sommeijer J-P, De Zeeuw CI, Hofer SB, Heimel JA, Levelt CN. 2012. Elimination of inhibitory synapses is a major component of adult ocular dominance plasticity. Neuron 74:374–383.

Vialou V, Robison AJ, Laplant QC, Covington HE, Dietz DM, Ohnishi YN, Mouzon E, Rush AJ, Watts EL, Wallace DL, Iñiguez SD, Ohnishi YH, Steiner MA, Warren BL, Krishnan V, Bolaños CA, Neve RL, Ghose S, Berton O, Tamminga CA, Nestler EJ. 2010. DeltaFosB in brain reward circuits mediates resilience to stress and antidepressant responses. Nat Neurosci 13:745–752.

Villalobos CA, Wu Q, Lee PH, May PJ, Basso MA. 2018. Parvalbumin and GABA Microcircuits in the Mouse Superior Colliculus. Front Neural Circuits 12.

Wang Y, Toledo-Rodriguez M, Gupta A, Wu C, Silberberg G, Luo J, Markram H. 2004. Anatomical, physiological and molecular properties of Martinotti cells in the somatosensory cortex of the juvenile rat. J Physiol 561:65–90.

West MJ, Slomianka L, Gundersen HJ. 1991. Unbiased stereological estimation of the total number of neurons in the subdivisions of the rat hippocampus using the optical fractionator. Anat Rec 231:482–497.

Whissell PD, Cajanding JD, Fogel N, Kim JC. 2015. Comparative density of CCK- and PV-GABA cells within the cortex and hippocampus. Front Neuroanat 9:124.

Wiesel TN, Hubel DH. 1963. SINGLE-CELL RESPONSES IN STRIATE CORTEX OF KITTENS DEPRIVED OF VISION IN ONE EYE. J Neurophysiol 26:1003–1017.

Willard SS, Koochekpour S. 2013. Glutamate, Glutamate Receptors, and Downstream Signaling Pathways. Int J Biol Sci 9:948–959.

Wohleb ES, Wu M, Gerhard DM, Taylor SR, Picciotto MR, Alreja M, Duman RS. 2016. GABA interneurons mediate the rapid antidepressant-like effects of scopolamine. J Clin Invest

126:2482–2494.

Wong DT, Perry KW, Bymaster FP. 2005. The Discovery of Fluoxetine Hydrochloride (Prozac). Nat Rev Drug Discov 4:764–774.

Woodruff AR, McGarry LM, Vogels TP, Inan M, Anderson SA, Yuste R. 2011. State-dependent function of neocortical chandelier cells. J Neurosci Off J Soc Neurosci 31:17872–17886.

Xerri C. 2008. Imprinting of idiosyncratic experience in cortical sensory maps: neural substrates of representational remodeling and correlative perceptual changes. Behav Brain Res 192:26–41.

Xue Y-X, Xue L-F, Liu J-F, He J, Deng J-H, Sun S-C, Han H-B, Luo Y-X, Xu L-Z, Wu P, Lu L. 2014. Depletion of Perineuronal Nets in the Amygdala to Enhance the Erasure of Drug Memories. J Neurosci 34:6647–6658.

Yuste R, Majewska A, Holthoff K. 2000. From form to function: calcium compartmentalization in dendritic spines. Nat Neurosci 3:653–659.

Zingg B, Chou X-L, Zhang Z-G, Mesik L, Liang F, Tao HW, Zhang LI. 2017. AAV-Mediated Anterograde Transsynaptic Tagging: Mapping Corticocollicular Input-Defined Neural Pathways for Defense Behaviors. Neuron 93:33–47.